STARS

Electronic Theses and Dissertations, 2004-2019

2010

Particle Separation Through Taylor-couette Flow And Dielectrophoretic Trapping

Christopher Paul Bock

University of Central Florida

Part of the Engineering Commons

Find similar works at: https://stars.library.ucf.edu/etd

University of Central Florida Libraries http://library.ucf.edu

University of Central Florida

Showcase of Text, Archives, Research & Scholarship

PARTICLE SEPARATION THROUGH TAYLOR-COUETTE FLOW AND
DIELECTROPHORETIC TRAPPING

by

CHRISTOPHER PAUL BOCK
B.S. Stevens Institute of Technology, 2006

A thesis submitted in partial fulfillment of the requirements
for the degree of Master of Science in Miniature Engineering Systems
in the Department of Mechanical, Materials, and Aerospace Engineering
in the College of Engineering and Computer Science
at the University of Central Florida
Orlando, Florida

Spring Term
2010

ABSTRACT

As the world population approaches seven billion, a greater strain is put on the resources necessary to sustain life. One of the most basic and essential resources is water and while two thirds of the earth is covered by water, the majority is either salt water (oceans and seas) or it is too contaminated to drink. The purpose of this project is to develop a portable device capable of testing whether a specific source of water (i.e. lake, river, well…) is potable. There are numerous filtration techniques that can remove contaminants and make even the dirtiest water clean enough for consumption but they are for the most part, very time consuming and immobile processes. The device is not a means of water purification but rather focuses on determining the content of the water and whether it is safe. Particles within the water are separated and trapped using a combination of a Taylor Couette fluid flow system and Dielectrophoretic electrodes. This paper explores Taylor Couette flow in a large gap and low aspect ratio system through theory and experimentation with early stage prototypes. Different inner cylinder radii, 2.12cm, 1.665cm and 1.075cm, were tested at different speeds approaching, at and passing the critical Taylor number, 3825, 4713 and 6923 respectively for each cylinder. Dielectrophoretic (DEP) electrodes were designed, fabricated, coated and tested using latex beads to determine the method of integrating them within the fluid flow system. Taylor Couette theory, in terms of the formation of vortices within the large gap, small aspect ratio system, was not validated during testing. The flow pattern generated was more akin to a chaotic circular Couette flow but still served to move the particles toward the outer wall. Fully integrated tests were run with limited success. Recommendations were made to pursue both circular Couette flow as the basis for

particle separation and dimensional changes in the setup to allow for the formation of Taylor

vortices by increasing the radius ratio but still allowing for a larger volume of fluid.

This work is dedicated to my parents for instilling the idea that education is a lifelong journey and to never stop learning. To Dr. Chen for his support and patience. But mostly to my wife< Keri, for her belief in my educational pursuits, putting up with undesirable conditions to support our family and her unwavering faith in me.

TABLE OF CONTENTS

LIST OF FIGURES

LIST OF TABLES

x

CHAPTER ONE: INTRODUCTION

Biocharacterization is an important tool used within many research facilities including medical, environmental and weapons research. It can be used to identify unknown species or chemicals that may become present in nature due to pollution, toxins that may be harmful and the result of either industrial accidents or bio-weapons, it can be used to study biological reactions within living species and their response to various outside factors whether they are present in nature (plants, bacteria…) or artificially produced (drugs, processed foods…). As technology has progressed, it has become an important part of every industry and has varied uses. Some companies use it as the main means of fabricating their product, others as a means of maximizing their productivity and others as a quality control tool. Biocharacterization can be used as a fabrication tool but only during the initial experimental and conceptual phase of a product. It can be used as a way to determine the most efficient process to achieving a particular dose or level of a specific bio-specimen. But it's most useful purpose is as sensors to detect and characterize harmful particles whether as an early detection tool for biowarfare, in healthcare facilities for the monitoring and containment of viruses introduced by patients or as a means of monitoring natural resources (drinking water) and crops. Many issues with respect to all these areas involve symptoms and reactions that are discernable to the human eye and biocharacterization is used to identify to the toxins present, this investigation is more concerned with microparticles and bacteria that is invisible to humans and if not identified early can cause devastating results.

There are several issues that present themselves when targeting particles of this nature. The most obvious and important problem is the size of the particles which generally range from 0.1 µm to 10 µm (micrometers, microns, 1×10^{-6}m) for bacteria and even smaller for viruses. The fact that some diseases, implying the viruses and bacteria that cause them can be transmitted by air speaks to the miniscule nature of these particles. The most common visual reference used when discussing micron sized objects is a human hair which has an average diameter of 100 µm. The combination of the micro sized targets and the vastness of the area that needs to be monitored make this task impossible prior to the advent of MEMS technology. MEMS, Micro Electro Mechanical Systems, devices are the tools available to modern scientists to bridge the gap between the macro world and the micro world. These devices are the result of advances in fabrication techniques with the main driving force within industry being the manufacture of computer chips. MEMS devices are, as the name implies, systems that can be combinations of both electrical aspects, such as microcircuits, and mechanical components, such as cantilever beams. The reason MEMS technology is the right tool for the job but also the only solution for micro sized particle interaction is because the system operates at that same size. The detection of potentially harmful biospecimen occurs at a one particle to one receptor on the MEMS device which yields much better results than concentration chemical reactions. BioMEMS, a branch of MEMS technology, deal with very specific devices which have certain receptors which dictate what particles can be detected but with great precision, even if there is only a single particle of that particular variety a BioMEMS device can detect it. There a various mechanisms that interpret that reaction having taken place and transmit the presence of that species in the area. An example is the cantilever beam with the receptors deposited on the end of the beam so that a

reaction creates a micro change in the weight and can be interpreted with a great deal of resolution. While this is a definite solution to biocharacterization, the most popular means of particle analysis is performed within microchannels as a part of a microfluidic process. These processes are used to recreate real world experiments at a micro level. The main issue for these devices is that the particles have to be brought to them and introduced into the system to detect which particles are present where as the previously mentioned devices are placed in the general detection area and left until a reaction occurs. The difficulty of this system is obviously found within the concentration portion of the process. The idea of this process is to separate the specific particles of interest making sure that they remain viable, reconcentrate them and then introduce them into the microfluidic array. The separation and subsequent concentration for analysis is the main aim of this research. The ability to separate out particulates from a large volume without extensive throughput times would contribute to a great many applications.

The main focus of this research is the particle separation for the purposes of analyzing those particles. The first goal is to steer clear of filters as they have extensive throughput times and are more focused on the fluid rather than the particle and it can be difficult to retrieve the particles from the filter membrane. The overall design was to use fluid flow patterns in combination with dielectrophoresis (DEP) electrodes to trap the particles. The fluid flows explored are circular Couette flow and Taylor-Couette flow; these are meant to direct the particles toward the DEP electrodes where they will be held by the trapping force generated. The flow pattern needs to be able to push the particles toward the electrodes while not creating too much force that the electrode can not hold it. Finding this balance is essential to this research. Overall the design of the system is meant to be portable while still being complete.

The dimension limits can affect the flow patterns substantially and will be another major factor in the design and experimental setup.

CHAPTER TWO: LITERATURE REVIEW

The ability to isolate particles and characterize them is an important aspect in research today with the need to defend against the new weapon of choice, biowarfare, as well as the increased focus on the environmental impact human existence is having on the planet. These are the most recent and headline grabbing reasons for pursuing this research but there are many more basic everyday uses for this technology. Bashir et al. [1] explain that BioMEMS chips that feature cell isolation and characterization on one device could be used as more efficient, both in cost and time, replacements for current diagnostic tools in the health and food industry along with the aforementioned prevention of biological and chemical hazards. With such a broad range of applications, there are many variations on cell sorting and trapping with each different approach being geared toward the application. There are three main sections of cell isolation that were explored for the purposes of this research: microfiltration, cell separation and cell isolation.

Microfiltration

Filters regardless of there design are made up of porous materials whether they be man made such as screens or naturally occurring such as charcoal. The pore size determines what can be filtered out and what remains in the passing liquid. The basic filtering setup is to have an entry point for the liquid and an exit port for the filtrate with the filter material obstructing the passage. Filters can either work by gravity where the liquid is pulled through slowly or the flow can be pushed through under pressure. Filters that operate without a pressurized flow are mainly small scale drip water filters or screens set up to keep larger particles from entering a chamber. They are either not meant for small particles, let alone microparticles, or they are inefficient as

they require a filtering period and the filtrate comes out too slowly to be used as a part of a particle removal system. Filtering using a flow can be done in two different ways. First, dead-end filtration is when the flow is coming perpendicular to the filtering membrane. The issue with this type of filtration is the build up that occurs over time from the filter stopping particles from passing. These particles build up forming a caked on layer that eventually becomes impenetrable and renders the filtering system worthless after some time. This occurs even with systems that are gravity fed, it just takes much longer and the system as a whole has a long enough life cycle that it is a viable system. The difference with the flow system is that the cake buildup occurs so much faster that this type of filtering can only be used for small volumes with the buildup being removed between runs. Cross-flow filtration has the same set up but the fluid flow occurs parallel to the filter membrane and allows for less particle build up with two fluids coming away from the filter membrane, the filtrate/permeate and the retentate as Cheryan calls them [2]. Having the flow move across the membrane keeps the particle buildup low enough to still allow the fluid to pass through the membrane. This happens because the larger particles are not trapped by the pores and keep moving along with the flow. This method allows for longer periods of flow but much like dead-end filtration is more focused on the filtrate.
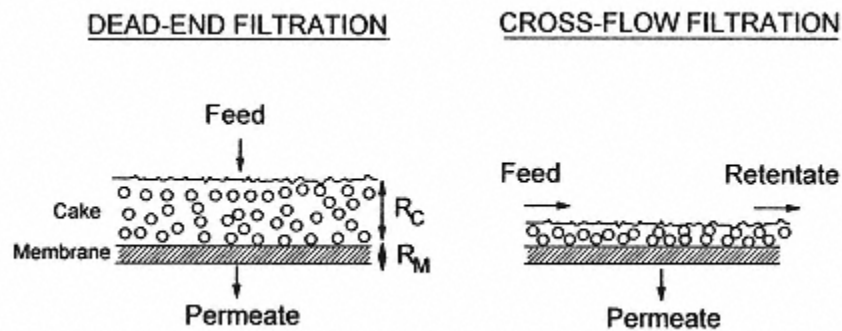
Figure 1 Straight flow filtration method [2]

There is another type of filtration which follows the goal of cross-flow filtration of limiting the particle build up on the membrane by having a flow running across it. The filtration method is called Reverse Osmosis. Lee and Lueptow [3] explain that it is used to remove ions and organic chemicals from contaminated water. The system is based on Taylor-Couette flow patterns which generate from an inner cylinder rotating within an outer cylinder. They conclude that the Taylor vortices formed help to keep particles from accumulating on the inner cylinder where the membrane is located. Wereley et al. [4] show that the Taylor vortices formed between the two cylinders help to pull away particles away from the filter and minimize cake buildup. This rotating filter is used in fields such as desalination and water treatment. The reason that this filtration is very efficient is the same reason that it is not applicable for research where the primary focus is the particle itself. Rotating filtration efficiently pulls particles away from the fluid/particle separation point and moves them along. There is a layer built up but there is no control of what is trapped and what moves along through the exit port of the filtration system as more fluid is pushed into the system. The very nature of filtration, although performing the task

7

of particle removal from a larger environment and thereby meeting are basic need, is focused on the filtrate and the particles that are removed are of little importance other than knowing they have been removed. While some of the aspects of filtration are pertinent to this investigation a more important focus on the cells and particles being separated is needed.

Cell Separation

While filtration techniques are used for removing pollutants from a substance, this investigation is mainly interested in creating a method that can isolate those particles from the fluid but with the main goal of being able to analyze them. This analysis is performed using biological techniques aimed at identifying cells, which requires sorting the cells out of a larger group. It is not the analysis techniques that are important at this point but rather the lab work and procedures used to get those cells in a position to be characterized. The first of these techniques is a simple premise based on gravity and cell properties known as sedimentation [5]. Cells will settle based on size and density of the particle as well as the density and viscosity of the medium. Although the cells would settle over a long period of time, because they are such small particles they settle at a much slower pace, a centrifuge is often used to increase that downward gravitational force dramatically. This allows a way to not only make this process efficient but also gives it some control over the final result. This control however can only be applied if the properties of the fluid and cells contained differentiate from one another in terms of density. Patel et al. [5] explains that the separation conditions must be chosen carefully because the cells are sensitive to the surrounding environment. While effective for small amounts, in terms of a method to isolate unknown species from a larger volume of water, this separation method is not ideal. A similar method based on centrifugal forces is elutriation. The basic principle is the

8

same where the centrifuge is forcing the cells downward but in this system, there is a flow pushing against the centrifugal force. According to Figdor et al. [6], this set up allows for large scale cell separation without need for pretreatment or major differences in cells. The process which uses opposing forces from the centrifuge and the in flow to allow the cell to settle based on sedimentation velocity and remain unharmed. The problem with this system is that it requires a somewhat complex setup but also knowledge of the process to achieve the correct opposing forces for a given sample in order for equilibrium to be achieved and for the cells to become ordered. This process also requires a group of cells to be present within a smaller volume and is more directed towards sorting that isolation of particles from a large volume. Hausmann et al. [7] describe another separation technique known as free-flow magnetophoresis. This process uses magnets to separate to sort particles. It requires the introduction of magnetized particles labeled with a specific antibody that allows it to attach to the desired particles which will be sorted using a magnet. The marked particles can either be the goal of the separation or one of the particles that must be removed to obtain the desired filtrate. Hoffman and Houck [8] present a cell separation technique known as flow cytometry where cells are rapidly sorted one at a time based on optical and fluorescent properties. This technique while fantastic in its ability to differentiate between particles is hugely inefficient in terms of bioseparation because the sorting process occurs on a particle by particle basis. Free flow electrophoresis is another separation method that uses surface charge to differentiate between cells according to Eggleton [9]. As particles flow through an electric field in a fluid chamber, the particles are separated based on the movement of the particles to either the anode side or the cathode side and the distance they move.

9

Cell Isolation

Bashir et al. [1] explain how dielectrophoresis (DEP) can be used to separate living and dead cells because they have different dielectric constants and are thus affected differently by the electric field generated. Cell isolation is different than cell separation in that the particles are trapped not sorted. There is more emphasis on the nature of the particle and trapping it for later use. While the goal of this paper is to separate particles from a solution much like filtration techniques and other cell separation processes, the better process to meet the needs of the separation device is dielectrophoresis, a cell isolation technique. The reason is that of the two components that come out of a cell separation procedure, fluid free from particles and the particles, the particles are the only part that is of any interest to this project. While it is true that cell separation effectively removes particles, another important factor to this removal is the state of the particle post-process. In most filtering techniques, the particles become layered onto the filtering membrane which would require further operations to separate them out from one another to be characterized. DEP traps the particle, individually or in clumps, the difference is that the electric field effect can be turned off and the particles are released for further analysis. There is no force compacting the particles into a layer and making them essentially waste.

Dielectrophoresis

Dielectrophoresis is a mechanism that allows control over particles by inducing motion or holding by generating a non-uniform electric field. The strength of this field is dependent on the electrical properties of the medium and the particle, the shape and size of the particle and the frequency of the electric field.

$$F_{DEP} = 2\pi\varepsilon_m R_p^3 \, \text{Re}[K(\omega)]\nabla E^2$$

Figure 2. Equation for Dielectrophoretic Force

In this equation, the geometry of the particle is expressed by $R_p{}^3$ where R is the radius, ε_m is the

permittivity of the suspending medium and ε_p is the permittivity of the particle, ∇E^2 is the

gradient electric field squared and *Re[K(ω)]* stands for the real part of *K(ω)* which is in the form

of Figure 3.

$$K(\omega) = \frac{\epsilon_p^* - \epsilon_m^*}{\epsilon_p^* + 2\epsilon_m^*}$$

Figure 3 Clausius Mossotti factor

Claussius Mossotti is the frequency factor of the DEP force arising from the permittivity

and it is also what determines DEP to be negative or positive. If the conductivity of the particle

is larger than the conductivity of the medium, *Re[K(ω)]>0*, and positive dielectrophoresis occurs

which is characterized by particles moving towards the edges of the electrodes where the electric

field is highest. If *Re[K(ω)]<0*, negative dielectrophoresis occurs and the particles are be pushed

away from the edges and corners of the electrodes by the electric field and grouped at the lower

electric fields. There are two kinds of DEP positive and negative and they are dependent on the

conductivity of the particle compared to the medium. Positive DEP is attractive and will pull

particles closer to the points where the electric field is the strongest (i.e. the edges) and negative

DEP is where the particles are repelled from these points but still grouped together in a 2 dimensional system based on the characteristics of the particles.

Dielectrophoresis is a great tool for holding particles but they require the particle to be within a certain distance of the electrode to feel the effects of the electric field. Dürr et al [10] fabricated a microdevice to manipulate, trap and separate micro and nano particles that involved having electrodes around a micro channel that deflect particles to certain outlets using negative DEP. The system highlights an issue that this paper aims to solve and that is the interface between micro electrodes and the macro world. The system puts the particles within a certain range of the electrodes by using a micro channel. The macro world is then made micro by pumping the fluid into the channel but it is inefficient for the large volumes that this project needs to use. Pethig and Markx [11] discuss the advantages of microelectrodes and state that by reducing the size of the electrodes, there is a substantial decrease in the reduction of operating voltage to maintain the same DEP force. They state that an n-fold change in electrode scale will result in a an $n^{3/2}$ fold change in operating voltage. They also state that for interdigitated electrodes (mostly associated with bioparticle separation) the electrical gradient generated decays exponentially with distance from the electrode surface. These two factors mean that the electrode design must have interdigitated teeth with minimal cross section and gap between them and that the particles must be pushed as close as possible to the electrodes where the gradient is the highest. Pohl and Hawk [12] come to the conclusion that with a difference in permittivity between live and dead cells due to cell wall denaturing at cell death, live and dead cells can be separated using dielectrophoresis. Certain constraints are necessary, high frequency alternating fields, media of very low conductivity and non-uniform electric fields. This same differentiation

between cells exists with more than just living and dead cells. Based on permittivity of a particle it can be separated from other particles with differing properties using dielectrophoresis and the non-uniform electric field that creates a certain polarity in each particle and moves the particle based on this induced polarity. Deval et al [13] explore chaotic mixing at a micro level using dielectrophoresis. At such a small scale the ability to disturb the medium by moving particles within create a mixing mechanism. This is the idea behind their project. An important aspect of their work was determining that the Clausius-Mossotti factor can effectively change the DEP force from attractive to repulsive by varying the frequency. Important for mixing mechanisms but also important in knowing whether particles are going to be held or pushed back when pushed toward the electrode and to create a range of particles that will be held which allows for some pre-characterization of cells. Gascoyne and Vyhoukal [14] discuss the low frequency effects of AC electroosmosis and the effect of pushing particles onto electrodes without holding them there. This is a phenomenon that has been encountered in this project and there seem to be no ill effects and it serves to keep particles near the electrodes. They also discuss Field-flow fractionation which is the use of DEP in trapping or placing specific particles at a certain height from the electrodes where a velocity profile pushes them through and allows for the characterization to be performed by the fluid and position of the particle with respect to this fluid. Chou et al [15] discuss electrodeless DEP and the fact that very high electric fields can be used without fear of electrolysis. This paper also serves to give weight to our DEP trends such as increased voltage and frequency will lead to an increase in dielectrophoretic force. Green and Morgan [16] show that the Clausius-Mossoti factor becomes negative at frequencies greater than 10^6Hz so that frequencies below that level display positive DEP and frequencies above it display

13

negative DEP. Positive DEP is the better suited direction for this project but the ability to change the direction of the signal based on frequency could prove useful in terms of releasing the particles after the fluid is drained away. Green, Morgan and Milner [17] discuss trapping of a virus and beads at the sub-micron level. Their experimental data again shows that at 500kHz DEP was positive while an increase to 10MHz made the DEP negative. Knowing at which frequencies the electrodes should operate at even before doing any tests will allow for confirmation experiments much more than investigative testing. Morgan, Hughes and Green [18] show that sub-micron particles can be separated on the same device without fluid flow based on the differences in polarizability of the particles in question. Any means of differentiating particles based on their properties before and characterization is performed makes a more efficient system.

<div align="center">Taylor-Couette Flow</div>

Taylor Couette is a fluid flow system developed as a means of exploring the flow patterns that develop between two rotating concentric cylinders. Donnelly [19] explains that the interest in rotating cylinder flow can be traced back to Isaac Newton. Taylor-Couette flow was used in the filtration example earlier in this section and the same flow patterns may apply to the designs for this investigation. Taylor-Couette flow patterns are generated in the gap between two concentric cylinders. The flow pattern develops as the angular velocity of the inner cylinder increases and the flow pattern goes from laminar circular Couette flow pattern to a more controlled chaotic flow that features vortices that rotate perpendicular to the surface of the fluid.
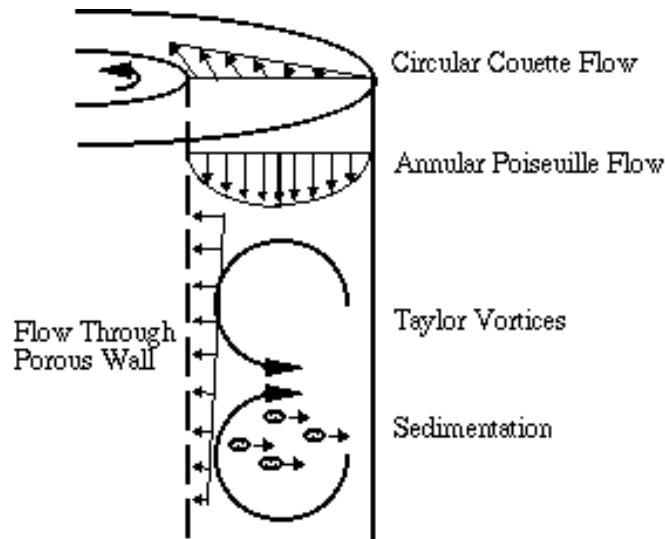
Figure 4. Types of flow through concentric cylinders

Taylor-Couette flow arises when a critical Taylor number has been crossed. This critical point is determined by the square root of the gap size divided by the inner radius and then the rotational Reynolds number of the inner cylinder.

$$Ta_{crit} = Re\sqrt{(d/r_i)}$$

$$Ta_{crit} = [(\Omega\ d\ r_i)/\nu\ ]\sqrt{(d/r_i)}$$

Substituting we find that the rotational Reynolds number is based on the angular velocity, gap size, inner radius and the viscosity of the system. The critical Taylor number is based on the dimensions of the system and the viscosity of the fluid filling the system and most importantly the angular velocity. All the other variables describe the system, the path the fluid is going to have to be pushed to create the vortical formations. The angular velocity of the cylinder is the force behind the vortices. It must surpass the point necessary to create a large enough vortex that

15

it reaches the outer wall and gets bounced back where the angular velocity continues to turn the inner cylinder at the right speed to keep the vortex moving. Lim, Chew and Xiao [20] describe the formation of Taylor vortices by accelerating the flow at a certain rate. This acceleration has to be maintained for the flow regime to be maintained. This is indicative of the nature of Taylor Couette flow and its dependence on the movement of the inner cylinder with respect to the system. The motion starts with the inner cylinder and even though most experiments use small gap systems, the inner cylinder speed/acceleration can be used to overcome a larger gap in theory. Another important part of Taylor Couette flow that is not present in the determining equation is the aspect ratio of the system. The aspect ratio is the height of the fluid that is present in the system compared to the gap size. If a vortex is to be formed across a gap, it has to have a vertical dimension. That is why the aspect ratio is important, it quantifies how many cells must be stacked to vertically fill the gap and more importantly is there enough vertical space for a vortex that spans the gap to form. In our design, the emphasis is on portability and using the angular velocity of the inner cylinder to make everything work perfectly. Mahamdia, Dhaoui and Bouabdallaha [21] discuss the aspect ratio of the system and determine that below a critical aspect ratio, $\Gamma < 10$, the transition from Taylor vortex flow to chaotic flow bypasses the azimuthal wave regime. This is particularly important for the dimensional design of the particle separator as the aspect ratio is well below 10. The Taylor vortex flow within our device is at risk of just being bypassed and moving from circular Couette flow to chaotic flow. Having a better understanding of the formation of the vortex is a big part in working with it. A more appropriate method to view Taylor vortices is by understanding the particle movements within them as those are the true objective of this project. Henderson, Gwynllyw and Barenghi [22] describe the

16

motion of particles in Taylor vortex. They describe how particles will move toward a limit orbit

regardless where they are initially. Particles at the edge will work their way in towards it and

particles contained within the vortex will spiral out. Understanding this limit orbit and its

distance from the outer wall will help quantify the DEP force necessary to trap particles.

Wereley and Lueptow [4] have also done work on the inertial particle motion in Taylor Couette

flow but for a rotating filter which has some axial flow. They describe the particle as travelling

around the center of the vortex as it moves through the gap. The azimuthal velocity propelling it

at high velocities around the inner cylinder but slowing it way down when it begins to reach the

outer wall and the azimuthal velocity is diminishing. This slowing works great with DEP

electrodes at the outer wall as they try and trap the particles. The structure of Taylor Couette

flow is such that the vortices are stacked on one another rotating in opposite directions with in

flow and out flow sections between each vortex depending on the direction of rotation. A

particle will quickly move out from the inner cylinder towards the outer cylinder through the

outflow band. Once it reaches the outer cylinder it slows down and will remain out there moving

axially before getting pulled back towards the inner cylinder. Part of Taylor Couette flow that

could also prove to be a big help in characterization is the separation that comes from centrifugal

forces in terms of particle differentiation based on size and density of the particle. Ohmura,

Suemasu and Asamura [23] deal with classifying particles using Taylor vortex flow. They

describe Taylor Couette flow as having two distinct mixing regions. The active mixing region

consists of the outer edges of the vortex and the flow around the inner cylinder and outer wall.

The isolated mixing region is at the center of the vortices. The larger particles end up in the

active mixing region and are the first to be captured by the DEP electrodes while the smaller

particles are pulled into the vortex. These self sorting moves could allow the particles to do a pre-separation by doing multiple runs. Although Taylor Couette flow is a well known experimental tool and has been used in labs for quite some time as a means of understanding fluids, there are few areas where it has been adapted for an industrial purpose. The main area that it is used in was mentioned before and that is in rotational filtration. The mechanism is used in plasma extraction from blood and water treatment. Min and Lueptow [24] use an porous inner cylinder to filter out particles as the fluid is passed through the inner cylinder and various Taylor Couette flow phases were investigated for their ability to pull particles away from the inner cylinder. The same principle is used for this paper but instead of keeping particles from the inner cylinder, the goal is to push them towards the outer cylinder where they will be trapped. Many other experiments are being performed involving Taylor Couette. Weisberg, Kevrekidis and Smits [25] were studying the effects of delaying transition to Taylor Couette flow by using axial motion and changes in pressure gradients within the axial cylinders. By delaying the formation of Taylor vortices, they were able to enhance the long term stability of the vortices. For this project being able to maintain Taylor vortices during the separation phase would be ideal. Serre, Sprague and Lueptow [26] examine the stability of Taylor Couette flow in a finite length cavity. The goal is to determine if radial throughflow will impact the stability in cylindrical Couette flow. Through simulations they conclude that small radial outflow lead to vortical transition at a lower Taylor number but for radial inflow and large outflow vortex formation is suppressed. This work could have some affect on this project should a flowing mechanism be developed to allow for a larger volume to be processed using the same wafers.

CHAPTER THREE: METHOLODGY

The focus of this research is on creating a separating mechanism that uses dielectrophoretic electrodes to trap and hold the particles of interest and specific fluid flow patterns that push the particles out towards the electrodes while minimizing the forces on them once they reach a point where they can be held. The literature review centered on methods of particle separation and arrived at the pairing of DEP electrodes and Taylor-Couette flow patterns. The process to create and test this apparatus is detailed in this section. The basic approach was to first create the electrodes and test them and then focus on the container and fluid flow mechanism that will push the particles out to the electrodes which will be placed on the inner surface of the outer cylinder.

Initial Electrode Design

The initial electrode design was created as a means of testing a couple parameters for the final electrode design. The fabrication process used to create these electrodes was to use microfabrication techniques to produce micro gap sized electrodes. There were numerous steps in this procedure, the first of which was the mask design. The goals of the mask design were two fold: knowing just how small the gap size in the electrodes needs to be for a certain size particle and knowing which direction the electrodes should be aligned on the cylinder walls to have the most effect. These goals were the main criteria in the design process and basically shaped the mask. The first goal was met by including four different gap sized electrodes within the mask ranging from 10 microns to 100 microns. This allowed us to cut the wafer after fabrication to see how well each electrode performed. The second goal was taken into account by having four

parts to each electrode, two vertical segments and two horizontal segments. This allowed us to identify how best to fabricate the electrodes for the final design. Once the mask was designed, the clean room fabrication was performed.
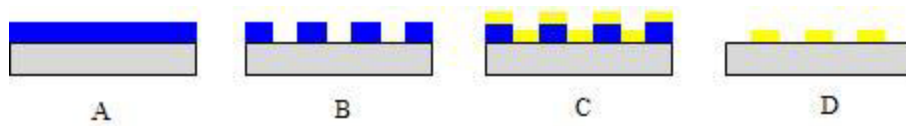
Figure 5 Fabrication process A) Photoresist deposition B) Photolithography patterning the photoresist C) Metal deposition using filament evaporation D) Removal of photoresist using Acetone bath

As Figure 5 shows, the procedure involved spinning a layer of negative photoresist with the spin speed determining the thickness of the layer which was important because it must be thick enough to separate the two metal layers and allow a clean pattern to form. The wafer was then baked to prepare the photoresist for UV exposure. The wafer was exposed using UV light and a prefabricated mask that patterns the photoresist by allowing only the desired photoresist to be crosslinked by the UV light. After exposure, the photoresist was again baked to solidify the crosslinked pattern. Once the desired pattern had been exposed, the wafer was rinsed in Acetone to remove the photoresist that was not exposed and open the wafer up for metal deposition. Once the excess photoresist was removed, the wafer was put into the vacuum chamber for metal evaporation. Metal evaporation works by heating up the desired metal so that it first melts and then flash evaporates depositing a thin layer of the metal on the wafer as the particles expand from the evaporation point. The chamber is pumped down using a cryo-vacuum to remove as many air molecules as possible so that the metal particles expand uniformly until reaching the target without being deflected. During evaporation, a chromium sub-layer was deposited first because gold does not bond well to the wafer. After the metal layers have been deposited, the

20

wafer was placed in Acetone and agitated to peel away the photoresist along with metal layers covering it to leave the DEP electrodes. With such small gaps in the pattern, the Acetone bath was conducted in an ultrasonic machine to remove all excess layers much faster and resulted in much cleaner pattern edges. The difficulty in this procedure was the lift off process which was a balance between removing all the photoresist while not altering the electrode shape. Once a suitable looking sample was achieved, it was cut and readied for the particle holding experiments.
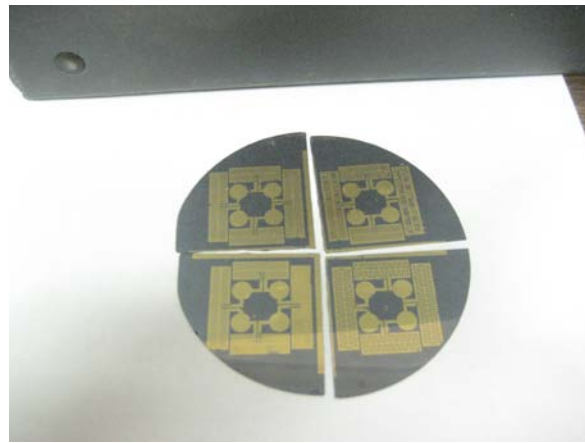
Figure 6 Test pattern for DEP electrodes

The experiments were based on visual confirmation and the setup to run and monitor the experiments consisted of a microscope mounted with a video camera as well as two probes. The camera allowed the experiments to be recorded for comparison purposes and the probes were used to apply the signal to the electrode pads. The signal was generated using Virtual Bench on a computer which allowed for the manipulation of multiple variables while monitoring their effect on the motion of particles. The function generator produced the signal and the scope allowed it to be monitored throughout the experiment.

Figure 7. Experimental setup for electrode testing

The electrodes were first hooked up to the system using the probes to make sure that the photoresist had released completely. This is to say that the original mask design was completely formed and intact. Since the design consists of two opposite electrodes that do not actually touch, the only way that the process will work is if they truly are not in contact. This was tested by applying a signal and monitoring it on the scope. If it remained unchanged, there was no contact. If the output voltage decreased it would mean that there was contact resulting in a resistance throughout the circuit which decreased the initial voltage. After making sure that the patterns had fully released, the voltage was slowly increased and the pattern monitored using the video feed from the microscope. Unfortunately at higher voltages, the electrodes go through electrolysis releasing hydrogen in the form of bubbles.
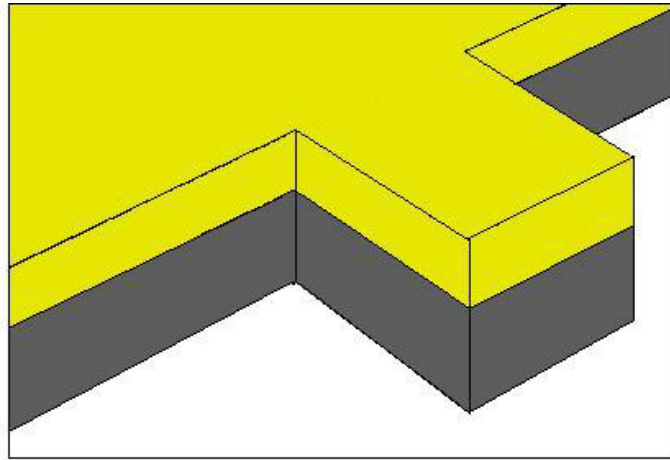
Figure 8 Gold and chromium layers

These bubbles can be seen escaping the electrode teeth and forming along the edges of the pattern. Electrolysis occurs at the edges of the pattern because it is the chromium sublayer that is reacting with the hydrogen in the water not the inert gold layer.
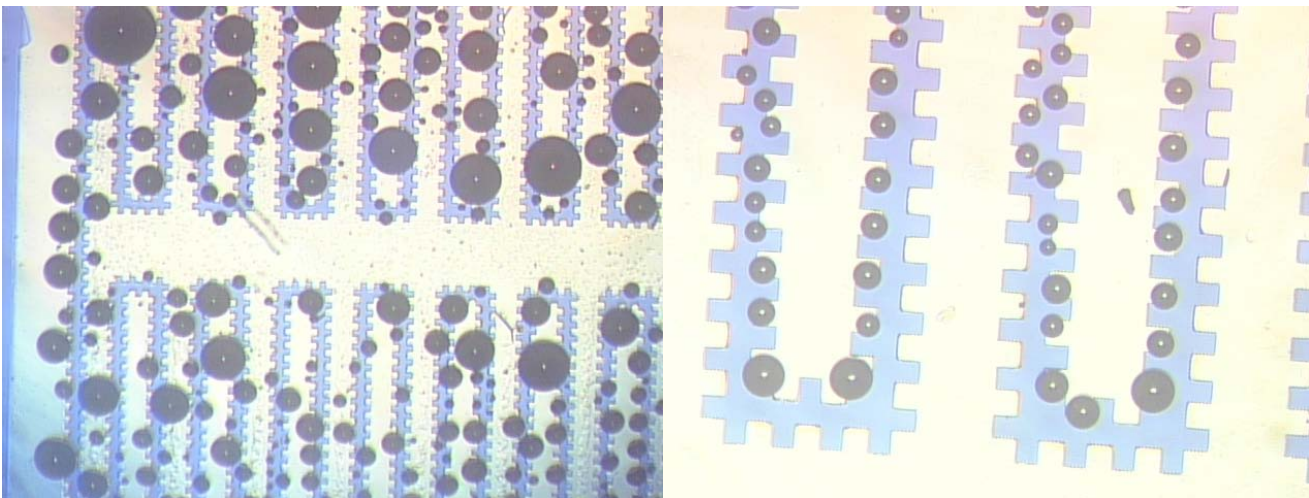
Figure 9 Bubbles formed through electrolysis are shown at various levels of growth. On the left, later stages of electrolysis show the chaotic result of the process as the electrode deteriorates. On the right, the early parts of electrolysis prior to electrode degradation

This effect must be removed or at least minimized to make the dielectrophoretic holding force effective. In order to control the process of electrolysis, the electrodes must be covered with a thin dielectric layer to prevent the electrodes from reacting with the water molecules. This investigation was pursued with its purpose being to develop an appropriate coating for the electrodes that would minimize electrolysis while still allowing the dielectrophoretic holding force to be effective on the particles. To meet these requirements the coating had to be thin and uniform throughout. Thin to allow the force to still be felt and uniform to minimize weak points in the layer which would eventually lead to its tearing. The proper coating would insure both the minimizing of electrolysis but also extend the operating life of the electrodes by separating them from the water molecules that react and release the bubbles. The dielectrophoretic electrode patterns were examined under the microscope and the four different gap sizes are shown in Figures 9-12. Once the issue of electrolysis was resolved, the optimal gap size, operational voltage and frequency were determined through Microbead experiments and are discussed later in this paper..
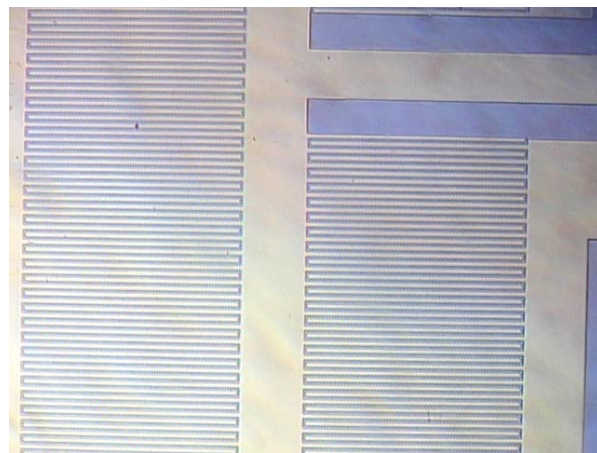
Figure 10. 10 micron pattern at 2.25X
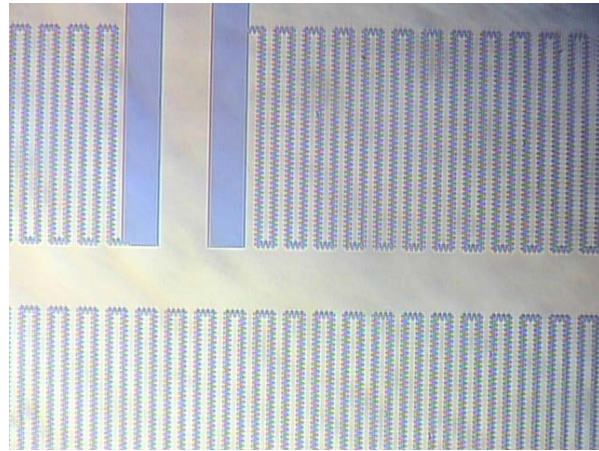
Figure 11. 20 micron at 2.25X
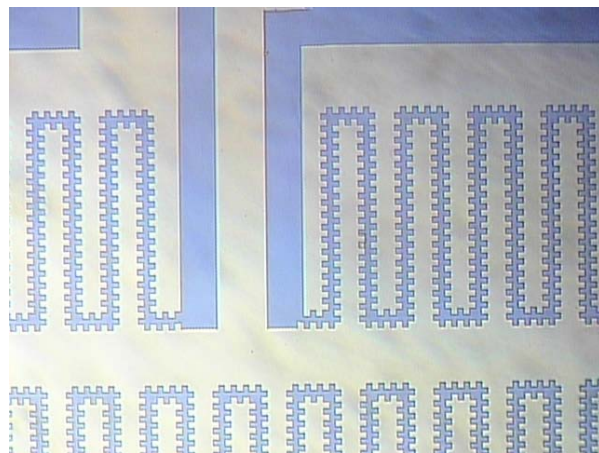
Figure 12. 50 micron at 2.25X
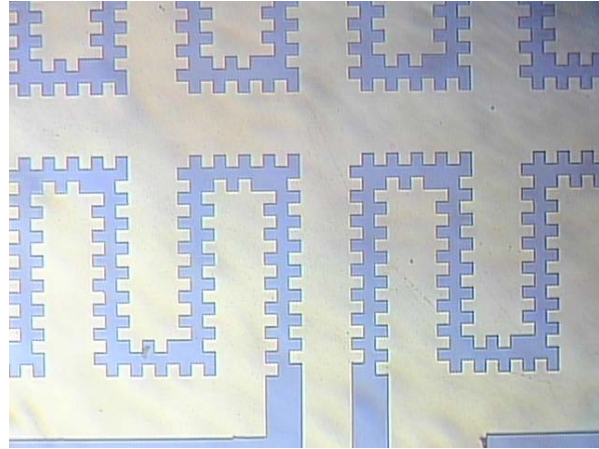
Figure 13. 100 micron at 2.25X

Electrode coating

The first coating that was investigated was Omnicoat which is normally used to

encourage the adhesion of SU-8 to metals. The main reason for choosing Omnicoat was because

of its very thin nature once spun onto a substrate. There were two main problems with this

substance that may have ultimately led to electrolysis still occurring. First, it was difficult to tell

whether or not the probe had pierced the layer and was in contact with the gold electrode pad and

often led to both the Omnicoat and gold being peeled off by the probe being over manipulated.

The second issue was that its surface was not uniform and appeared bubbly. This was most

likely due to a wrong post-spin baking step which may require a slower ramping up of the

temperature to allow for a more uniform surface. Electrolysis still occurred and Omnicoat was

ruled out as a possible dielectrophoretic electrode shielding layer.
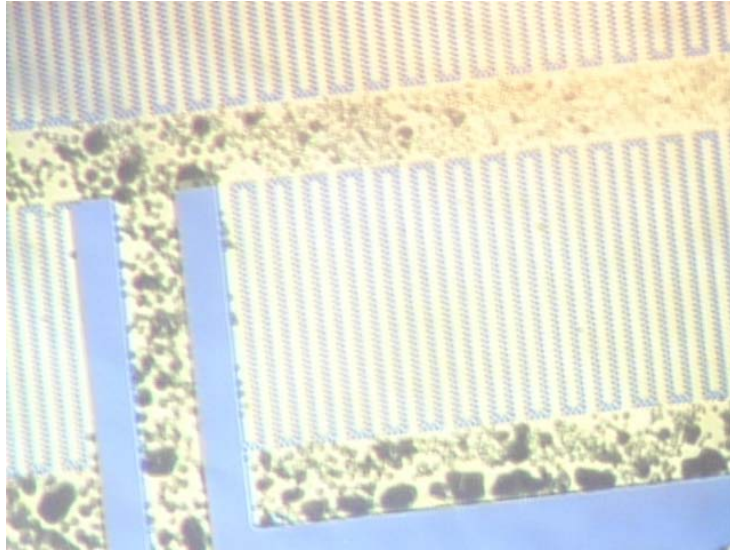
Figure 14. Bubbles formed due to Omnicoat baking

After failing to find a solution with Omnicoat, the effort to achieve dielectrophoretic electrodes that not only demonstrate bead or cell attraction but minimize the effects of electrolysis if not eliminate it entirely was continued with the main goal of preventing electrolysis by covering the electrical conducts with a dielectric layer to separate them from the water and bead suspension. The key to this solution is two fold. First, the layer needs to be uniform and defect free to allow for bead trapping across the whole pattern without the opportunity for water to get under the layer causing electrolysis and ultimately electrode destruction. The second part of this solution is that the layer can not be so thick that it prevents the necessary attraction of the beads to the pattern. Besides Omnicoat, he other coatings tested were Spin-on-Glass (SOG) and thin SU-8 (2000.5). The SOG coating created a similar layer to Omnicoat including the bubbles on top of the gold pattern from the heating process. The similarities continued in the testing phase and SOG did not show signs of preventing electrolysis.

27

Electrodes were then fabricated taking care to lower the amount of defects that could cause failures when applying a protective layer. Better releasing of the pattern was achieved using an ultrasonic bath. This allowed the electrodes to be independent throughout and the coating to be more uniformly applied. The thin SU-8 was then spun on using a mask to block the electrode contacts from being covered so that probe contact would not be an issue. Once these wafers were ready, testing began to determine if SU-8 eliminates the electrolytic effect on the electrodes. In order to maximize the significance of each test and attempt to reproduce the goal of pushing the beads or cells within a certain distance of the electrodes so that they can be trapped more readily. This task was performed by using a small amount of solution and a glass slide. The glass slide is also useful in making the pattern and beads easier to see with the microscope. Without the slide the solution formed a bubble on the surface in which case only the very top allowed light through to see anything and even then it was hard to get a good image or a lot of solution had to be used minimizing the concentration of microbeads which meant that there was no guarantee that the microscope would feature enough beads to make any results significant. The result of testing the electrodes with the SU-8 coating was that electrolysis was not eliminated. It did, however, appear to be minimized to a point where there was clear evidence of bead attraction and trapping at higher frequencies. The key to achieving DEP without having electrolysis interfere, was balancing voltage and frequency, higher frequencies allow for higher voltages. From these initial experiments, it was unclear whether it was purely manipulation of the function that minimized the effects of electrolysis or if the SU-8 layer was minimizing the effect. Having observed DEP, it was important to characterize the variables affecting the phenomenon and how best to manipulate them. Various patterns, frequency and

28

voltage manipulations as well as concentrations were tested to better understand DEP and the involvement of electrolysis in the process and those results are presented further on in this paper. Without conclusive evidence that the either the SU-8 or SOG helped in preventing electrolysis, a fourth potential coating substance, Teflon, was tested. Teflon was purchased in liquid form which allowed it to be applied by spin coating. The spinner allowed the user to control the thickness of the Teflon by using specific speeds. A couple of problems were encountered with Teflon that were namely due to the curing process as well as the fact that it was being spun onto a substrate that already had a structure on it. The defects caused during the heat curing process after depositing the Teflon were formed because spin coating traps little pockets of air that when heated expand to burst through the layer. This is called pinholing and the fabrication process was changed to prevent it. By preheating the substrate and then allowing it to cure at room temperature, the trapped air pockets did not expand but decreased in volume as the substrate cools and actually pulled the Teflon tight to the pattern.
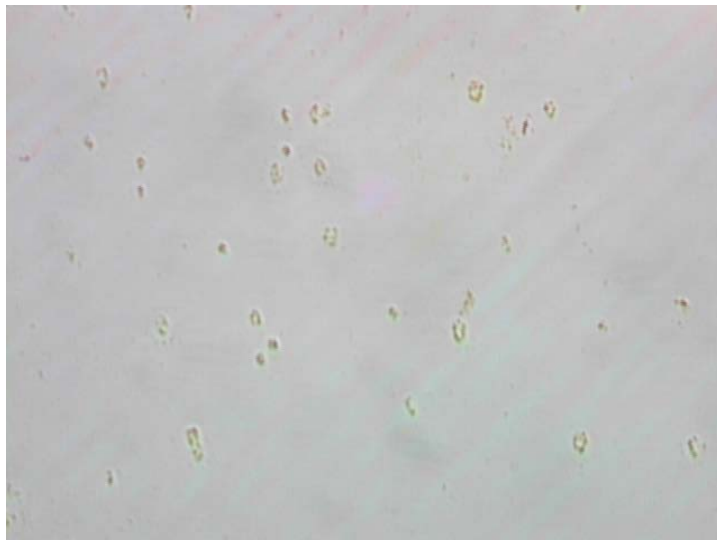
Figure 15. Pinholing in Teflon

The irregularities caused by the presence of the gold electrodes created a unique effects on the substrate surface. The wave pattern in Figure 15 was created when the Teflon was spun on and came in contact with the structures already present on the wafer in this case, the side of the electrode and created a ripple effect. This same principle applies to microscopic dust particles or any foreign object on the substrate prior to spin coating. That is why the cleaning process is so important to the uniformity of the Teflon layer. Allowing the spun on layer to settle prior to curing also helped prevent these irregularities as the Teflon was able to flow into the crevices.
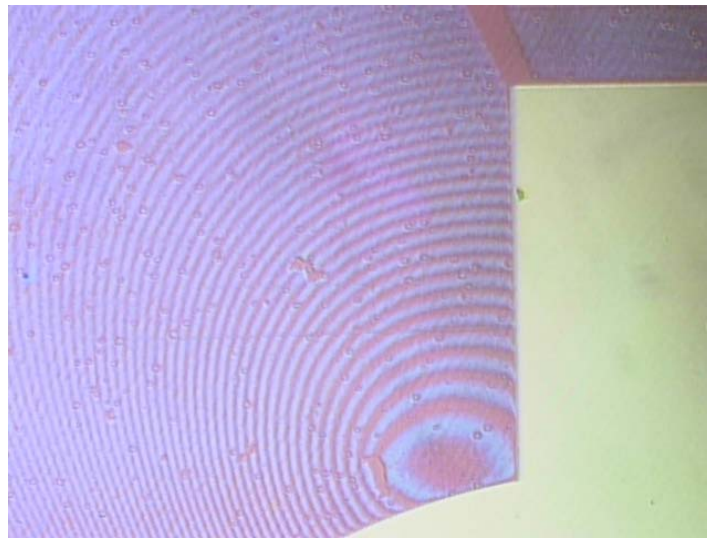
Figure 16. Irregularities caused by presence of electrodes during spin coating process

The many issues with the deposition of Teflon coupled with the fact that there had been no evidence of DEP particle manipulation during any of the experiments meant that it was not the solution the DEP electrodes required. A more suitable solution would be a layer that could truly be deposited uniformly regardless of the structures present on the substrate and that was capable of ultra thin layers without pinholing or other defects that could create fluid entry points

that could compromise the integrity of the layer. A material that fit both of these characteristics was Parylene.

Figure 17 Parylene deposition machine

Parylene is a polymer coating that is uniform and highly conformal as it deposits molecule by molecule on the surface in a vacuum chamber. The Parylene layer protects the electrodes from water with a pinhole free coating (down to the nanometer thickness level) that has excellent dielectric properties that cause less interference with DEP. The most beneficial aspect of the Parylene deposition system to us is the uniformity of the layer regardless of the sub-layer shape. For the dielectrophoretic electrodes, this means that the corners and edges which

have an increased trapping force are not coated with a larger layer than the top side of the electrodes. In other coating mechanisms (spin coating, dip coating...), the deposition process would cover these corners with a larger amount of substance.
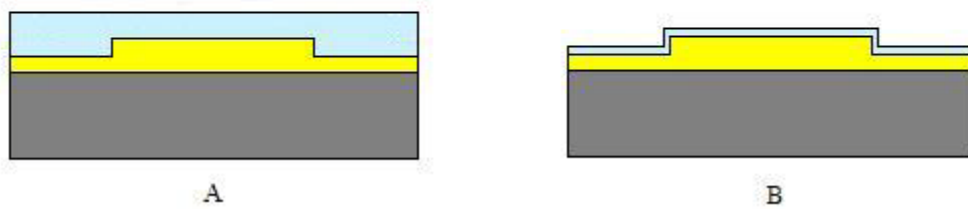
Figure 18 A) Regular means of layer deposition (spin coating, dip coating,…) B) Parylene deposition creates a uniform layer

There was a need to better understand our particular deposition system and the relation between the weight of Parylene dimer and the final layer thickness. The deposition thickness is dependent on two main factors. First there is a direct correlation between the amount of dimer used and the ultimate thickness, this is fairly straight forward in that the initial amount of material has an affect on the final amount of material. It was however essential to understand the relationship between the two. This relationship is based on temperature and vacuum pressure as they determine the rate of deposition but the main correlation is the surface volume. This is because Parylene deposits uniformly throughout the entire deposition chamber. Rather than attempting to account for all the surfaces present in the chamber it is easiest to run several different amounts of dimer and then measure the resulting thickness. The graph below shows the results. Each different weight class was averaged prior to graphing.
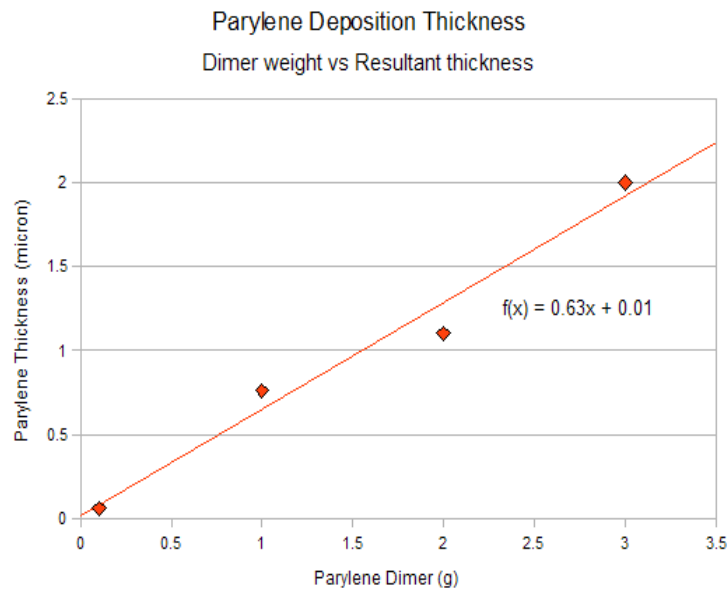
Figure 19. Graph of Parylene Deposition Thickness

The result is a linear relationship and will help in determining the amount of dimer to use for future depositions at desired thicknesses.

Initial Separator Prototype

The fabrication of the initial prototype involved three specific components: the container and inner cylinder, the motor to move the particles and dielectrophoretic electrodes. The focus of this section will be the basic structure consisting of the container and inner cylinder. The motor will come in to play in a later section and the electrodes have already been discussed on a basic level but will be of greater focus in other sections as they are redesigned and fabricated based on the container dimensions and experimental results. The basic design principle for a Taylor-Couette flow based particle separator was to have a cylindrical container with a rotating inner cylinder powered by a motor that pushes the particles to the outer wall. Once pushed to the

33

outer cylindrical boundary, the particles are held by DEP electrodes that have been attached to the cylinder. This principle was the guide to designing a functional prototype. The fact that the approach utilized individually cut electrodes to cover the inner surface of the outer cylinder meant that that surface would not be perfectly cylindrical but faceted. There were two options for the build of the design, fabricate every part of the prototype or buy a product that can be modified to fit the project needs. Rather than creating a faceted outer cylinder, the container was adapted from a purchased food processor. The container was already faceted to make the electrode attachment easier and a shaft for mounting the various removable blades made fabricating inner cylinders to work with the container easier. The theory with which this work was approached was that Taylor-Couette flow can be produced regardless of radius ratio. It would only require the inner cylinder to spin faster so as to transfer enough energy to the particles that they could move across the gap and create Taylor vortices. This premise facilitated the use of readily available materials to build the initial prototype with controlling factors to be applied through the motor.

Figure 20. Food Processor with top mounted motor

After purchasing the food processor, the first step was to design and fabricate the inner cylinder that would be used to produce flow within the container. There are two points of attachment for the inner cylinder in the food processor. The base container had a centered metal pin that kept the mixing tool centered. The second point was on the top attachment which features a three point gear that gets inserted into the mixing tool to transmit the motor rotation to the cylinder. These two points would be the basis of the reverse engineering of the food processor to design the inner cylinder. The difficulty in this process was the internal portions of the cylinder that had to be designed and fabricated. The design would not allow this part to be machined using a CNC machine due to the internal contours. Since this part could not be easily manufactured using traditional methods, Rapid Prototyping was selected instead. This technique allows the complex structures to be built by fabricating them layer by layer. After several

designs and discussions with the head of the RP lab at UCF, it was settled that two separate

pieces be manufactured for the top and bottom attachments and then fitted to a pre-made

cylinder. The advantage of this design choice and the fast turnaround time of Rapid Prototyping

was that several different cylinder diameters could be used and compared to determine optimal

flow conditions. With the aim of maximizing fluid volume during testing, three different PVC

pipes were chosen to be used for the cylinders. There diameters were 4.25 cm, 3.4 cm, and 2.15

cm which translated to aspect ratios of 0.385, 0.303, 0.195 respectively. These dimensions were

applied to the 3D CAD design and taken to the RP lab. All three pairs of adapter bits were made

on the same platform shortening fabrication time. Once the parts were finished, they were fitted

to the precut PVC pipes and bonded using a strong adhesive. The three different inner cylinders

were ready to be used along with the food processor to evaluate flow patterns.

Figure 21. Fabricated cylinders next to the top gear that transfers spin
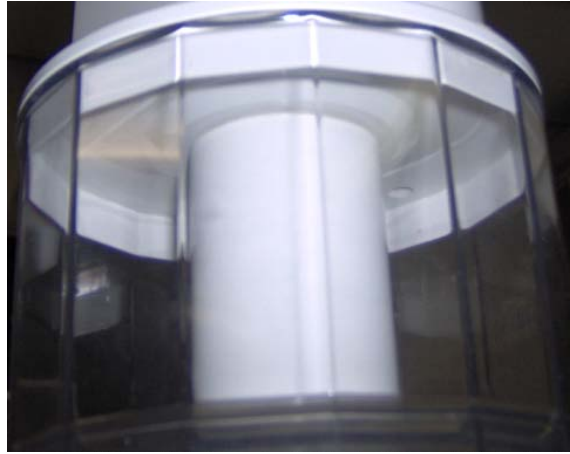
Figure 22. The largest cylinder fitted in the container

The food processor had three speeds which created unknown angular velocities and made

demonstrating fluid flow differences with each particular inner cylinder diameter rather difficult.

Tests were done on using each cylinder and dye to determine the affect inner cylinder radius has

on flow. The images are presented in Appendix C. They clearly show that an increase in inner

radius creates more turbulent flow at a given speed. This is an easily understood principle

because more surface area to move the fluid will push more fluid in the same instant as a smaller

radius. Also, and more important in determining the long term flow pattern, a smaller gap

between the two means the outward spinning fluid contacts the boundary faster. The fluid

bounces off the outer wall and pushes back towards the inner cylinder opposing the outward

motion. This creates the whirlpool effect around the inner cylinder and an increase in turbulence

in the gap as the radius of the inner cylinder increases. The images also show the three different

speeds for each cylinder size. These images show that an increase in speed will increase the

turbulence of the flow

<u>Microbead flow pattern experiments</u>

As tests were being performed on different electrode coatings to prevent electrolysis and

extend electrode life, experiments were performed to determine whether limiting the frequency

range could minimize electrolysis. The experiments were performed using the same setup in Fig

8 where the electrode was placed under the microscope, the probes coming from the function

generator were attached to the contact pads, a sample of microbead solution dropped onto the

electrode with a slide pressing down the drop to insure viewing through the microscope and the

attached CCD camera and the signal turned on. Having performed several tests using different

frequencies and voltages, there was a need to understand the relationship. The effects were

clearly visible but not defined. The procedure was to begin at a low frequency and increase the

voltage slowly to find the initial electrolyzing point and then increase the frequency and change

signal structure once the max frequency was tested.

Using the knowledge of coating-less DEP electrodes that can minimize electrolysis, the

same test setup was used to investigate DEP holding force as the fluid is suctioned away. The

process of trapping and removing the water while maintaining the electrical connection is shown

below. It was important to show that the particles will not just move away with the water but are

actually trapped by the electrodes.

1   *2*   *3*
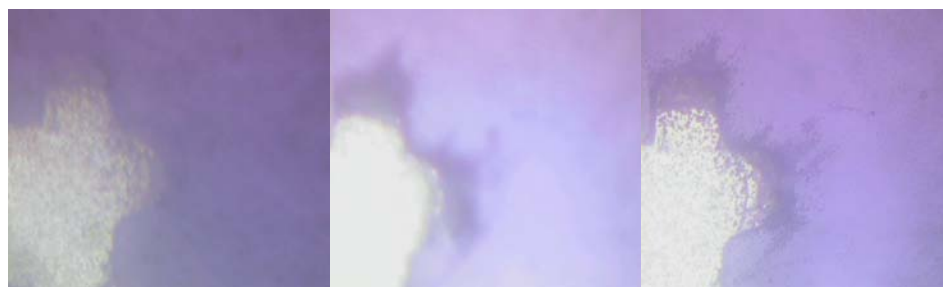
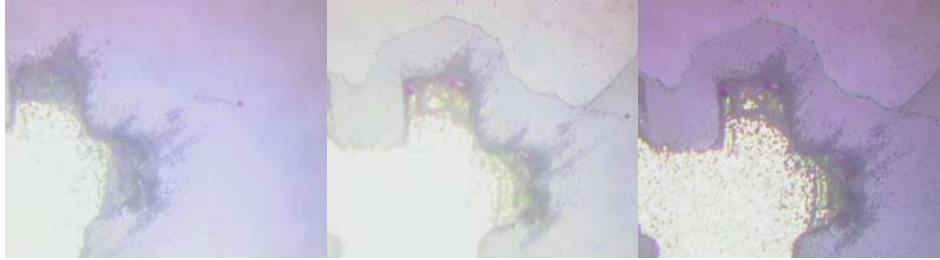*4*   *5*   *6*

Figure 23. Beads are held at the edges of electrodes as water is removed and voltage held constant

In the above pictures, a droplet of beads in water was placed on the electrodes to test the trapping effect and also the holding of beads as the water is removed using a syringe. In the first picture although blurry due to the curved surface of the droplet, the electrodes were clearly trapping beads from the solution. As the pictures move along and the water was removed, the electrodes become clearer and the extent of the trapping can be clearly seen. The beads were held on the electrode despite the suction power of the syringe acting upon them which was a good sign for the future of this project. The pictures also gave a glimpse of the electric field that is being produced by DEP as the beads are moving towards the electrodes in straight lines.

AC Electroosmosis

During the microbead experiments, the latex spheres were viewed gathering along the horizontal line of the electrodes, see Fig 31. The particles were not still, as if trapped, but the edges were moving as if pushed by the fluid towards the center of the electrodes. This is caused by a phenomenon called AC Electroosmosis (ACEO) which according to Gascoyne et al [14] consists of convection cells created by currents that start at the electrode edges and fall back in the electrode gaps.
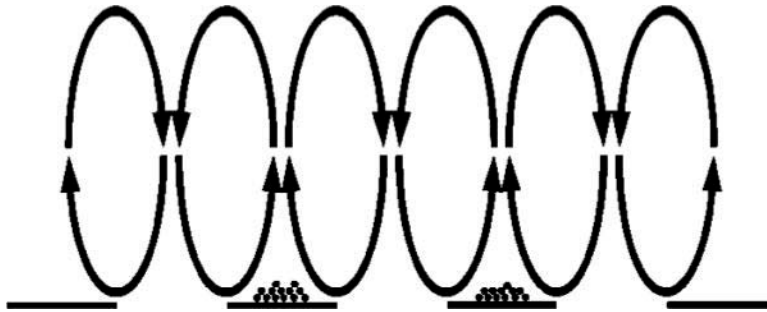
Figure 24 Convection cells created by ACEO at low frequencies [14]
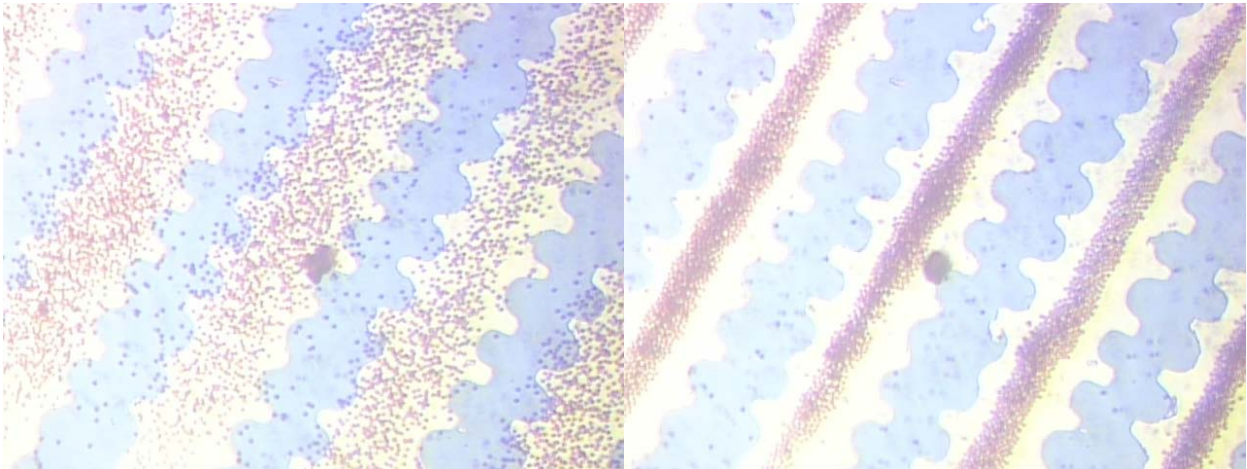
Figure 25 The AC electroosmosis effect before and after the signal was turned on. Difficult lift off process leaves electrode edges misshaped

AC Electroosmosis (ACEO) was explored as another means of particle control using electrodes. ACEO is a phenomenon where fluid motion is created by an AC signal which pushes the particles towards the center of electrodes by moving in and then up (shown in figure 24). This phenomenon was investigated using Coventor, modeling and simulation software that allowed micro scale analysis. Ultimately, it will only increase the ability of our electrodes to trap particles as the motion created by it will not be greater than the DEP attraction force of most particles and it will aid in keeping particles at the outer wall as long as possible. Experiments

40

were run to determine the effect increases in voltage, frequency, signal shape and particle size

have on, not just whether or not ACEO cells form but the power of the cells and how they effect

the particles.

Electrode redesign based on initial results

The microbead experiments were performed and the resulting information compiled.

Three factors that have an influence on the DEP force generated are frequency, voltage, and gap

size. These three factors were the focus of the redesign process because they are the controlling

variables. Frequency is not pertinent to the redesign because it can be adjusted throughout the

process but it should be said that high frequencies help prevent electrolysis and prevent electrode

damage by allowing higher voltages to be used thereby increasing holding power. Voltage can

also be adjusted at a later date but the higher the better as far as holding strength. Max voltage is

largely based on the frequency used because of the electrolytic factor. Both frequency and

voltage are tests that will need to be re-explored once the separator system is finalized and fluid

is moving across the electrodes at the required speed. It should be noted that the frequency and

voltage limits using just the Virtual Bench function generator were enough to demonstrate

particle holding and if greater frequencies and or voltages are needed for greater holding power,

an increase in both would do the job. With max voltage dependent on frequency which can be

manipulated and made different for each test, the only factor that has a direct effect on DEP force

in terms of from an initial deign stand point was gap size. The trend is the smaller the better

meaning the smaller the gap size the greater the holding force for two reasons. First, the smaller

structure require less power for a larger force which means that those electrodes would allow for

a greater range of frequency and voltage giving the device the flexibility it needs to adapt to different scenarios. Second, with less empty space on the wafer surface, there is a greater possibility of a particle encountering an electrode surface rather than a gap which could allow for less instant attraction and let the particle push past. The small gaps concentrate the field across the gap. The chosen gap size was 20 um because the 10 um was difficult to fabricate repeatedly. The lift off process was particularly difficult as removing an intricate design means more points of attachment that have to be broken. Also, there was always a section that was left undeveloped after lift off. Minimizing the potential for problems in fabrication is a good choice for this design approach especially since all gap sizes demonstrated dielectrophoretic properties and the function generator can always be increased if needed.

Figure 26. Mask for the fabrication of DEP electrode wafers

The most important factor was to have well formed electrodes without potential for shorts or missing portions of the electrodes. The power can be adjusted based on the frequency and voltage. The orientation of the electrodes also came into play, vertical electrode body or horizontal electrode body. Horizontal is the better choice because the desired flow pattern, Taylor Couette flow, creates vertical movement with the vortex being perpendicular to electrodes as the particles are pushed outward and then move up or down depending on the vortex direction. This allows for the particle to be pushed across multiple different attraction points when it reaches the outer wall. The faceted container and wafer holder provided us with the dimensions for the new electrode design. With the use of a coating layer to prevent electrolysis and other structural decaying issues, aluminum electrodes where made for cost effectiveness and then cut using the dicing saw. The first step will be to cut the electrodes using the dicing saw which allows for micro cut paths and at high speeds no wafer cracking. Initial tests were run using only a few wafers but once the entire process tested and confirmed. The required fifteen electrodes will be fabricated in the clean room using eight wafers and aluminum for the electrode body. After fabrication, they will follow the rest of the process that will be determined during the testing phase to produce a functional particle trapping electrode. This process will start with the cutting of the wafer to match the electrode size to the slots that have been created by the container. This will ensure a proper fit. Once cut to size, the electrodes will go through the wire bonding procedure which will allow power to be easily transmitted to the electrodes. This process will be made easier through the use of aluminum electrodes as the aluminum wire will bond much better to its surface. After wiring the electrodes, they will be cleaned to prevent any contaminating particles from being coated and permanently affixed to the electrode after the

coating process. By wiring first then coating, there is no need to have to strip the coating from the bonding pads to allow a better wire connection. Once cleaned using an Acetone, Methanol and DI water bath and ultrasonic tools, the wafer will be coated using the Parylene deposition system and will require covering the contact pads if pre-wire bonding or covering the wire to prevent the uniform deposition to include the wire. Parylene is a thin film that is biocompatible and will allow us to produce the thinnest most uniform coating possible that will not interfere with the electrodes. The uniformity is created because Parylene is applied as a monomer after being vaporized Vapor and not spun on. Once the wafers were complete, the full experiments began.

<u>Electrode holder design</u>

While the flow and electrode experiments were being conducted, another part of the project took shape, the electrode holder. The idea behind the holder was to create slots for the electrodes that follow the contour of the outer wall allowing the wafers to slide down and be held in place. The design was based on the dimensions of the container and the electrodes on the mask. After numerous design changes, the electrode holder was built using the same Rapid Prototyping technology used for the inner cylinders. The final design featured a minimal amount of material to keep the wafers held in place but without blocking the DEP electrodes from the fluid sample. The inner and outer rims worked to sandwich the wafer together and held them in place. Holes were drilled to allow set screws to better attach the two rims together. A section of the top of the inner rim was removed to allow the electrodes to slide into place without interfering with the wire bonded portion of the electrodes.
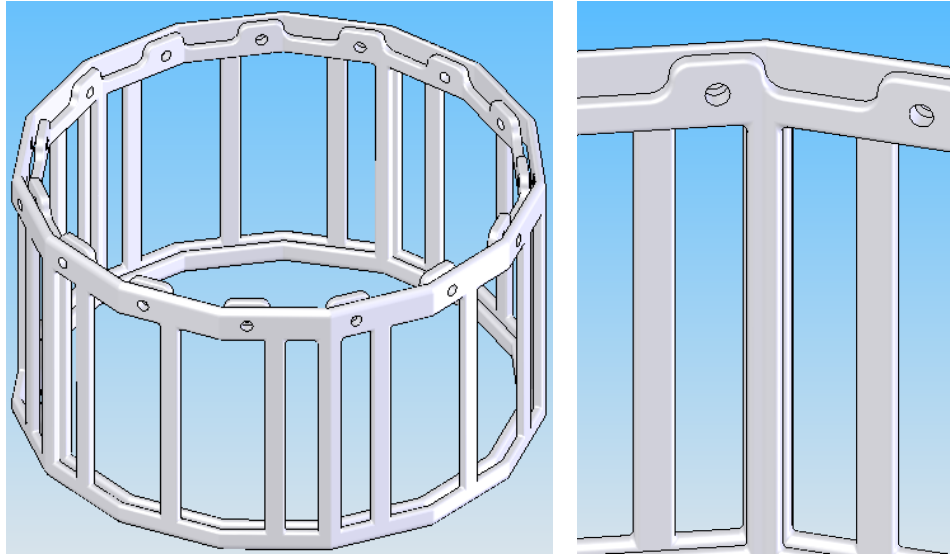
Figure 27. Solidworks 3D model of slotted wafer holder for Rapid Prototyping

Figure 28. Rapid Prototype for slotted wafer holder

<u>Motor control</u>

A motor and microcontroller combination was purchased to provide greater speed control over the inner cylinder as well as allowing for lower speeds than the original motor and a variable voltage supply. The first step was to understand the software that controlled the

microcontroller in order to translate the theoretical speed to the motor speed. The program

operated by first creating a reference speed that the motor controller attempted to match. The

reference speed is generated in steps not RPMs which led to our investigation into determining

the conversion rate between steps and RPMs. The first test was done using a stop watch and

manually timing the spin rate of a propeller attached to the motor. At 1 step, the measured speed

was 30 RPM. This rate was able to be timed at 2 steps but higher step rates were impossible

with the propeller seemingly forming a solid disk. While this rate was true for the minimum step

rates, it was not sure that the speed was uniform as it increased. To ascertain whether the speed

was linear, an experimental setup was devised using a photo-resistor, laser and an oscilloscope.

The photo-resistor registered changes in frequency on the oscilloscope depending on whether the

laser was being blocked by the propeller blade or was hitting the resistor and measuring the

frequency of the laser. The wave profile created on the oscilloscope was then used to calculate
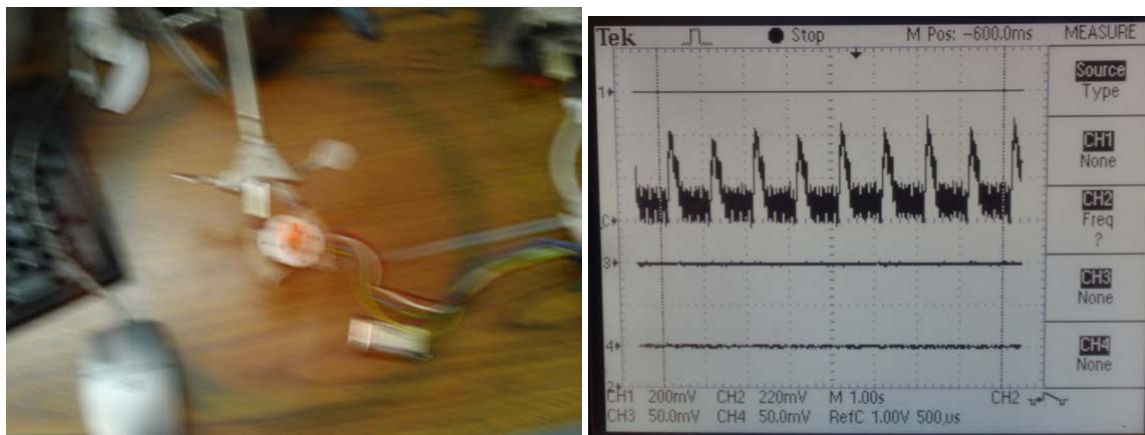
the RPMs at higher step rates.

Figure 29. Setup for calculating conversion between software motor speed and actual RPM. a) propeller attached to motor spinning. b) frequency of propeller as determined by laser and photo-resistor

46

The resulting speed conversion factor was 30 RPMs per step and linear as it increased as shown graphically in the figure below.
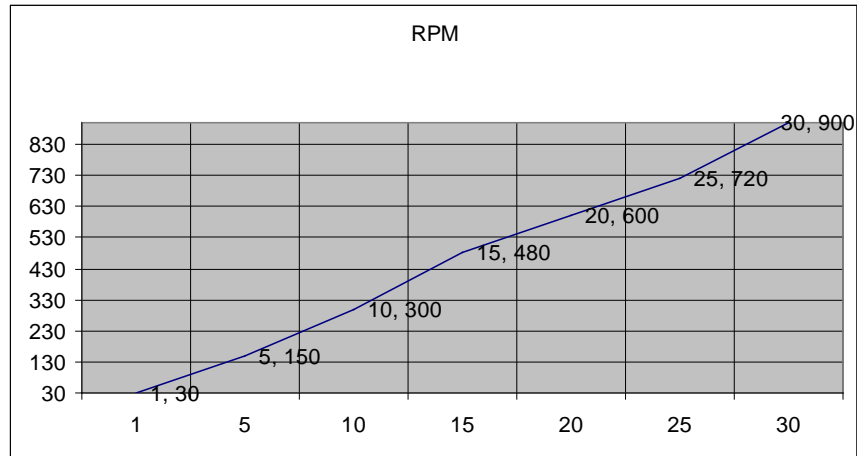

Figure 30. Graph of RPMs per step

Once the conversion rate was figured out, tests were performed using water and larger particles to determine if the specific RPMs would carry over during experiments with cylinder loads applying a resistance to the motor. The figure is a snapshot from a video of one of those experiments.
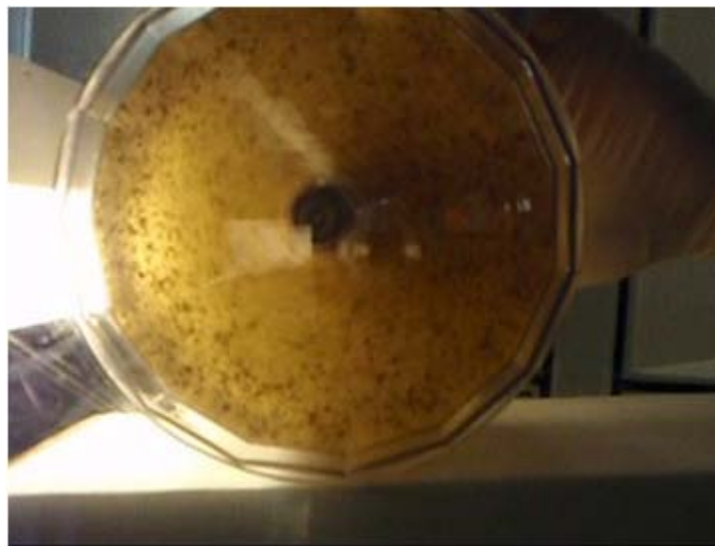

Figure 31. Larger particles being pushed towards the outer wall

It shows the particles being pushed outward towards the cylinder wall. All three of the cylinders demonstrated the ability to push particles outward. The main difference in that process is the time it takes a particle to traverse the liquid from the inner cylinder to the outer. The smallest cylinder would however allow for the greatest volume of liquid. The main concern was the transfer of speeds from the motor to the inner cylinder. Even from these early tests, it became apparent that the desired speeds were lower and the motor did not produce enough torque to create a constant spin speed. There were two ways to solve this problem. The first and most obvious was to purchase a more powerful motor but this would be difficult to mesh with the controller board and would most likely lead to a burnout. The second potential solution was to create a housing unit that would stabilize all the components of the experimental setup: the container, the lid with the gears, motor and controller board. This was the idea pursued with the thought being that creating a perfectly aligned motor and gear would run into less resistance and run much smoother and more efficient. The design basis was to have a location to lock in the container and lid and allow them to be tightened together to eliminate any unnecessary vibrations or misalignments. Another platform fit on top of this and was aligned using pillars to both the base and the middle platforms creating the desired verticality of the motor link. On this top platform, a hole was drilled for the motor and it was tightened down for testing using a bracket.
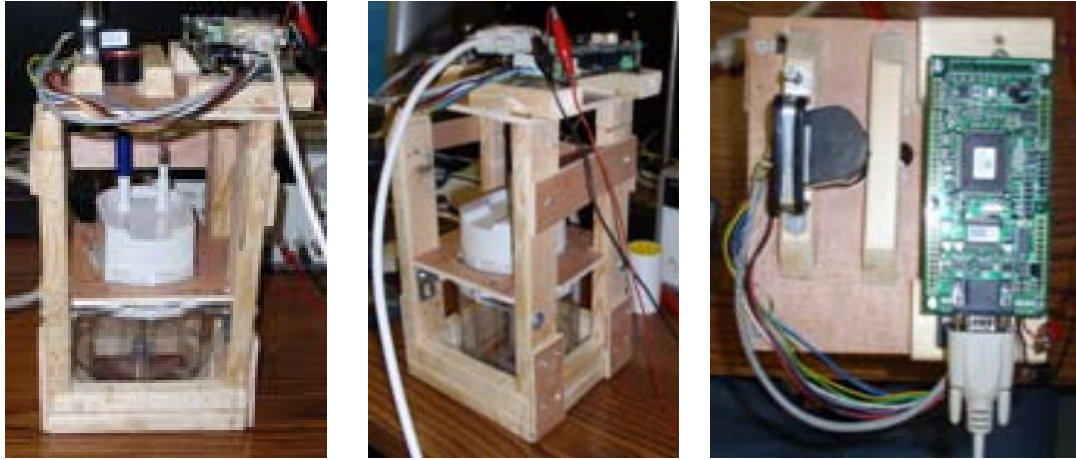
Figure 32. Experimental apparatus to help increase stability during test runs

After building structures to contain and align the motor and the shaft to allow for uniform speed without resistance causing the motor to accelerate or decelerate constantly, a powerful enough motor to maintain a set RPM was acquired, the Fisher Scientific Steadystir. This motor was attached to a standard lab standard and the container placed beneath it. The gearing which had been taken apart allowed for the cylinder adapter to be inserted into the Steadystir and held much like a drill press. The adapter and motor were then lowered to the cylinder and eliminated the need for holders and motor control boards and power supplies. The Steadystir did not replace the motor in terms of final system design because the minimum speed was 50 RPM and the control board allows for a more accurate change between speeds during tests for multiple run experiments. It was, however, the means of characterizing fluid flow visually at specific RPMs and with quickly interchangeable cylinders.
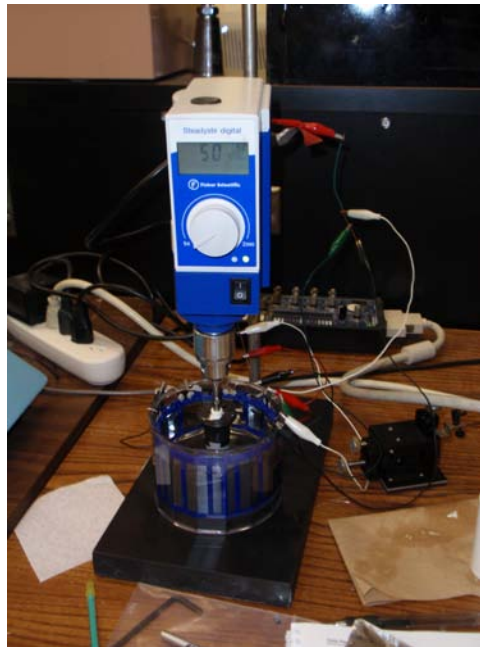
Figure 33 Fisher Scientific motor

<div align="center">Taylor Couette Flow Experiments</div>

The dielectrophoretic electrodes are crucial in trapping the particles for characterization but the particles must first come within range of the electric field generated by the electrodes. Taylor Couette flow is a flow pattern that continuously moves particles between the cylinders with the slowest point being at the outer cylinder wall due to azimuthal velocity loss. The pattern is well understood and experimented with for small gap and large aspect ratio systems where the vortex can much more readily be formed. This work, as has been stated, requires a large volume of fluid to be characterized in order to make any kind of statistical proclamations about the safety of the water source. The container and cylinders for the system have been fabricated and assembled. The main issue that needs to be tested and evaluated is the idea that Taylor vortices will be formed in this large gap, small aspect ratio system should the critical

Taylor number be surpassed. This involved an increase in the speed of the inner cylinder to compensate for the increase in gap size. The first step in the flow experiments was determining the critical Taylor number needed to be exceeded for each cylinder. The critical Taylor number calculation was done by graphing known critical Taylor number data for different radius ratios from Koschmieder's [40] book, Benard cells and Taylor Vortices. The data was extrapolated out using a power trend line to determine the critical Taylor numbers for each radius ratio in the setup. Once these values were known, the speed was derived from the Reynolds number and the critical speed for each cylinder to transition into Taylor Couette flow were 69RPM for the small cylinder, 47RPM for the medium cylinder and 41RPM for the large cylinder. This data was graphed along with angular velocities for each cylinder size. Using the most stable motor available, the Fisher Scientific Steadystir, food dye as well as dyed micro particles were dropped into a fluid while in motion to examine the fluid flow. The flow was recorded and analyzed later with the goal of identifying repetitive patterns. If a flow pattern can not be characterized, it is independent of controlling variables and in the turbulent realm.
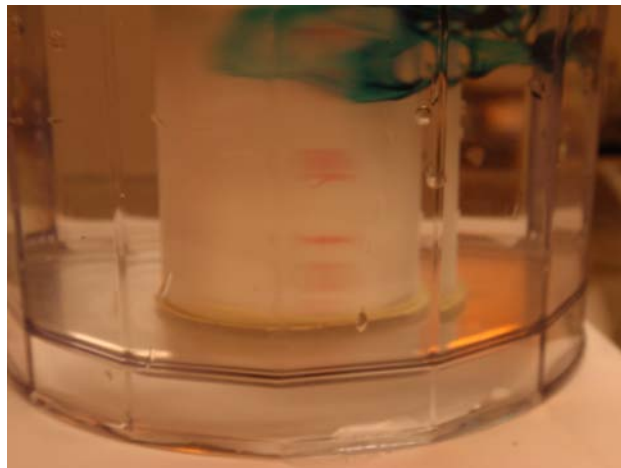

Figure 34 Vortex formation as dye is set in motion by inner cylinder angular velocity
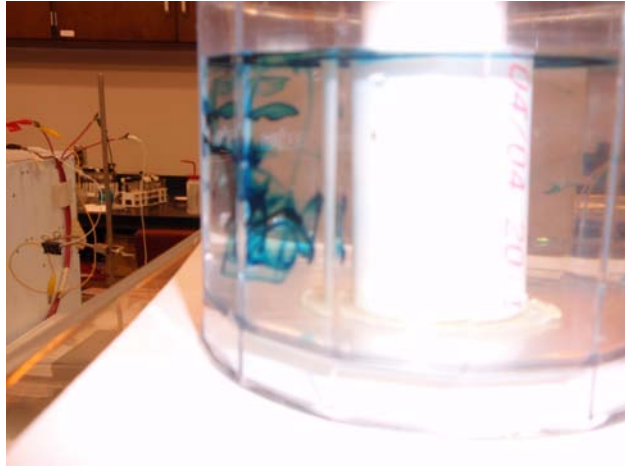
Figure 35 Chaotic vortices as dye spun off from inner cylinder flows through gap and approaches wall

Figure 36 Chaotic Circular Couette flow

After demonstrating that the flow pattern works to push the dyed particles, experiments were done to determine the speed at which the flow pattern pushes the particles to the outer wall. For these experiments, the principle was the same; drop dye in and analyze the trajectory. The major difference was the angle of the camera. For these tests, the camera was placed beneath the container so as to watch the particles get pushed to the outer wall.

Figure 37 Bottom view of dye drop experiment

The data generated although highly dependent on human repeatability allowed for a trend to be developed and the project to move forward. The idea behind these tests is to determine the best cylinder size for the full system tests. A balance between time to wall and force upon particle once it reached the outer wall and the electrode.

Secondary container rough prototyping

After experimenting with the RP electrode holder, it was determined that the holding force while great for a system that uses a drain and does not need to slide the wafers in and out during testing. For those initial tests, the easiest means of determining whether particles were being trapped was to run the system, create the outward push, and while maintaining the DEP process, turn off the motor, slide the electrode out and move it to the microscope and examine it. The wafers could not be removed easily from the holder and maintaining electrical contact proved impossible. To solve this experimental issue, a second rough prototype was fabricated using simple materials that allowed the electrodes to be removed and placed under a microscope without interrupting the signal from the function generator. The experimental prototype was made of PVC pipe and pipe coverings. The PVC was shaped using a drill press and dremmel to

shape the wafer slots that would provide the side to side stability for the wafers during fluid flow.

Pipe coverings were used to cap the bottom and create a pocket for the wafer to sit in keeping the

electrodes in place during the system run. A second pipe cover was used as a top side holder

while still allowing access for the inner cylinder as well as contact with the electrode pads.
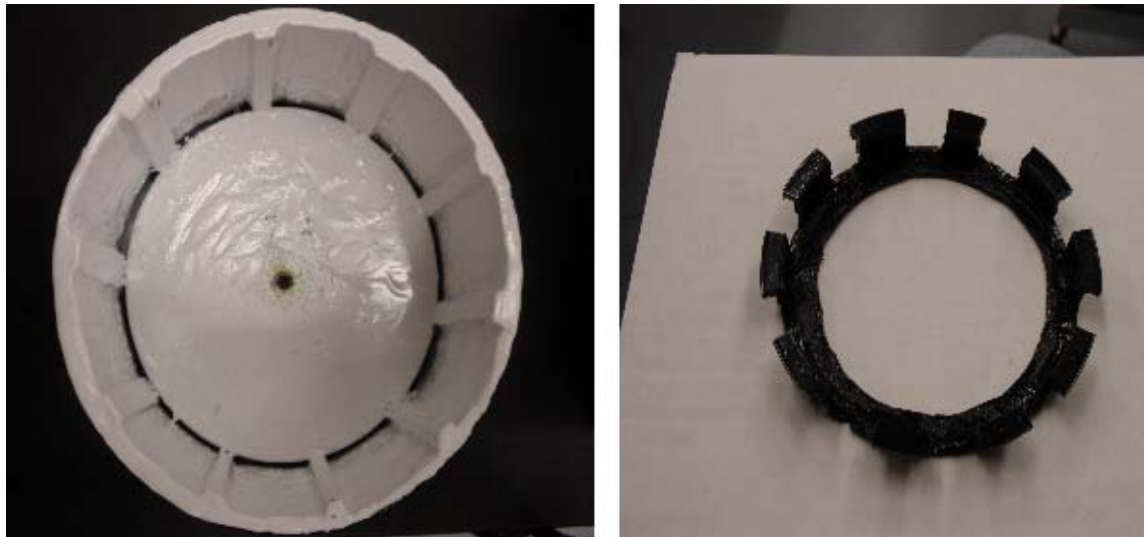

Figure 38. Slotted cylinder and cap which holds wafers in place.

This design created a simple structure that would allow the electrodes to be held throughout the

particle separation as well as allow for easy removal once complete. The extraction of the

electrodes without altering the trapped particles on their surfaces was essential to the
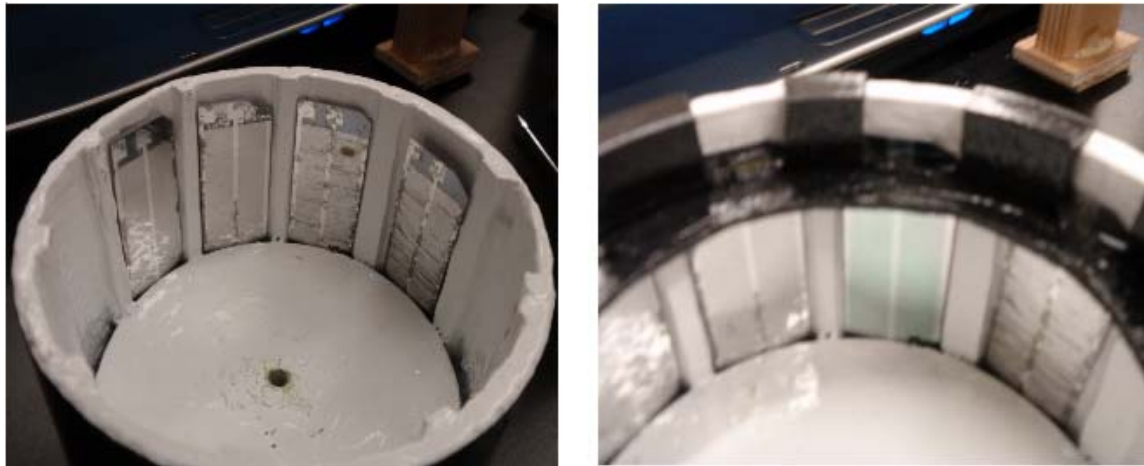
experimental process.

Figure 39. Wafer holder with slotted DEP electrodes in place.

Figure 35 shows how easily the wafers fit into the slots and the top covering prevents the

DEP electrodes from slipping out of the slots during fluid motion and subsequent draining. The

slotted cover allows access to the contact pads. Another benefit of this experimental prototype

was it created a better alignment between the motor shaft and the inner cylinder by simplifying

the setup from the previous multileveled device that used a prior piece of engineering which was

unnecessary and created a need to adapt the design at both ends of this piece of equipment. The

top connected the motor shaft to the gears already present using a piece that had to be fabricated.

Those gears transferred the power of the movement to the fabricated cylinder through a second

point that had to be made to fit the system. By eliminating the two adapters and the gearing three

points of potential increased resistance were removed from the link that connects the motor shaft

to the cylinder. The motor shaft was inserted directly into the inner cylinder using a press fit

which allowed the motor to run smoother and fluid motion was more dependent on the initial

input. The motor was firmly attached to the platform to minimize vibrations from the motor.

The need to create a point of attachment at the base to maintain verticality was a more complex

issue. The first idea was to create a second shaft that the cylinder spun freely around but that resulted in rubbing at the base when the motor reached high speeds and the cylinder started wobbling a bit. The solution was to fix a shaft to the cylinder and have it spin within a point at the base. The idea behind it was to have a sharp point spinning within a specific point at the center of the base. The task was accomplished using nails attached to the cylinders at their centers and attaching an enclosed nut with a domed interior that matched up with the nail so that it spun within the nut with minimal rubbing and resistance.
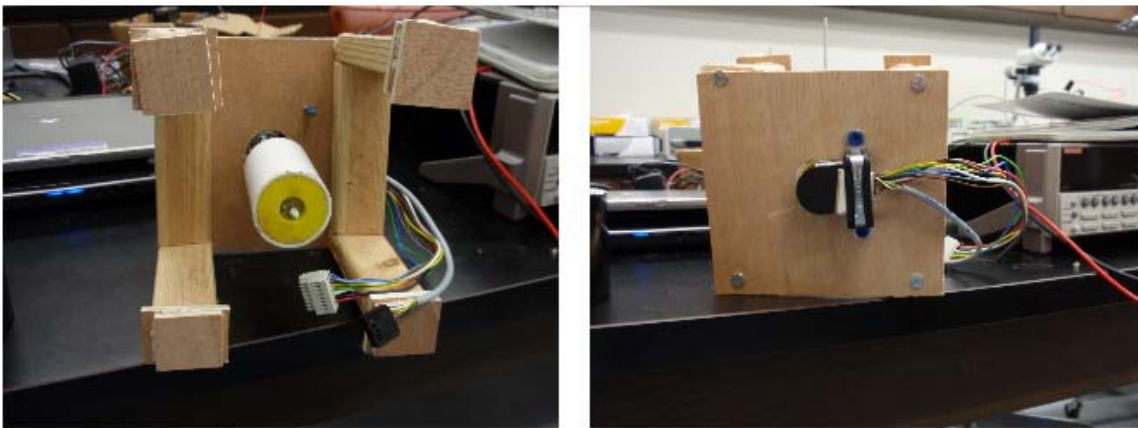

Figure 40. The pointed base of the cylinder and the motor mount work to maintain alignment

Full system test

Despite the lack of formation of Taylor vortices, the system still created an outward push on the particles based on Circular Couette flow. This evidence of particle motion although not using the expected flow pattern still would help to test the entire system in terms of proof of concept for the DEP electrode lined container trapping particles. The experimental prototype along with the results from the experiments on motor speed, function frequency, shape and amplitude as well as voltage for the motor control board, a full system test was setup and run.

The large inner cylinder was used to minimize the gap distance being crossed by the particles. The fluid flow generated above the critical Taylor number (at 41RPM for large cylinder) appears to be vortical in nature by the inner cylinder. At certain speeds, the high pressure on the particle as it is being pushed outward by the angular velocity of the inner cylinder, coupled with the low pressure region produced as the fluid and particles are pushed away from the center axis results in the formation of vortices. The gap dimensions make the formation of sustained Taylor Couette vortices impossible. The goal then is to employ circular Couette flow to push out the particles. When using the large cylinder, it was necessary to use the motor and motor control board to keep the speed of the inner cylinder below 41 RPM.
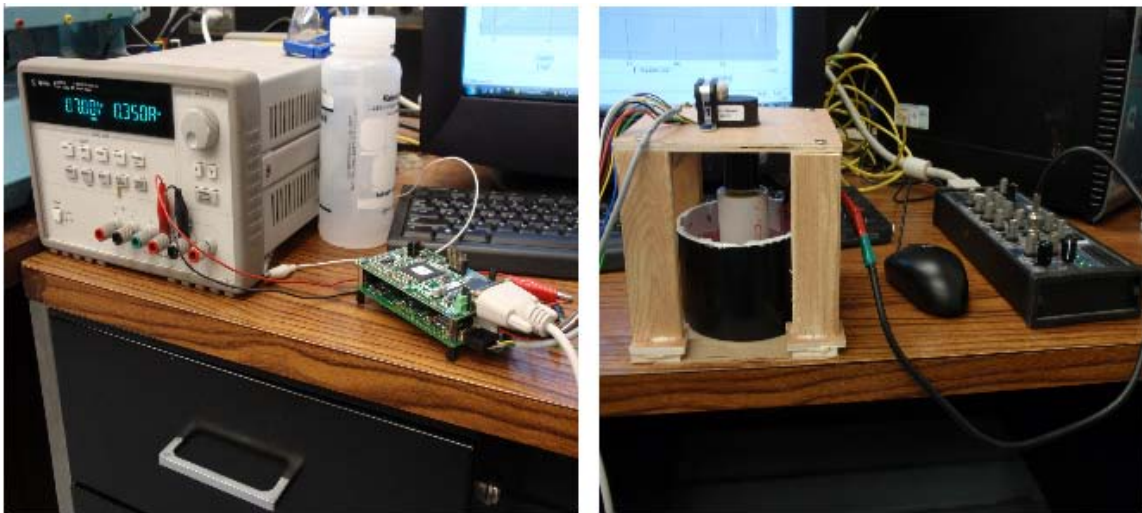

Figure 41. The full system test setup

The full system test required several different operations to be running simultaneously. There had to be a power supply for the motor control board which was also hooked up to the computer using an RS232-USB cable to allow the motor control reference for the speed to communicate with the board which was linked with the motor using two different sets of cables.

One set for the communication of instructions and transmitting power necessary and the other set for the feedback loop so that the motor operation could do the inverse communication path and be graphically reproduced after the run. The motor speed was controlled using the software provided by Technosoft and creating a reference profile for motor speed in terms of steps per millisecond. The board was run off of 10V a value that allows us to start the motor at lower speeds but does not endanger the board or motor. The voltage will stay the same throughout while the current fluctuates based on the resistance the motor encounters. The power supply current max is 1A which is a great feature in that it will not burn out the motor or board by going over that value when too much resistance is encountered. When running at low step rates the current jumped to 1A and would not start but giving the inner cylinder an initial spin allowed the motor to get up to speed and the current dropped to 0.75 and fluctuated at that point throughout the run. The reason for the push start was that it requires more power to start an object moving from a stationary position than it does to keep it in motion due to momentum. The next part of the full setup was the dielectrophoretic electrodes that were hooked up to the function generator which was operating off of the computer using LabView's Signal Express. For these rudimentary tests, the signal from the function generator was clipped directly to the contact pads instead of wiring them to insure contact was maintained during the transfer from container to microscope. The function generated and used for the runs was taken from our previous study into the effect each parameter had on the strength of DEP holding. From the findings we decided to use a 10 kHz frequency at the maximum amplitude for our function generator of 10V and a square wave signal was also found to be the most beneficial to holding force. The function

generator was left running throughout the process this time from run to transfer to under the microscope.
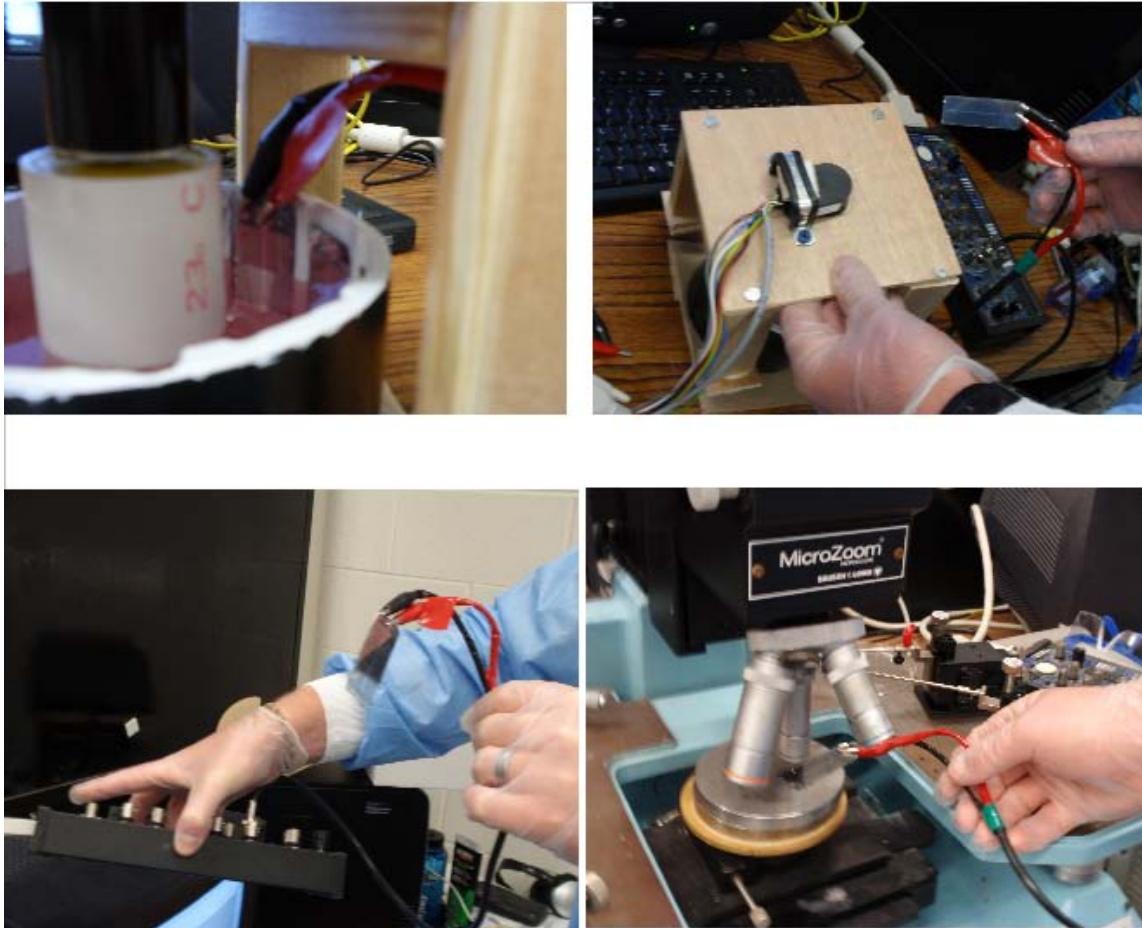

Figure 42. Transferring the slotted DEP wafers from the cylinder wall to the microscope for post test run analysis

Figure 42 shows the attachment of the function generator using the clips as well as the removal and transfer to the microscope stage for inspection. The ability to keep the electrode engaged with the function generator at this point in the research was a huge benefit as it maximized the electrodes ability to trap particles throughout the run as well as under the microscope.

CHAPTER FOUR: RESULTS

Microbead experiments

Frequency dependent electrolysis

Electrolysis can be a chain reaction and after the metal becomes weakened the reaction can only be stopped by removing the signal. The best solution to minimize the effect of uncoated, direct contact electrodes is to determine the variables that initiate the reaction and delay the process. The graph below shows the relationship between frequency and electrolysis for all three signals used (sine, square, triangle).
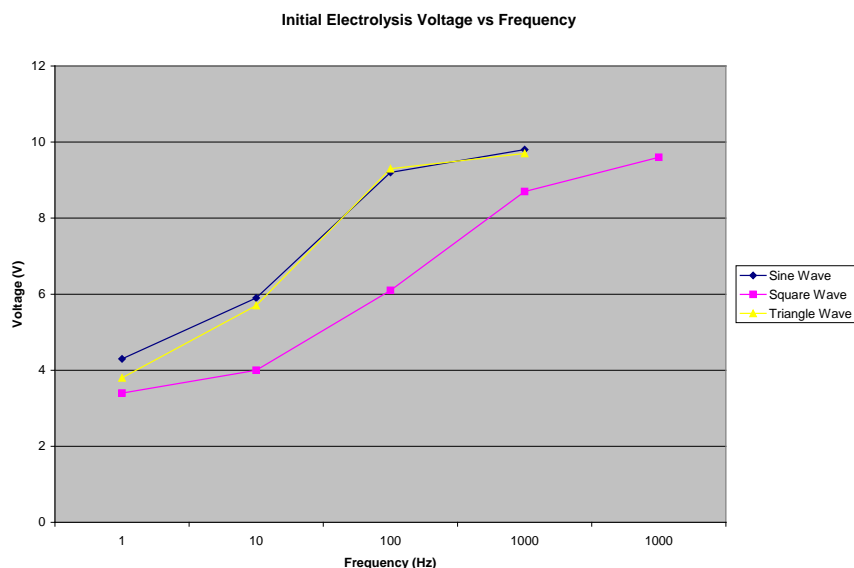

Figure 43. Graph of Initial Electrolysis. Voltage vs Frequency

When analyzing the effect the change in frequency had on electrolysis, there was a definitive trend. The above graph shows that as frequency increases, the maximum voltage the electrodes can take before electrolyzing increases. For frequencies above 1 kHz for both sine

and triangle waves and 10 kHz for the square wave, data is not available as the initializing

voltage exceeds the max voltage from the National Instruments Virtual Bench Function

Generator. This is not to say that electrolysis does not occur at these frequencies at high

voltages, it is possible that electrolysis beyond a certain frequency becomes impossible due to

the rapid changing signal. The graph also shows the differences in using different wave

functions, sine, square and triangle. The sine and triangle waves are very similar in their limits

for each frequency while the square wave exhibits electrolysis at lower voltages. Based on

observations of the structure under the microscope, it is clear that electrolysis occurred more

readily during drastic changes in voltage such as an increase in voltage by an entire unit as

opposed to 0.1 volts. This is the reason that the square wave electrolyses much more readily

because the wave structure is based on instant jumps in the signal as opposed to the gradual

increase or decrease exhibited by both the sine and the triangle wave. This electrolytic response

to sudden and large changes in voltage was observed both while increasing the voltage and

decreasing the voltage. This data although indicative of the general trends is by no means error

free. The error for this data was due to the method of collecting the data. It was compiled

visually by increasing the voltage of the function generator by small increments for each

frequency while observing a randomly chosen area on the pattern and once a voltage was

reached where electrolysis began to occur a data point was noted and the next frequency begun.

The error with this process was that the entire pattern can not be monitored and that electrolysis

begins randomly due to defects in the electrode patterns. There is no uniformity to electrolysis

and therefore attempting to characterize it using specific points can be difficult and inaccurate.

The general trend is that the higher the frequency the higher the voltage limit to achieve

electrolysis as well as the fact that once that voltage is reached and frequency is not changed any increase in voltage will lead to a more violent and rapid electrolytic reaction. It should be noted that although the occurrence of electrolysis can negate any trapping that happens, it is avoidable by having a specific operating procedure from the start of the experiment. All trapping mechanisms were operated at 100 Hz and at varied temperatures but all were able to reach 10 V without being affected by electrolysis; a triangle wave signal was used for all three because it showed signs of minimizing electrolysis. The conclusions we were able to achieve from these experiments propelled the project forward by helping to contain the issue electrolysis poses to the system. The strongest form of containment appears to be manipulating the frequency and voltage. It is important that both remain relatively stable. Frequency should be selected previously based on the medium being analyzed and geometry used. The voltage should be selected to minimize power consumption while still providing the necessary force to trap beads. Also, the smaller the gap size used for the electrodes, the less power is necessary to produce the same DEP force which means the more particles can be trapped and held with greater strength with less risk of electrolysis. The minimizing of electrolysis through frequency and variable selection and without the use of coatings meant adding another layer of control over the process. During some of the experiments, it appeared that some of the beads remain trapped on the teeth even after the removal of the voltage. It is important that they can be easily removed with a wash so that they can be analyzed by the microfluidic chamber. Ultimately, the best means of eliminating or minimizing electrolysis for the purposes of this project is the design that allows for trapping and releasing of particles repeatedly. Different situations and different fluid samples may call for frequency control, coatings or a combination of both. Having an understanding of

the relationship between the variables allows for the experiment/sample to have specific settings to aid in the separation process.

Dielectrophoretic Trapping

Over the course of manipulating the signal function while monitoring the trapping mechanism for changes in attraction, repulsion or electrolysis, several trends became apparent. As stated previously, low frequency greatly increases electrolytic reactivity and increases in voltage cause instantaneous breakdown of the electrodes. This effect changes at high frequencies which allow less time for the molecules to relax and react while the signal is changing. The larger the voltage of the signal, the greater the DEP force as it strengthens the electric field between the opposing electrodes. The smaller the gap between the electrodes the greater capacity for DEP trapping as less signal strength is necessary to produce and maintain the field. Several examples are shown below showing electrodes in various states of DEP.
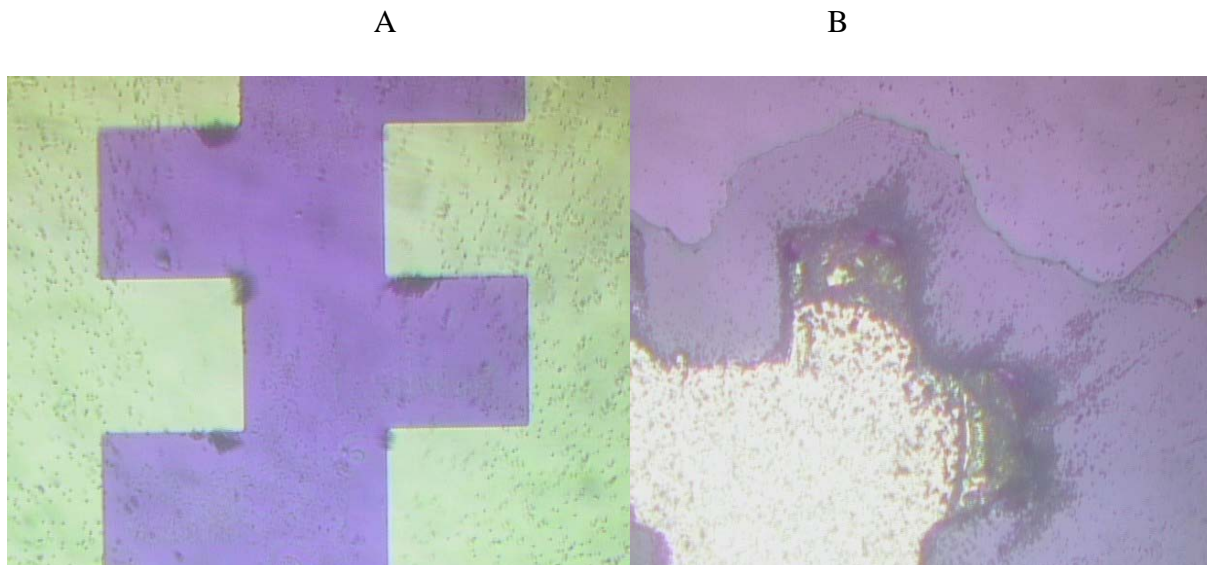
A   B

Figure 44. Positive Dielectrophoresis:

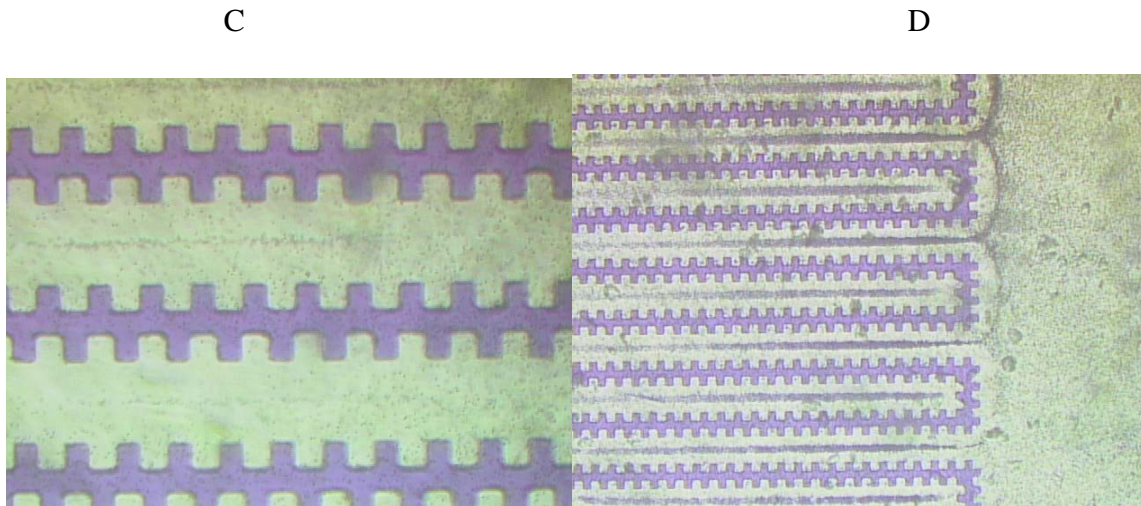C   D

Figure 45. Both Positive DEP and AC electroosmosis: C) The beginning of both phenomenon high magnification D) After some time has passed smallest magnification

By comparing figures A, B, E, F, and G with the other figures, we can understand differences between gap sizes and whether a change in dimensions truly will affect the number of particles trapped as theorized from the equation. From these images, it is clear that the 20 um electrodes in C, D, H and I are trapping more electrodes because they are using the entire electrode surface whereas the 100um electrodes in the other patterns can only trap particles that are near to the corners or edges in a short period of time. This whole pattern trapping is of course due to the effect of AC electroosmosis which creates convection cells pushing the particles towards the center of the electrodes. While not trapped, the particles are maintained within range of the electrode surface which could be advantageous to this project. Eventually, if left to work all particles within a certain height of the pattern would be trapped due to the electric field forces pushing towards the points of trapping.
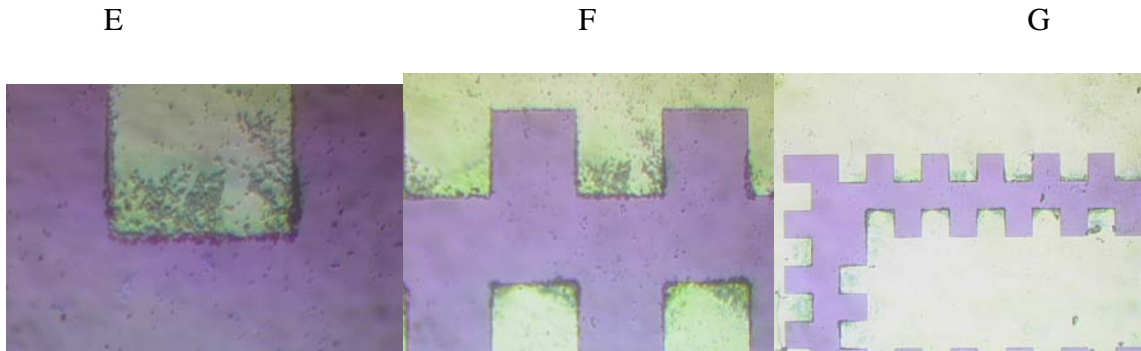
Figure 46. Positive Dielectrophoresis: E, F, G) Same image at decreasing orders of magnitude
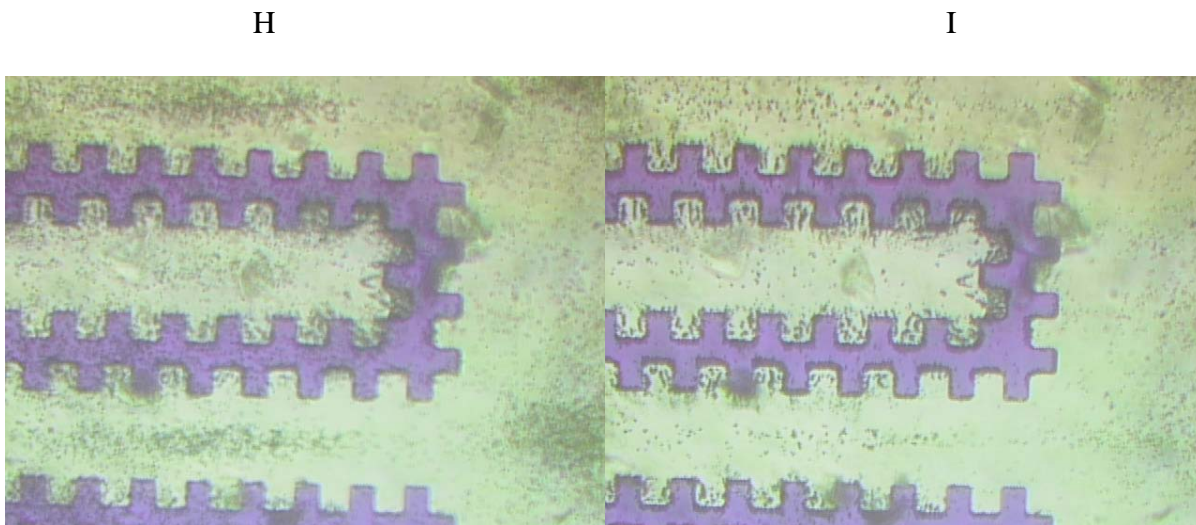
Figure 47. Positive DEP: H) Before voltage I) After voltage applied

<u>Motor control results and experimental yields</u>

The images below show a sequence of dye being introduced into the prototype during normal flow. The pictures give an indication to the type of flow being experienced but the dye becomes immersed in the water too readily and it is difficult to really characterize the flow using this material. The prototype clearly demonstrated the ability to distribute particles. The key is determining the right components of the flow for that particular inner cylinder radius and being

able to manipulate the motor with enough control to make accurately control the flow of particles.
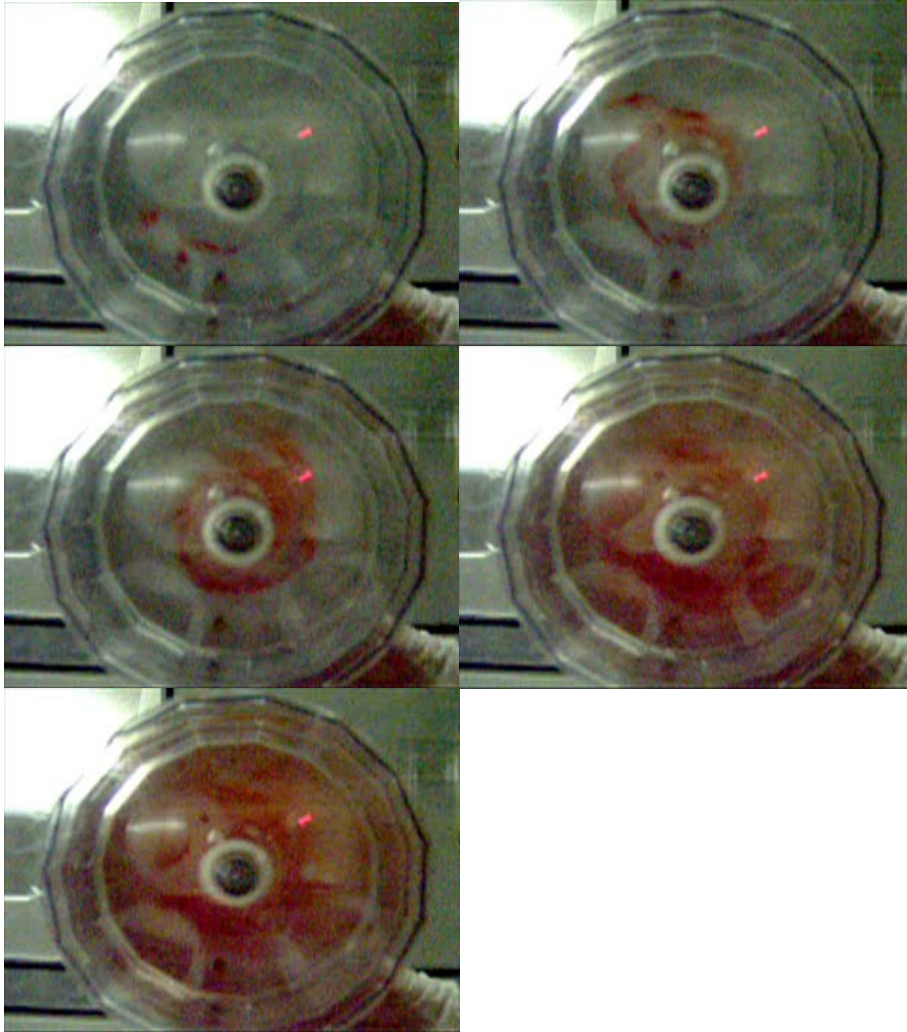

Figure 48. Sequential dispersal of dye (small particles) in a Taylor Couette System

<u>ACEO simulation vs. experimental</u>

The following graphs and images help to understand the effect ACEO has on the microbeads. The first set of images show the modeled results with the electric field vectors pointing in and up towards the center of the electrode beams along with a picture of our

electrodes using a 1 kHz 5V function. The image taken with the microscope camera shows the same bead movement towards the center of the electrodes as well as beads that have not yet reached there indicating their paths.
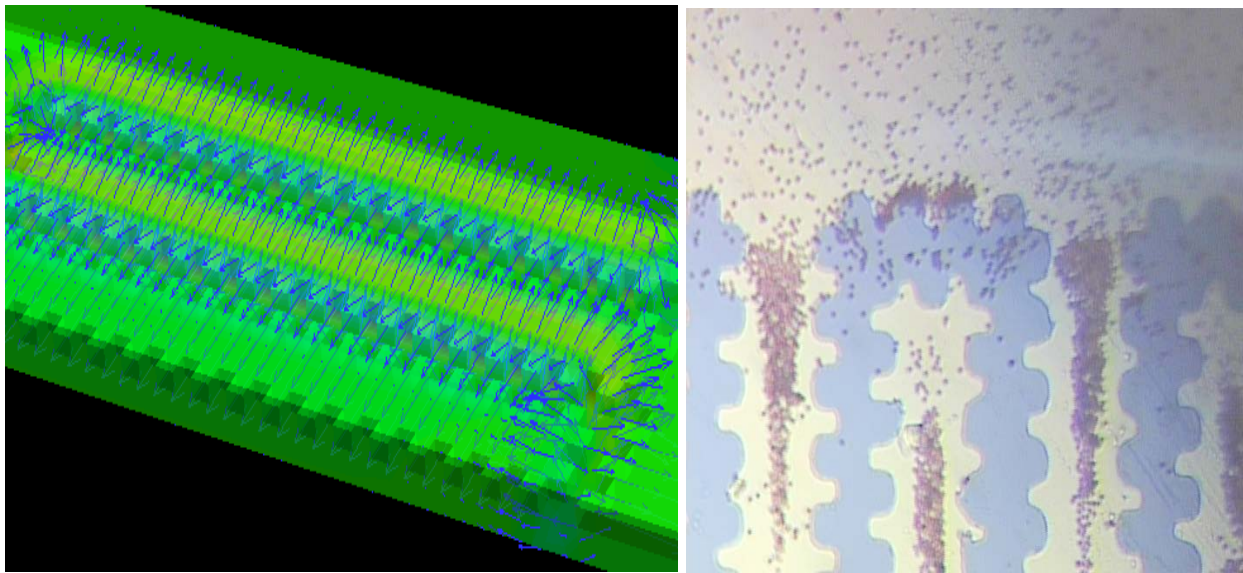

Figure 49. AC electroosmosis. A simulated electrode with vectors indicating particle motion and an experimental result

The next group of images contains the graph equivalent of the images that follow it. It helps us understand the trends of ACEO and how it ultimately affects our work. All images are taken at the 1 minute point of the experiment. This point was chosen to attempt to minimize the time dependent factor of AC electroosmosis which will be explored later. There are three trends that can be taken from this graph. First, the 10V image at each frequency interval generates greater particle holding that its 5V counterpart. This implies that the higher the voltage the greater the fluid motion. Second, as frequency increases, the percentage also increases for the most part. Therefore, a higher frequency will produce greater fluid motion and pull in more

particles. This trend does not however apply for the entire range of frequencies; it appears to be a lower frequency phenomenon for the most part. The lower frequency phenomenon was confirmed by Gascoyne et al [14]. The third trend is that smaller particles are affected much more readily. This is most likely due to a lower drag coefficient. These trends are much more visible with the video recordings and are consistent.
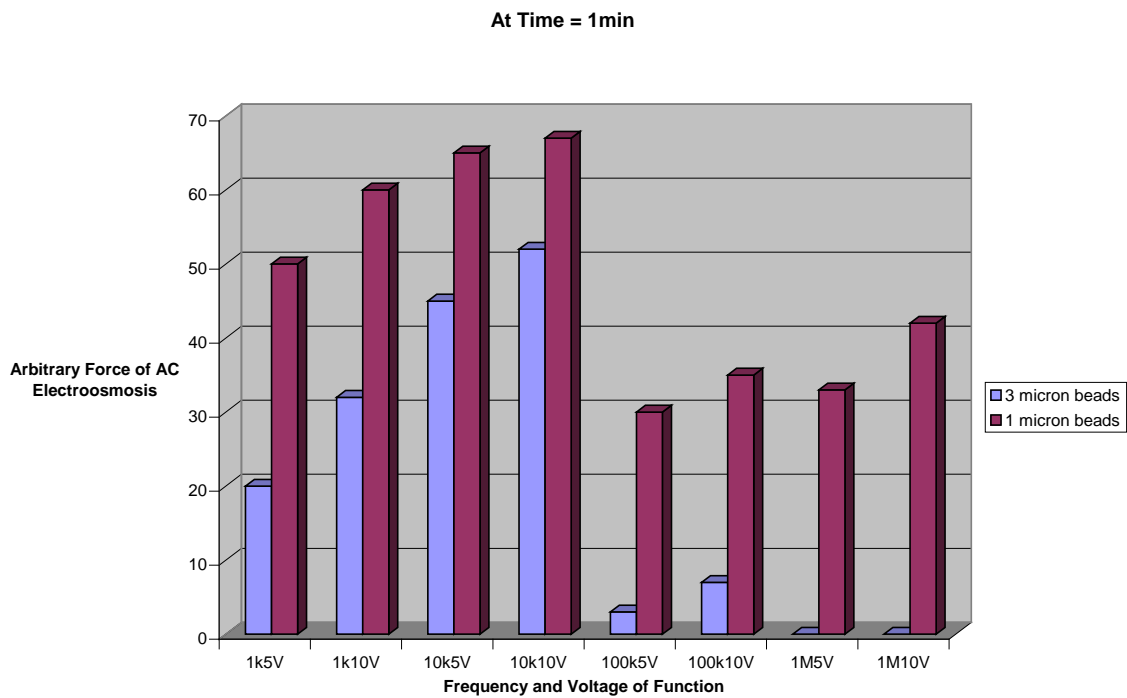
At Time = 1min

Figure 50. Graph representing the amount of particles being contained through ACEO after 1 minute for multiple frequencies, voltages, and particle sizes
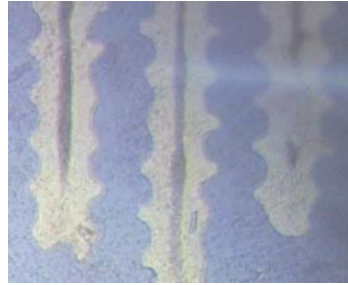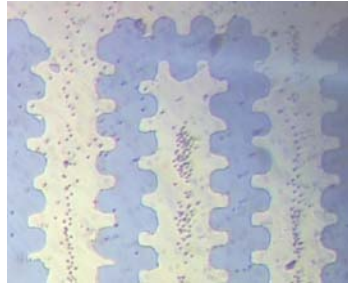
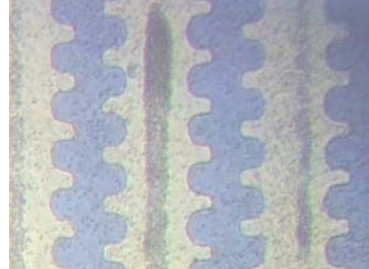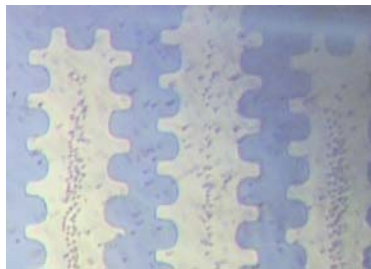**3um**   **1um**
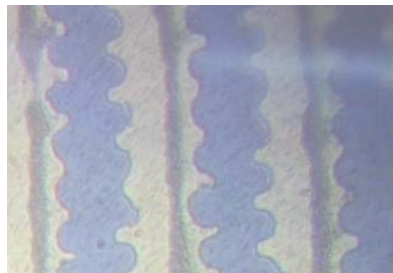

Figure 51. 1 kHz 5V @1min

Figure 52. 1 kHz 10V @1min

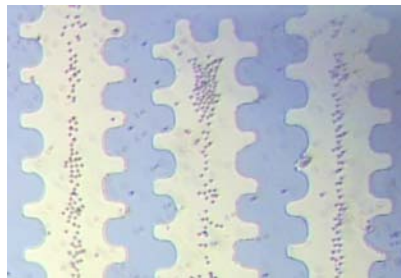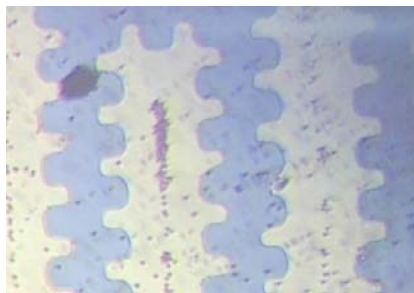**Figure 53. 10kHz 5V @1min**

Figure 54. 10kHz 10V @1min

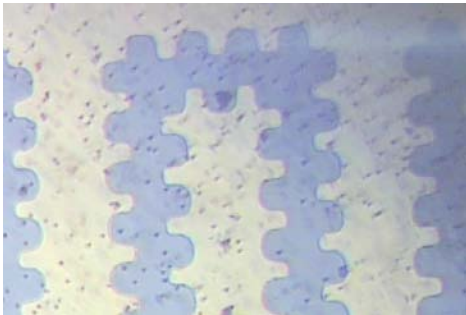**3um**   **1um**

Figure 55. 100kHz 5V @1min
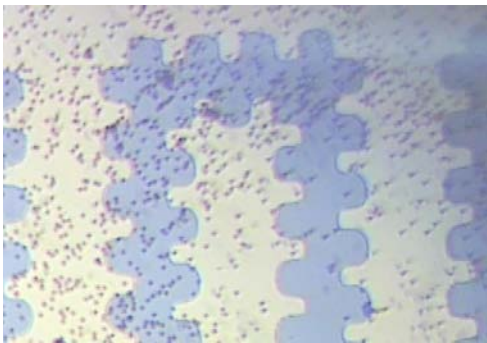

Figure 56. 100kHz 10V @1min

Figure 57. 1MHz 5V @1min

3um   **1um**

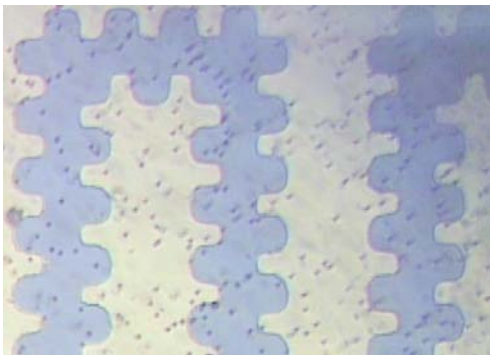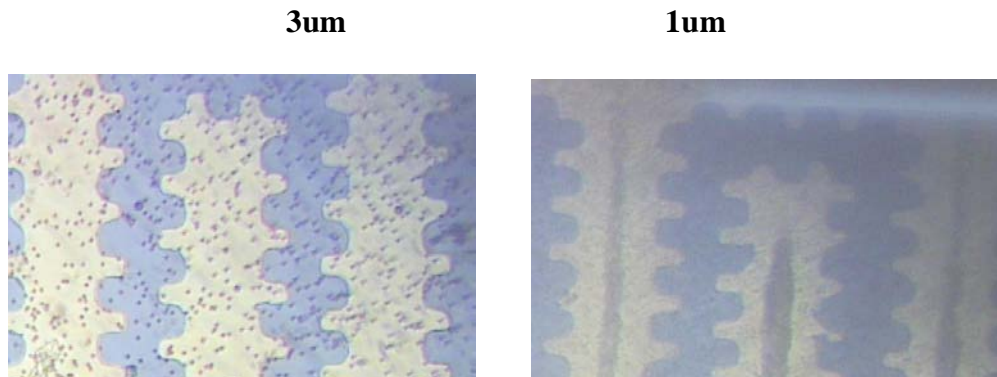**Figure 58. 1MHz 10V @1min**

The last set of images attempts to discover the time dependency of ACEO. Again these are arbitrary percentages taken from the images but the trend developed is consistent with the visuals from the video. The images and graph simply show that as time goes on the number of particles concentrated within the center of the electrodes increases. This makes sense as the fluid motion is constant and particles are being pushed towards that section. Occasionally beads will be pushed out and will catch the motion of the fluid and be pulled away but overtime these occasional exoduses will not affect the increase in bead trapping at this location.

Figure 59. 1kHz 5V 1minute intervals

Figure 60. Graph of particles held over time
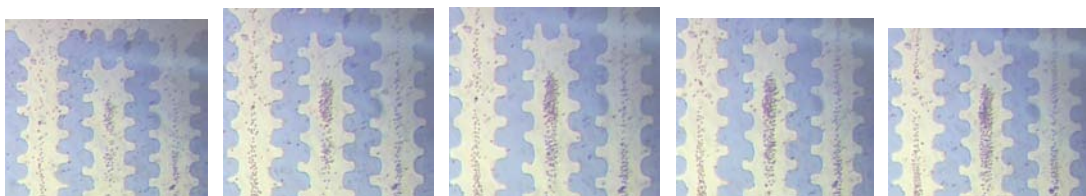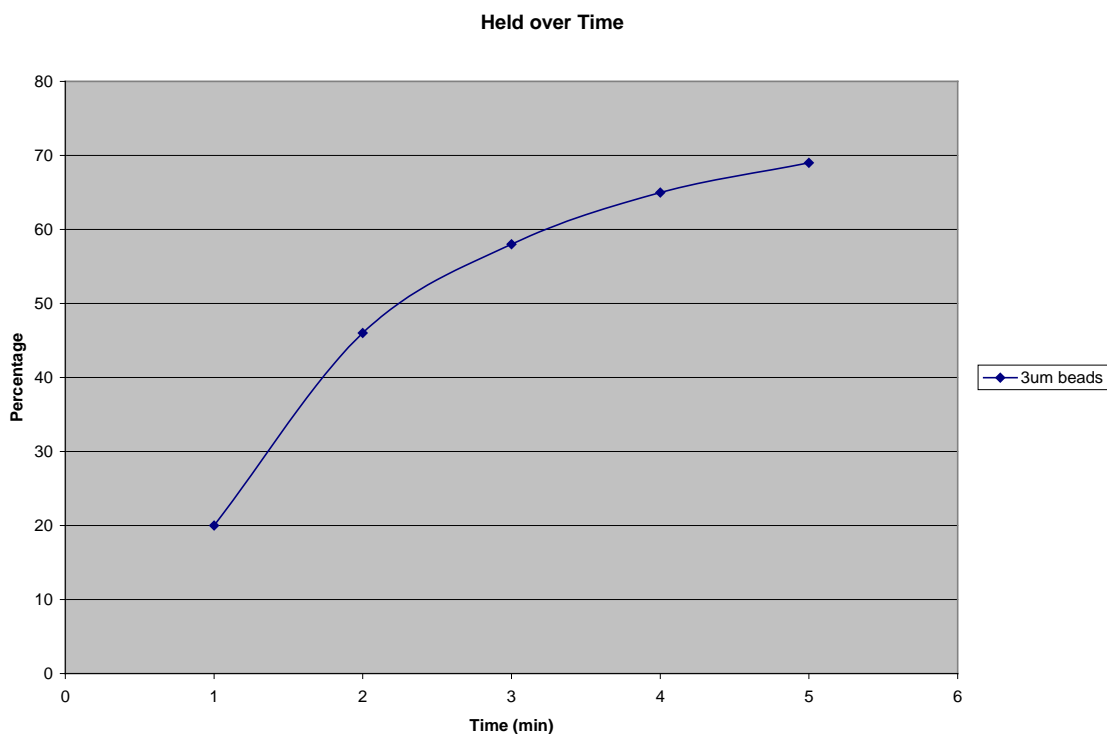
These experiments are real proof of the simulation results but also help understand a phenomenon that will affect the ability of the separator to trap particles and analyze them. A second group of experiments were performed to better understand the importance of signal shape. The following images and graphs are the results and they serve two purposes. First they help to understand the different signal shapes and which type will best serve the purpose of this research and second they allow us to narrow a frequency range that will serve that purpose. The images show a single electrode band with three different signal types: Sine, Square and Triangle. Each signal was applied to the electrodes using two different microbead solutions, 3 μm and 1 μm. The smaller beads have a higher concentration (~4.55x10^9 particles/mL) than the larger beads (~3.36x10^8 particles/mL). This results in higher AC electroosmosis percentages for the

smaller particles because the size difference requires less force to move and the interaction between the particles which are closer together causes them to clump more readily. Generally though, the percentage of the phenomenon will be in the same range despite the signal choice for each particle size. This is discussed further below.

Figure 61. 1 kHz 10V 1min. From left to right, Sine, Sine small, Square, Square small, Triangle, Triangle small
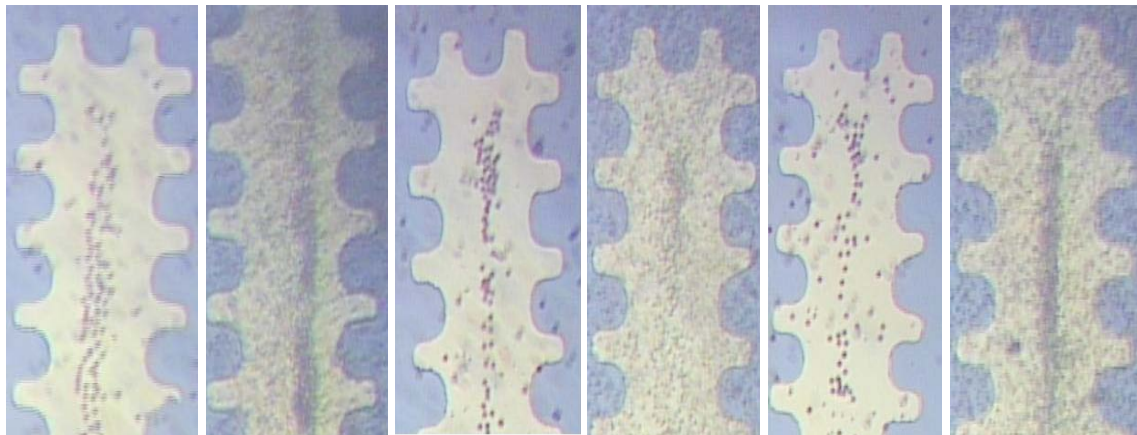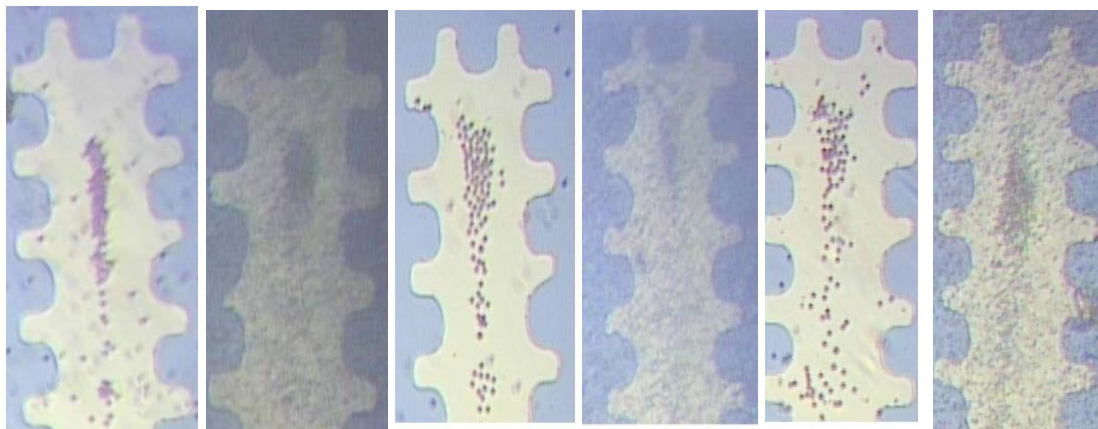

Figure 62. 10kHz 10V 1 min. From left to right, Sine, Sine small, Square, Square small, Triangle, Triangle small
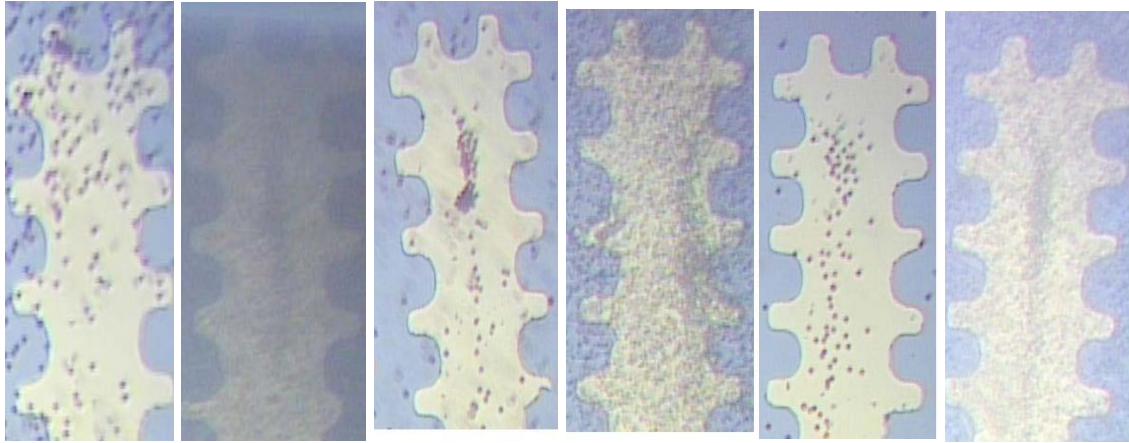
Figure 63. 100kHz 10V 1min. From left to right, Sine, Sine small, Square, Square small, Triangle, Triangle small
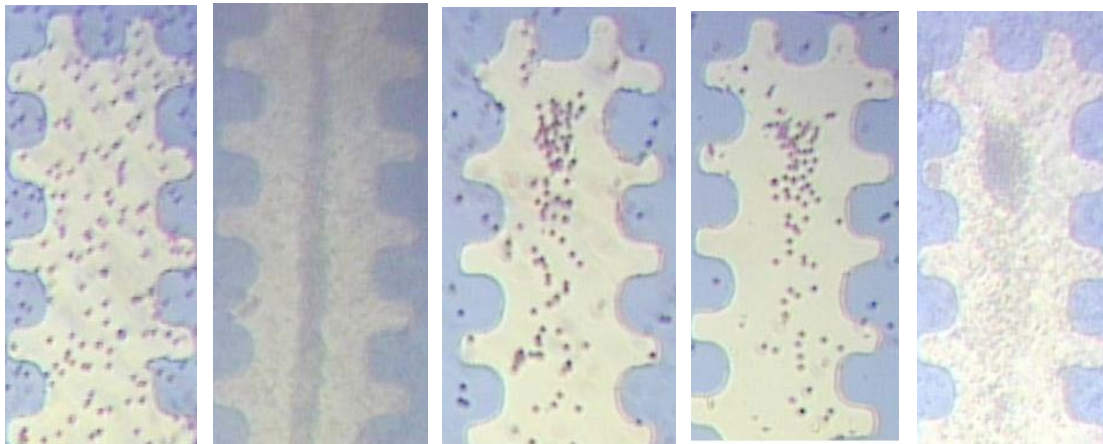
Figure 64. 1MHz 10V 1 min. From left to right, Sine, Sine small, Square, Triangle, Triangle Small

ACEO percentage vs Signal shape
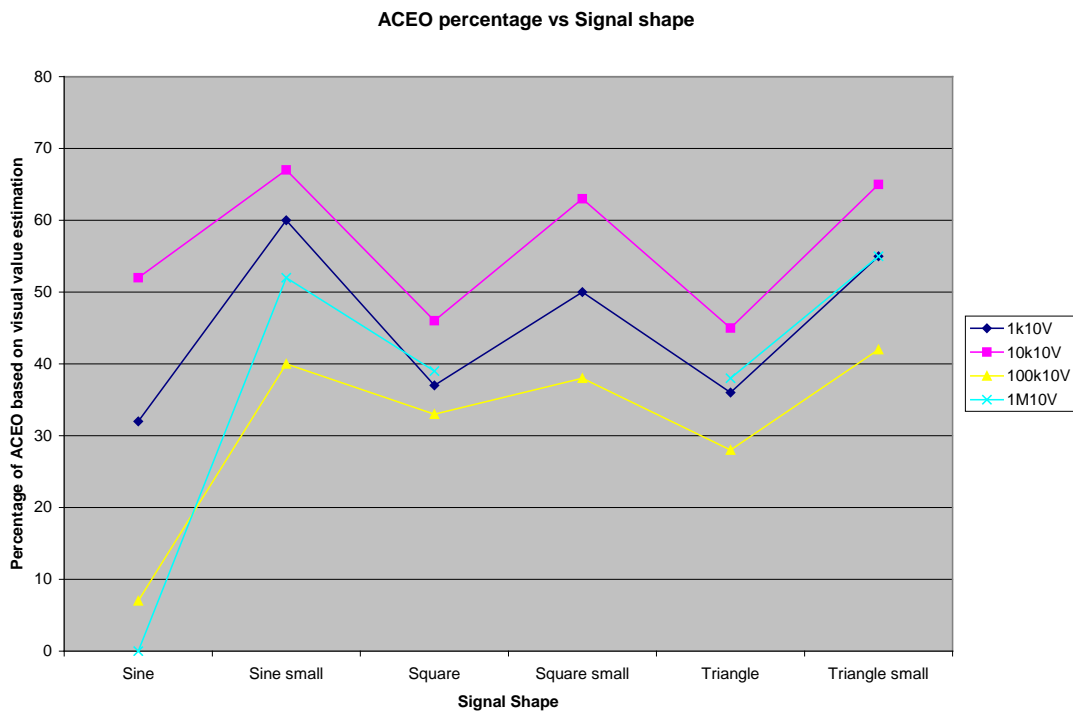
Figure 65. Line Graph of percentage of particles held by ACEO as the signal shape changes

The two graphs use the same data but different types to express different trends. The first

graph is arranged by frequency. The sawtooth shape of the line indicates the increase in ACEO

when the same signal is applied to a smaller particle. The percentage of each frequency per

particle size is within the same range, this is a sign that the signal shape does not affect the fluid

motion once the necessary sample rate is reached. The fluid motion is more dependent on

frequency (how often the signal goes from max to min) rather than the signal shape (the path

taken to get from max to min). The graph also shows that the 10kHz frequency is in the right

range for optimal AC electroosmosis generation. This trend is better indicated in the second

graph where the data is grouped by signal shape. The 10kHz frequency is clearly the highest

value of ACEO in each category. This is a good indicator of the operating frequency that will be

used for the separator tests.
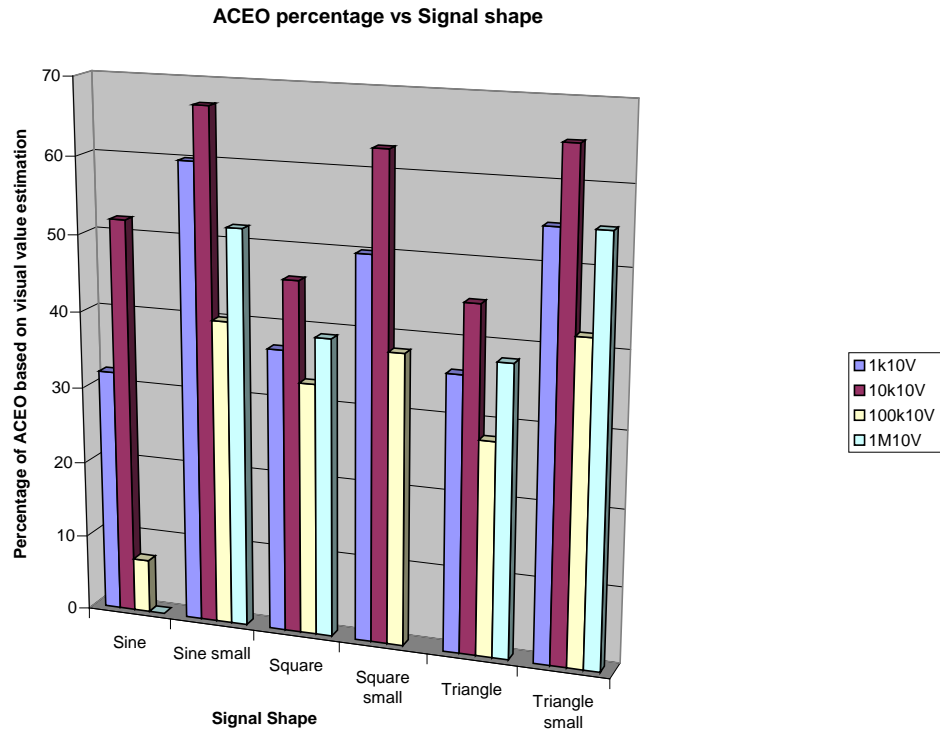
Figure 66. Bar Graph of percentage of particles held by ACEO as the signal shape changes

Taylor Couette Flow

The first step to determining the critical Taylor number for our parameters was to extrapolate from known data for critical Taylor numbers at decreasing radius ratios. These values were taken from Koschmieder's [40] book and are shown in Table 2. The data was graphed and then a power trend line was used to derive the equation and the critical Taylor numbers for each of the fabricated cylinders was calculated.
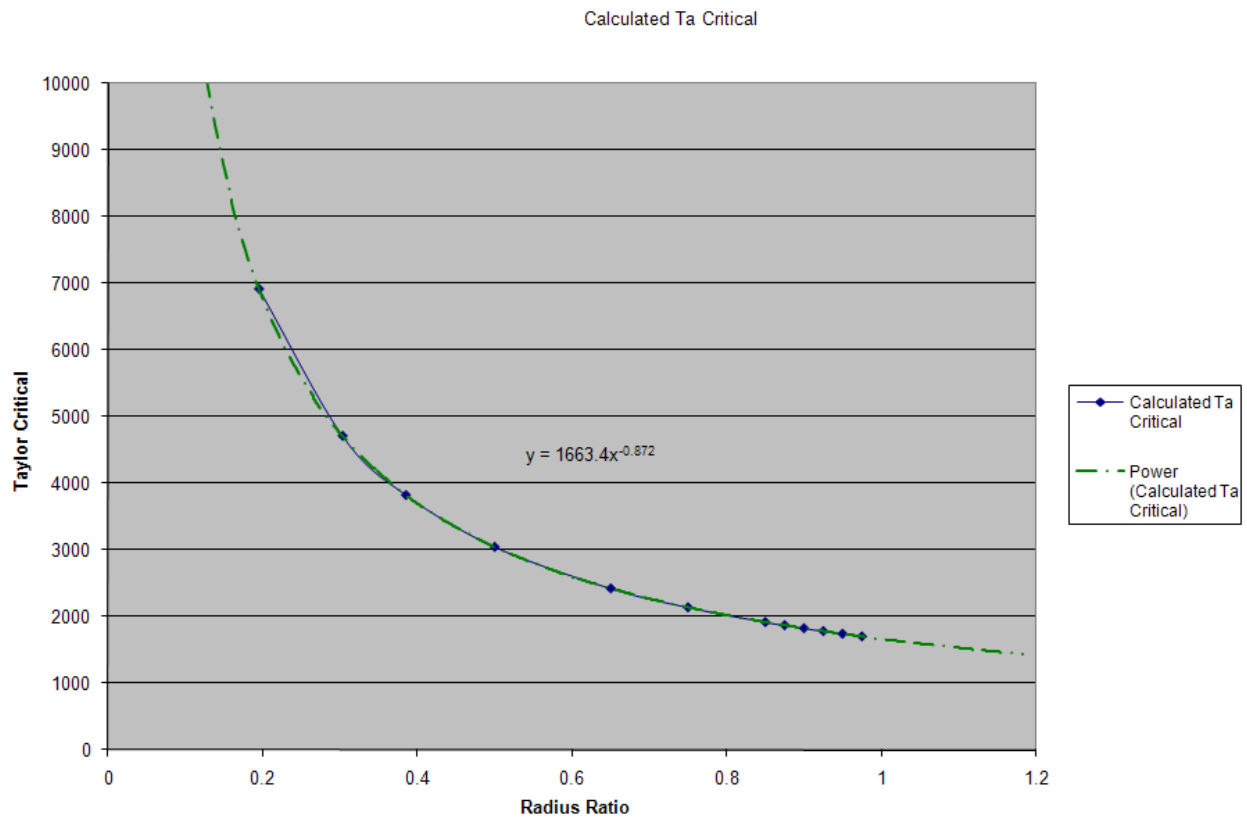
Figure 67 Graph to help calculate Critical Taylor number

Table 1 Data to determine critical Taylor number equation along with corresponding critical Taylor numbers

Radius Ratio	Given Ta Critical	Calculated Ta Critical
0.975	1723.89	1700.544382
0.95	1754.76	1739.515874
0.925	1787.93	1780.456074
0.9	1823.37	1823.521785
0.875	1861.48	1868.887127
0.85	1902.4	1916.746012
0.75	2102.17	2137.867362
0.65	2383.96	2422.101709
0.5	3099.57	3044.985034
0.385		3824.71697
0.303		4713.399944
0.195		6923.082479

Once these values were known, the Reynolds number was derived using the equation:

$$Ta_{crit} = Re\sqrt{(d/r_i)} \qquad (1)$$

The critical Taylor number is dependent on the rotational Reynolds number as well as the square root of the gap size divided by the inner radius. Having calculated the Reynolds number from the values this second equation was used to discover the angular velocity of the inner cylinder and converted to speed in RPM for testing.

$$Re = (\Omega\ d\ r_i)/\nu \qquad (2)$$

The Reynolds number is dependent on Ω (the angular velocity of the inner cylinder), d (gap size), r_i (radius of inner cylinder) and inversely dependent on ν (viscosity of fluid).

The tables below are data for different angular velocities from 0-10 for each cylinder size and the Rotational Reynolds number and Taylor number are calculated for each along with the critical Taylor number for that specific cylinder size using equations 1 and 2.

Table 2 Data for each cylinder: small, medium, large

Small						
Ang. Vel.	Radius (i)	Gap size	Visc. Kin.	Rotational Re	Taylor number	RPM
0	1.075	4.425	0.01	0	0	0
1	1.075	4.425	0.01	475.6875	965.1040646	9.549297
2	1.075	4.425	0.01	951.375	1930.208129	19.09859
3	1.075	4.425	0.01	1427.0625	2895.312194	28.64789
4	1.075	4.425	0.01	1902.75	3860.416258	38.19719
5	1.075	4.425	0.01	2378.4375	4825.520323	47.74648
6	1.075	4.425	0.01	2854.125	5790.624387	57.29578
7	1.075	4.425	0.01	3329.8125	6755.728452	66.84508
8	1.075	4.425	0.01	3805.5	7720.832517	76.39437
9	1.075	4.425	0.01	4281.1875	8685.936581	85.94367
10	1.075	4.425	0.01	4756.875	9651.040646	95.49297
20	1.075	4.425	0.01	9513.75	19302.08129	190.9859
30	1.075	4.425	0.01	14270.625	28953.12194	286.4789
40	1.075	4.425	0.01	19027.5	38604.16258	381.9719
50	1.075	4.425	0.01	23784.375	48255.20323	477.4648
100	1.075	4.425	0.01	47568.75	96510.40646	954.9297
200	1.075	4.425	0.01	95137.5	193020.8129	1909.859
300	1.075	4.425	0.01	142706.25	289531.2194	2864.789
500	1.075	4.425	0.01	237843.75	482552.0323	4774.648
1000	1.075	4.425	0.01	475687.5	965104.0646	9549.297
7.17	1.075	4.425	0.01	3410.679375	6919.796143	68.46846
Medium						
Ang. Vel.	Radius (i)	Gap size	Visc. Kin.	Rotational Re	Taylor number	RPM
0	1.665	3.835	0.01	0	0	0
1	1.665	3.835	0.01	638.5275	969.0700496	9.549297
2	1.665	3.835	0.01	1277.055	1938.140099	19.09859
3	1.665	3.835	0.01	1915.5825	2907.210149	28.64789
4	1.665	3.835	0.01	2554.11	3876.280199	38.19719
5	1.665	3.835	0.01	3192.6375	4845.350248	47.74648
6	1.665	3.835	0.01	3831.165	5814.420298	57.29578
7	1.665	3.835	0.01	4469.6925	6783.490348	66.84508
8	1.665	3.835	0.01	5108.22	7752.560397	76.39437
9	1.665	3.835	0.01	5746.7475	8721.630447	85.94367
10	1.665	3.835	0.01	6385.275	9690.700496	95.49297
20	1.665	3.835	0.01	12770.55	19381.40099	190.9859
30	1.665	3.835	0.01	19155.825	29072.10149	286.4789
40	1.665	3.835	0.01	25541.1	38762.80199	381.9719
50	1.665	3.835	0.01	31926.375	48453.50248	477.4648
100	1.665	3.835	0.01	63852.75	96907.00496	954.9297
200	1.665	3.835	0.01	127705.5	193814.0099	1909.859
300	1.665	3.835	0.01	191558.25	290721.0149	2864.789
500	1.665	3.835	0.01	319263.75	484535.0248	4774.648
1000	1.665	3.835	0.01	638527.5	969070.0496	9549.297
4.86	1.665	3.835	0.01	3103.24365	4709.680441	46.40958
Large						

Ang. Vel.	Radius (i)	Gap size	Visc. Kin.	Rotational Re	Taylor number	RPM
0	2.12	3.38	0.01	0	0	0
1	2.12	3.38	0.01	716.56	904.7799768	9.549297
2	2.12	3.38	0.01	1433.12	1809.559954	19.09859
3	2.12	3.38	0.01	2149.68	2714.33993	28.64789
4	2.12	3.38	0.01	2866.24	3619.119907	38.19719
5	2.12	3.38	0.01	3582.8	4523.899884	47.74648
6	2.12	3.38	0.01	4299.36	5428.679861	57.29578
7	2.12	3.38	0.01	5015.92	6333.459838	66.84508
8	2.12	3.38	0.01	5732.48	7238.239814	76.39437
9	2.12	3.38	0.01	6449.04	8143.019791	85.94367
10	2.12	3.38	0.01	7165.6	9047.799768	95.49297
20	2.12	3.38	0.01	14331.2	18095.59954	190.9859
30	2.12	3.38	0.01	21496.8	27143.3993	286.4789
40	2.12	3.38	0.01	28662.4	36191.19907	381.9719
50	2.12	3.38	0.01	35828	45238.99884	477.4648
100	2.12	3.38	0.01	71656	90477.99768	954.9297
200	2.12	3.38	0.01	143312	180955.9954	1909.859
300	2.12	3.38	0.01	214968	271433.993	2864.789
500	2.12	3.38	0.01	358280	452389.9884	4774.648
1000	2.12	3.38	0.01	716560	904779.9768	9549.297
4.23	2.12	3.38	0.01	3031.0488	3827.219302	40.39352
Small						
Ang. Vel.	Radius (i)	Gap size	Visc. Kin.	Rotational Re	Taylor number	RPM

Table 3 Experimental numbers with resullting critical values

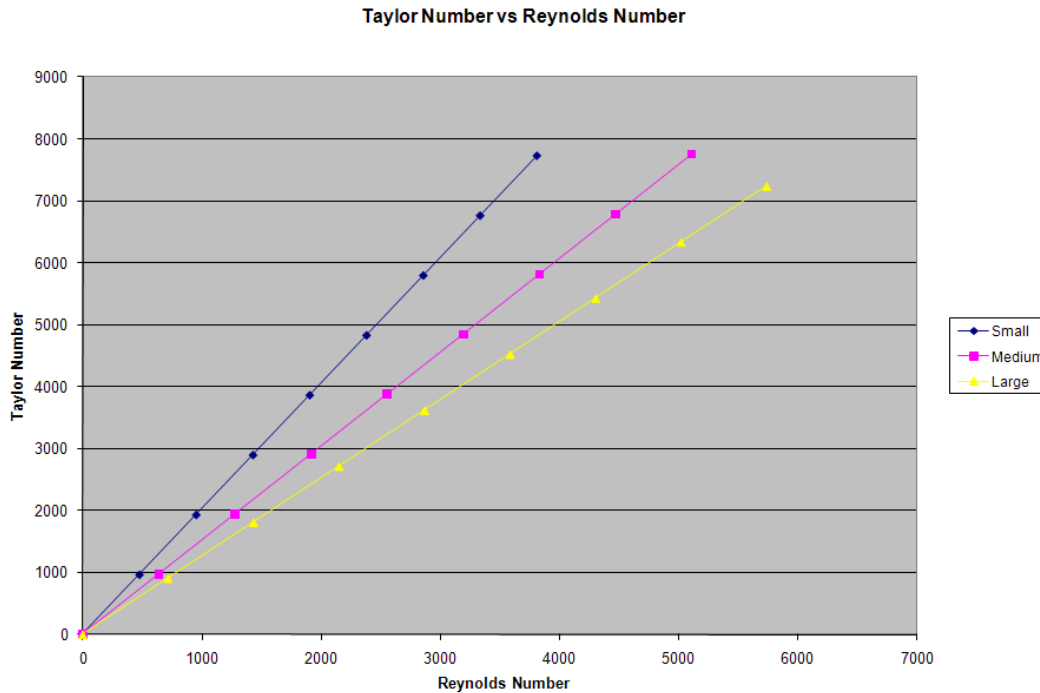|	Ang. Vel.	Radius (i)	Gap size	Visc. Kin.	Rotational Re	Taylor number	RPM
Small	7.17	1.075	4.425	0.01	3410.679375	6919.796	68.46846
Medium	4.86	1.665	3.835	0.01	3103.24365	4709.68	46.40958
Large	4.23	2.12	3.38	0.01	3031.0488	3827.219	40.39352

Figure 68 Taylor Number vs Reynolds Number

By graphing Taylor number vs. Reynolds number in Figure 67, it becomes clear that a larger cylinder speed will be necessary to achieve Taylor Couette flow for the smallest cylinder. This is due to the fact that vortical formation occurs as the particles are pulled outward to the wall by the velocity achieved from the inner cylinder and once the particle reaches the outer cylinder viscosity and drag forces have slowed it down and the pressure gradient changes and the particle causes the particle to return towards the inner cylinder until it obtains enough force to stop and be pushed back out. The smaller the radius, the larger the gap and the more force the cylinder has to put on the particle for it to reach the wall and form vortices. The following three graphs are representations of the point where the critical Taylor number occurs.
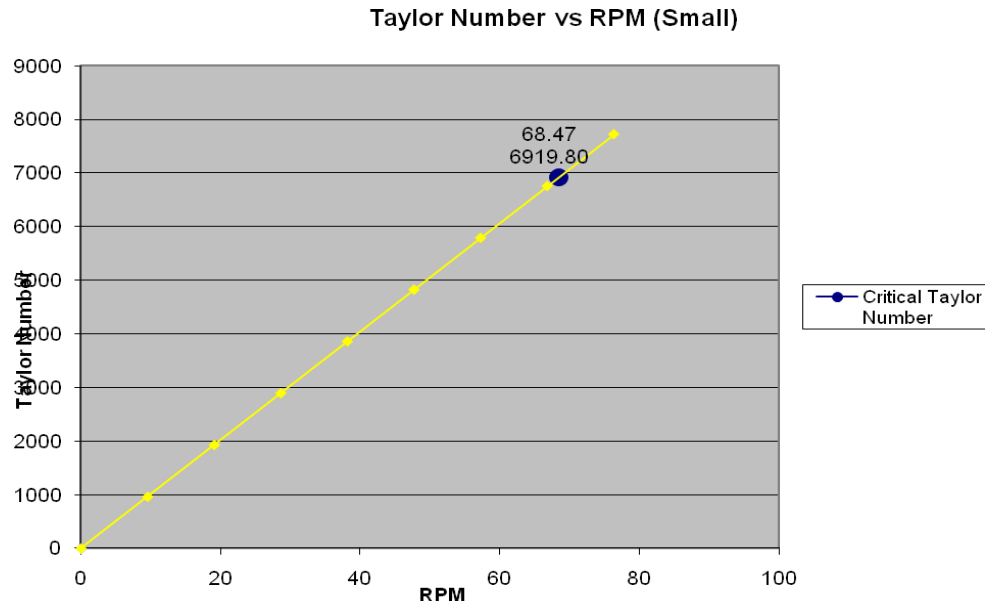
Figure 69 Taylor Number vs RPM for small cylinder with highlighted Critical Taylor number and speed
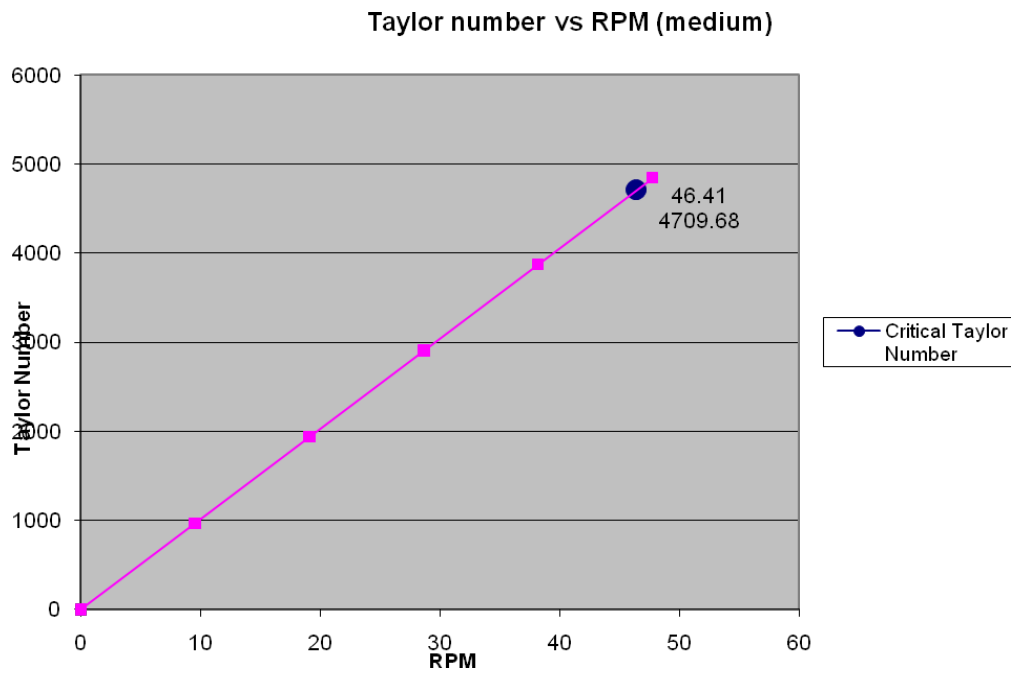

Figure 70 Taylor Number vs RPM for medium cylinder with highlighted Critical Taylor number and speed
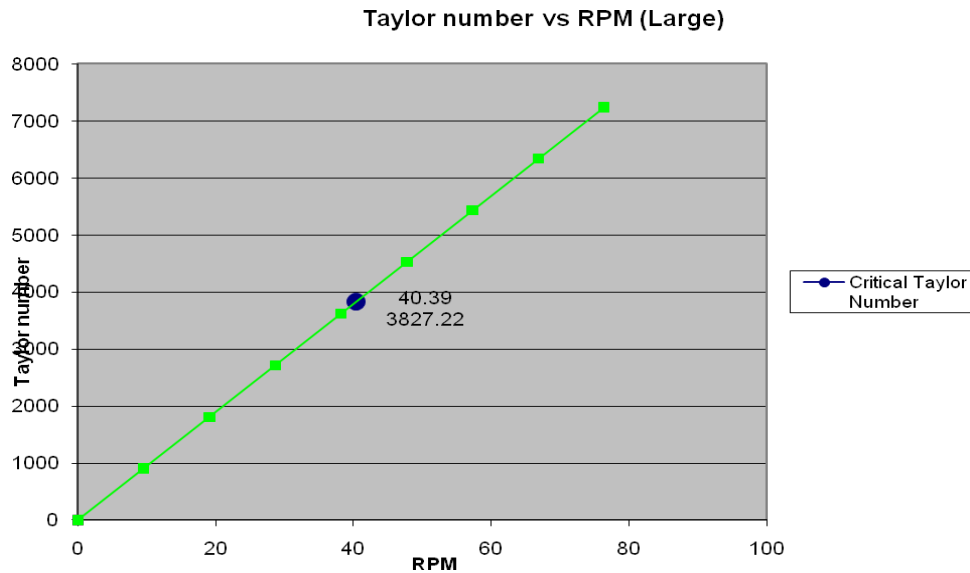
82

Figure 71 Taylor Number vs RPM for large cylinder with highlighted Critical Taylor number and speed

The cylinder speeds calculated for the onset of Taylor Couette vortices, the container and fluid tests were performed. Figure 72 shows supercritical Taylor Couette flow at 50 RPM for the medium cylinder (Ta_{crit} = 47RPM) at eight intervals in the flow. The flow is characterized by circular Couette flow in that the particles are pushed outward at decreasing speeds but it also shows turbulent signs created by the vortices that spin off of the inner cylinder but never reach the outer wall in time to form a closed vortex between the inner and outer cylinders. Instead, a form of chaotic circular Couette flow ensues and although there is a distinct outward motion generated by the inner cylinder spinning, the particle pathways can not be described using Taylor Couette flow.
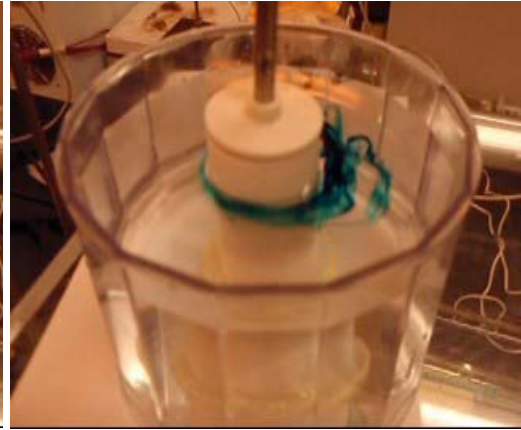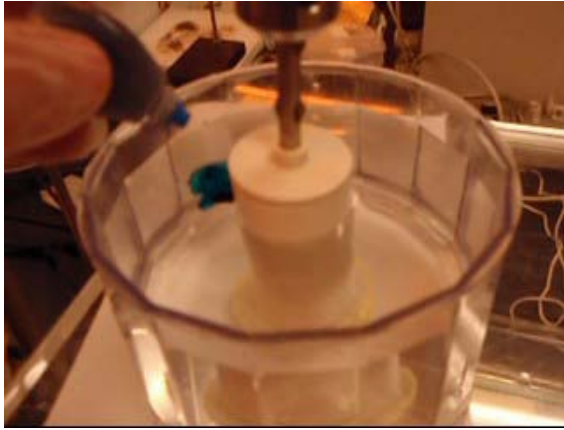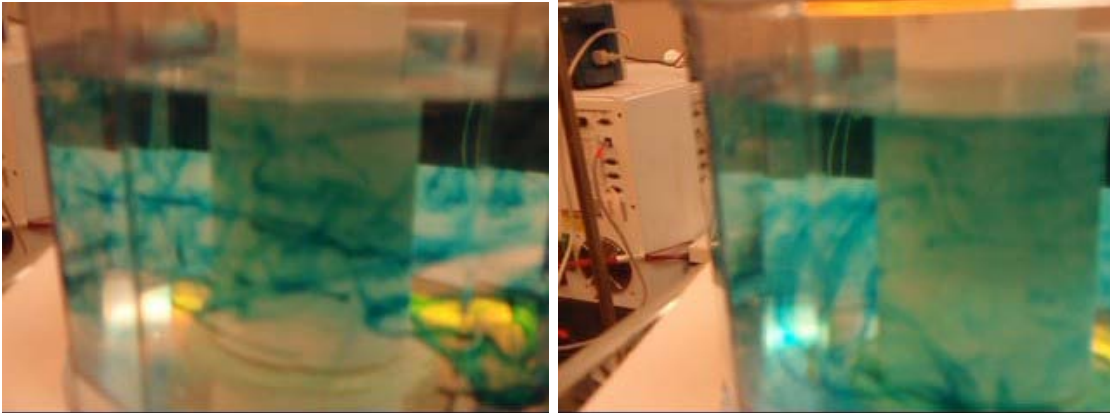
Figure 72 Pictures 1-8 of flow in Medium Cylinder at 50 RPM (super critical)

Figure 73 shows the progression of dye in a fluid flow for the large cylinder at 50RPM which is beyond the critical Taylor number of 41 RPM. Circular Couette flow is not as obvious with the larger cylinder as there is less of a gap and at the same speed and a larger circumference, the particles will travel around the cylinder less times to gather the velocity to cross the gap. The dye still is spun off from the cylinder in that characteristic vortex shape but the particles do not appear to cross the gap to form the Taylor vortex.
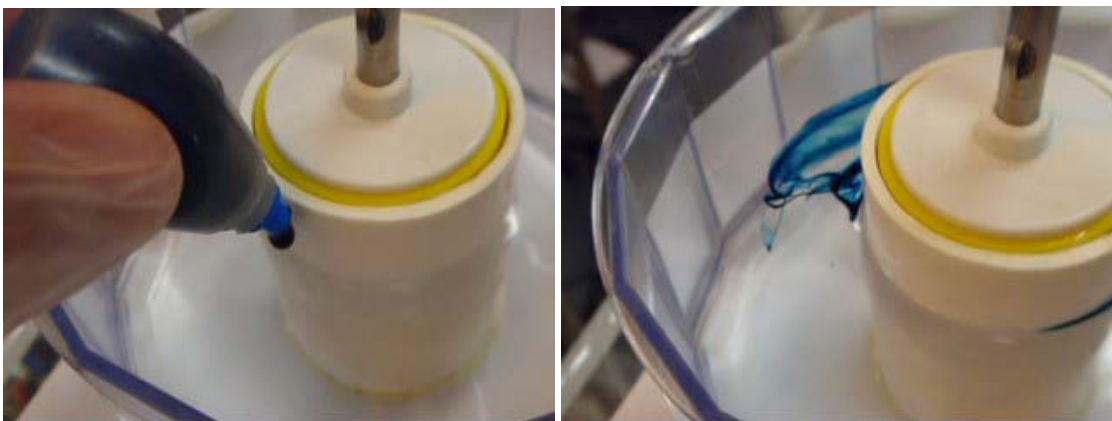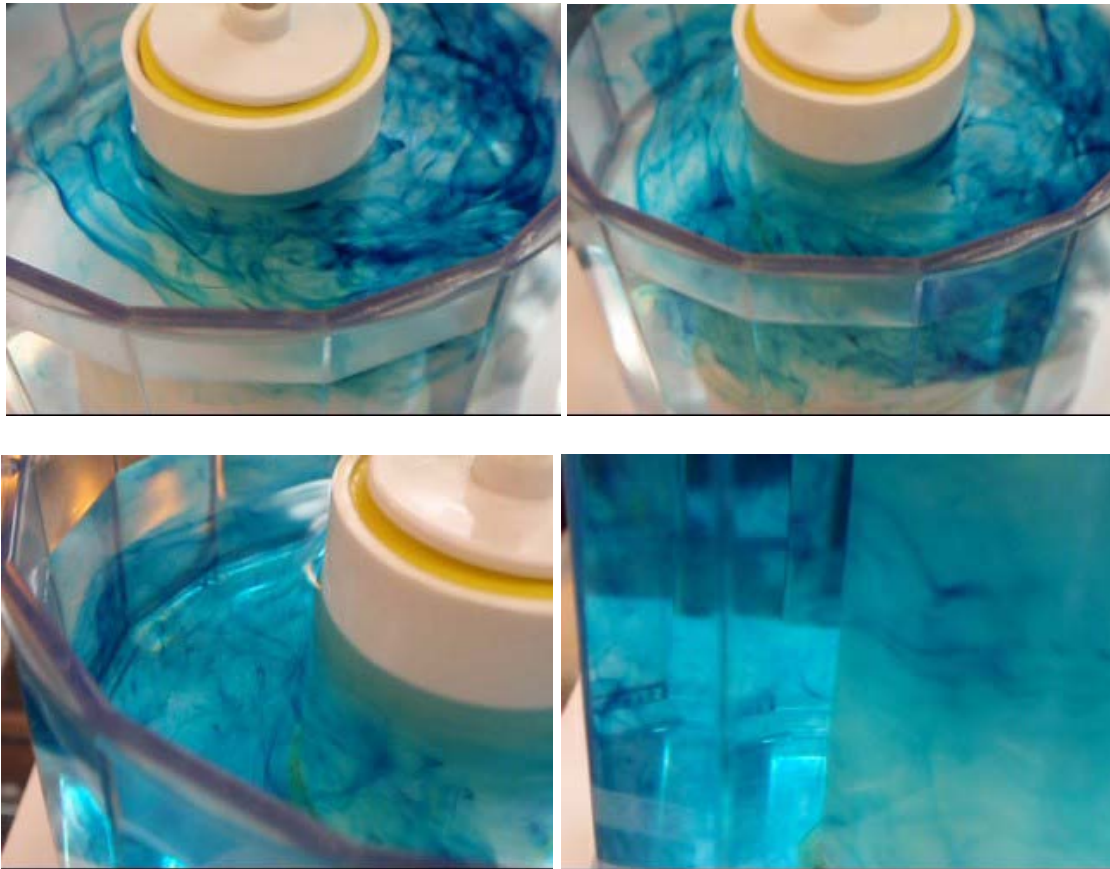
Figure 73 Pictures 1-6 of Large cylinder flow at 50 RPM (super critical)

Without the formation of vortices, the next step was to determine the speed of particles crossing the gap regardless of the fluid flow that pushes the particle to the electrode, it may still be trapped and a separation, albeit a chaotic one, would take place. The theories of why Taylor Couette flow did not form are numerous and will be pursued long term in hopes of finding solutions and making the necessary changes to the system to allow the process to work. Theories on failure involved, large gap, small aspect ratio, poor alignment between the motor and the central axis of the container among others. The large gap theory has been discussed earlier and is the most obvious possibility as the small vortical formations do not have enough power to

cross the large gap with the little force given the particle by the inner cylinder. Without crossing

the gap the vortices can not become fully formed and the result is turbulent flow. The small

aspect ratio which refers to the height of the container as compared to the gap between the inner

cylinder and the outer wall could be the issue because the vortex usually takes on the dimensions

that approach the gap, d and generally requires as much height in the cylinder as the gap. There

is more height in the cylinder than there is even for the small cylinder gap but with the

characteristic of Taylor Couette flow being the exchange of particles through the in flow and out

flow sections between the vortices, the expectation is for multiple vortices to form to achieve

better balance which is proving difficult with the current dimensions. Poor alignment was

mostly eliminated with the use of the SteadyStir as the speed was very uniform

To better examine the differences in the cylinders and view the time it takes a particle to cross

the gap, two approaches were used. The first shown in figures 74-76 are 3 second time jumps

from the left picture to the right picture with the left image being the initial introduction of the
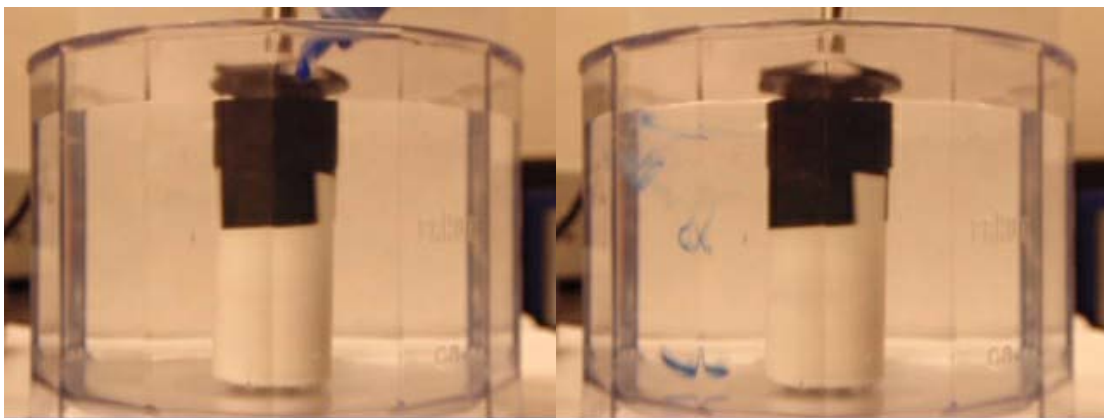
dye into the system.

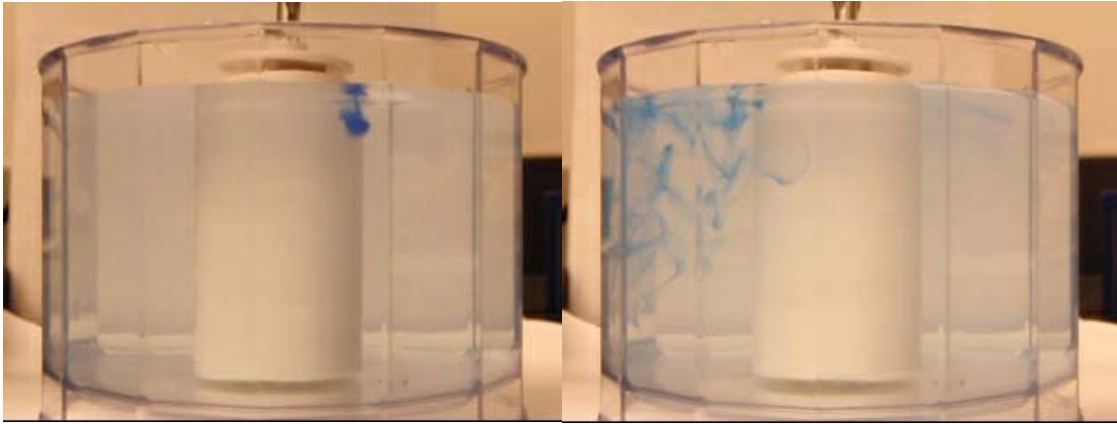**Figure 74 First 3 seconds of small cylinder flow at 80RPM**

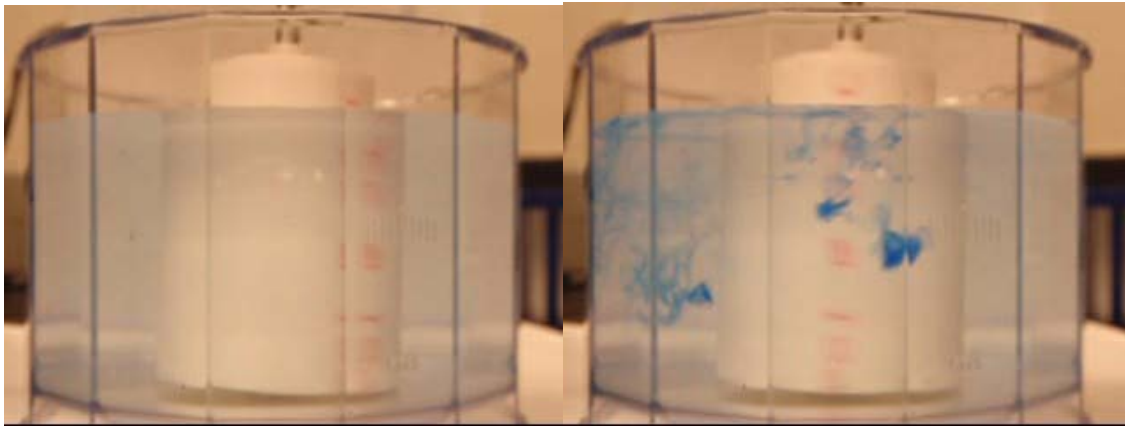**Figure 75 First 3 seconds of medium cylinder flow at 80 RPM**

Figure 76 First 3 seconds of large cylinder flow at 80 RPM

The largest and darkest blue spots in the right image of figure 76 were ignored as they were a second drop introduction and the focus was on the first. The first visual difference is that the dye became more spread out as the radius increased. A logical trend as the larger circumference causes greater displacement per time frame which spreads the dye out quicker. In fact, part of the drop in the first test with the small cylinder was not broken up upon entering the fluid and it sank towards the bottom of the container. The second trend ties into the first observation; it is the distance the particles travelled around the cylinder. In the small cylinder,

they have moved some but not a lot and moving around a smaller cylinder means they travelled less than the particles moving around the larger cylinders. These images show the importance of inner radius to the movement of the particles. The continued analysis of the movement of the particles regardless of flow pattern but more based on visual keys such as time to dissolution of the dye in the fluid and the time for the particles to reach the outer wall. The graphs below indicate dissolving time with the cylinder sizes coding as such: Blue: Small cylinder, Pink: Medium cylinder, Yellow: Large Cylinder
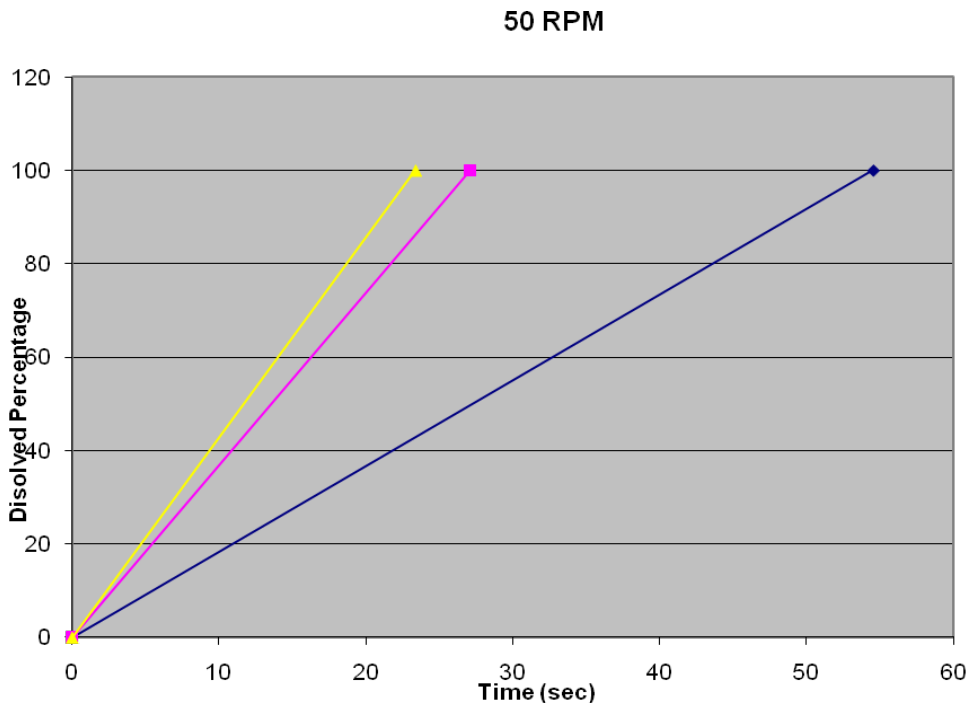
50 RPM

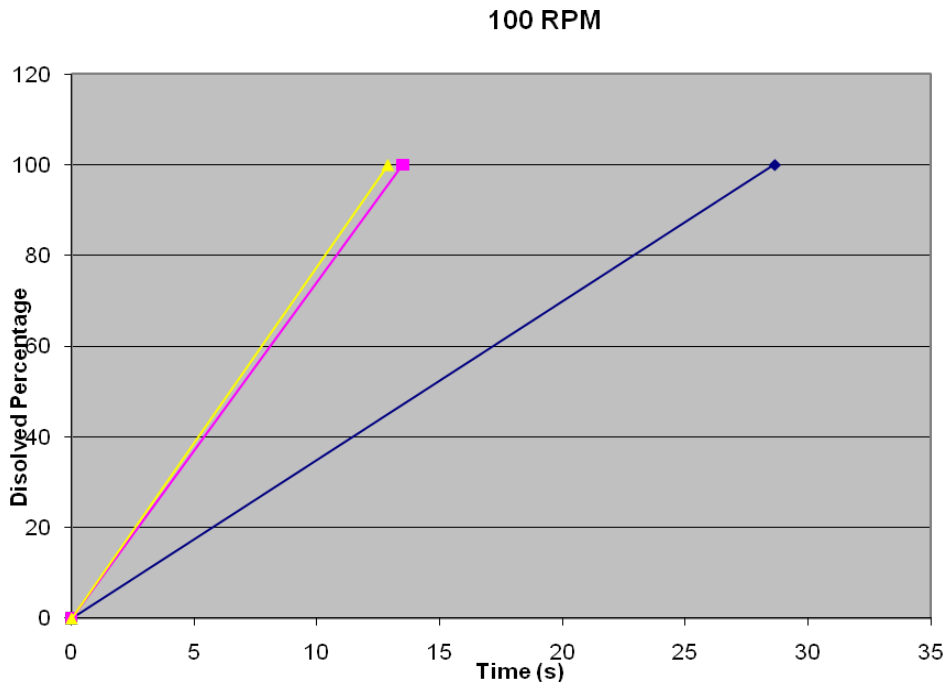

Figure 77. Time to complete dissolving of dye at 50 RPM

100 RPM

Figure 78. Time to complete dissolving of dye at 100 RPM
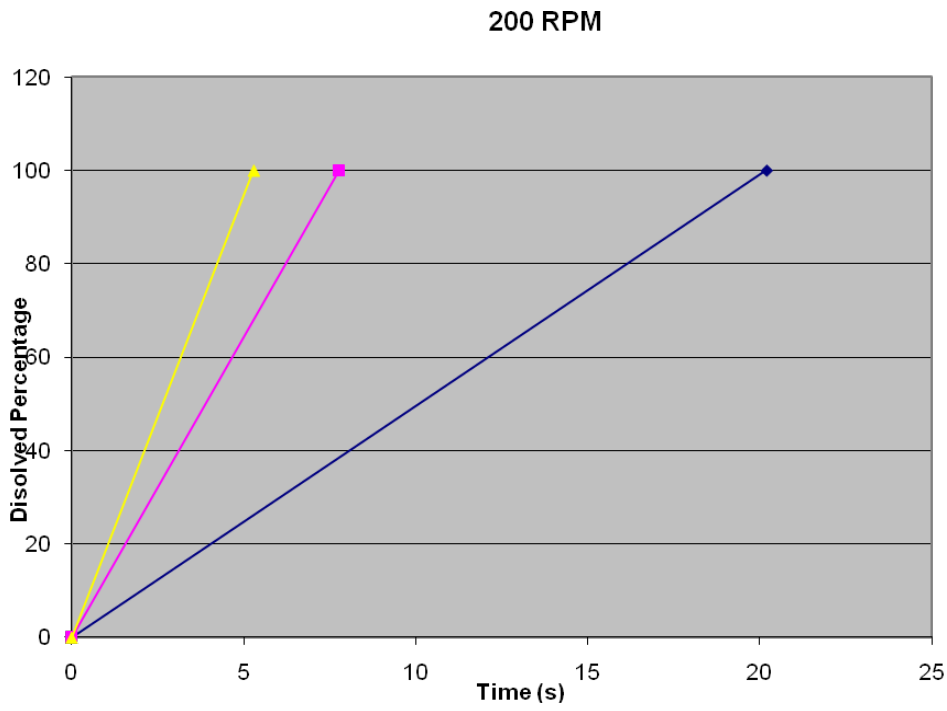
200 RPM

Figure 79. Time to complete dissolving of dye at 200 RPM

90

These graphs were based off of the visuals of the dye drop experiments filmed from beneath the container which allowed for the whole cylinder to be visualized. The larger cylinder has the clear advantage when it comes to moving the particles or dissolving the dye as the surface area is much larger allowing for greater interaction at each instant with the fluid and particles in contact with the cylinder. The next graph explores the same principle but this time with the goal being time to cross gap Blue: 50 RPM, Pink: 100 RPM, Yellow: 200 RPM
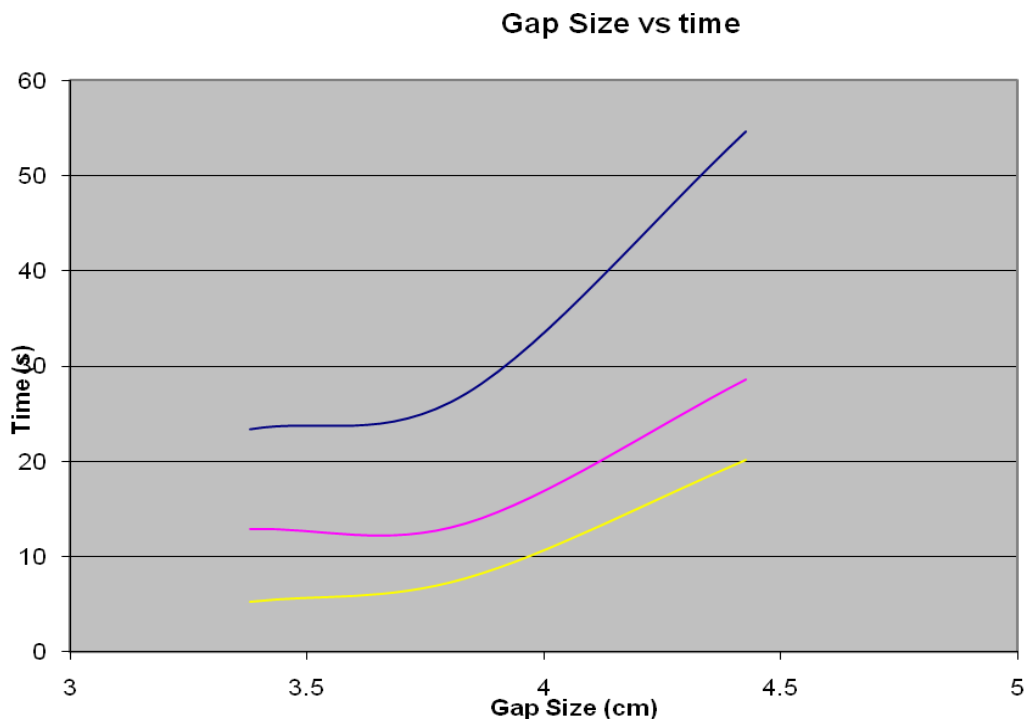
Figure 80. Time to cross gap

Table 4 Time to cross gap data

Speed		Small		Medium	Large	
	0	0	0	0	0	0
50	100	54.57	100	27.1	23.37	100
	0	0	0	0	0	0
100	100	28.64	100	13.5	12.9	100
	0	0	0	0	0	0
200	100	20.2	100	7.77	5.3	100

91

Gap Size	50rpm	100rpm	200rpm			
4.425	54.57	28.64	20.2			
3.835	27.1	13.5	7.77			
3.38	23.37	12.9	5.3			
Speed	Small	Medium	Large			
50	54.57	27.1	23.37			
100	28.64	13.5	12.9			
200	20.2	7.77	5.3			

Although the formation of Taylor vortices proved unsuccesful for this particular setup, the cylinder interaction with the particles provided some data that will prove useful for the full system test. Using the largest cylinder at low speeds will push the most particles to the outer wall and staying at a lowere speed prevents turbulent flow from occuring and circular Couette flow is the dominant flow pattern

Full system results

The figures below are three images from three different spots on one electrode under the microscope after a run. The red circles indicate microbeads present on the electrodes. It is impossible to tell if they are there due to trapping or chance because we can not view their approach to the electrodes and if there was a reaction.
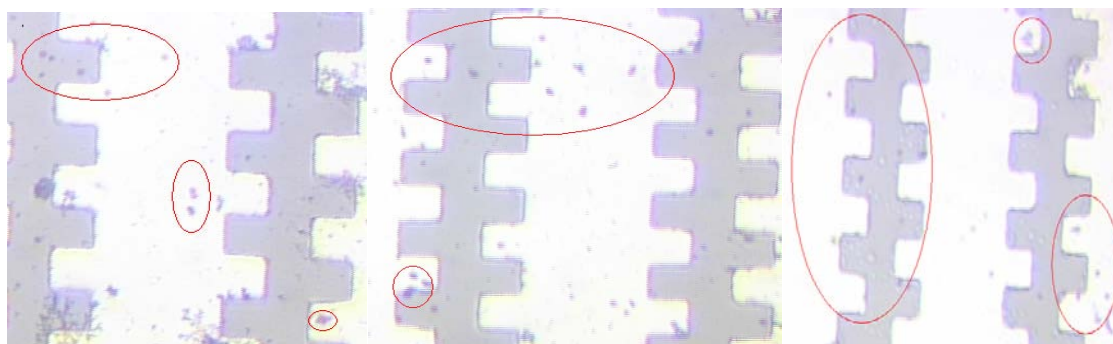

Figure 81. Electrodes under microscope after test run and transfer to microscope. Particles circled in red.

When performing experiments under the microscope, the particles clearly react in the presence of the electric field and can therefore be determined as being trapped or not. Unfortunately, that is not the case for these tests but the number of particles present in three different spots we would have to expect that there would be some that were trapped and some by chance. Especially when the tests were run with 220 ml of total solution 1.5 ml of which was Polybead dyed Red 3 micron microspheres at a 2.61% (solids-latex), making the solution 0.01% microsphere. This may seem like a minuscule percentage but certain bacteria can be a threat at a presence of one bacterium per liter of water. As it is, any microbeads held through the run and then during the transfer over to the microscope were a good sign. Despite the lack of the specific fluid formation that this work was attempting to use, there was some success using circular Couette flow. The laminar nature of this fluid structure helped in the capturing process as there was less force on the particles at the electrodes which meant that if particles were sufficiently pushed out to the electrodes they would be held for microscope visualization and future characterization.

CHAPTER FIVE: CONCLUSIONS

This project had one main objective that required multiple minor goals to be accomplished first. The main project was to create a particle separator that uses Taylor Couette flow to push particles out to electrodes where they can be trapped by dielectrophoresis (DEP). The first step to completing this large project was the design and fabrication of the DEP electrodes that would trap the particles as they reach the outer wall. The second step was to create the Taylor Couette flow fluid container that would serve as the particle control tool. Once both steps were complete and tested, the final assembly of the two sub-projects was performed and some particles were separated from a very diluted solution.

The first goal, dielectrophoretic electrodes, was well understood and the difficulty was going to be bringing the particles within the necessary range of the electrodes. A mask was designed and the electrodes fabricated in a clean room using chromium and gold at first and then aluminum. Issues with electrolysis led to investigations in coatings as well as frequency dependence of electrolysis. A coating called Parylene which is deposited uniformly on any surface structure and that has excellent dielectric properties was used as a means of not only minimizing electrolysis because ultimately that was found to be preventable if the signal function was chosen appropriately but the layer will serve as a protective barrier and prevent the corrosion of the electrode for repeated uses as well as increase the releasing ability of the DEP electrodes after the fluid has been drained and the particles need to be characterized. Experiments using latex microbeads were performed with great success and positive DEP trapping as well as AC Electroosmosis.

The second part to the project the Taylor Couette flow system was fabricated using three different inner cylinders for radius ratios of 0.385, 0.303, and 0.195. These radius ratios were chosen from readily available materials but with the goal of performing large gap Taylor Couette flow. The critical Taylor Numbers were calculated for each cylinder and the speeds were calculated from these numbers as small 69RPM, medium 47RPM and large 41RPM. The supercritical Taylor experiments did not result in Taylor vortices most likely due to the combination of the large gap and small aspect ratio which were design specifications for this device. Nevertheless, circular Couette flow which is laminar in nature was used to perform full system tests where there was evidence of multiple microbeads being trapped on the outer wall electrodes and held while the wafer was transferred to the microscope. While some successes occurred during the course of this project, a large disappointment was the Taylor vortices. Thankfully the initial fluid flow structure, circular Couette flow helped to at least prove the idea that particles can be separated out of a source by pushing the particles toward DEP electrodes.

Obviously the future of this work involves restructuring the design of the container to allow for the production of Taylor vortices without having to sacrifice portability and sample test volume. The first step will be to increase the height of the system and determine if the aspect ratio was the issue. The second will be to use a more conventional Taylor Couette system with an external reservoir and have multiple runs preformed while replacing the water but not the electrodes so that the particles present on the DEP electrodes accurately reflects the source of water. Once the system is perfected, then data can start being collected on experimental yields over time and based on concentration and particle nature.

APPENDIX A: INITIAL TESTING

Blender options

Figure 82Different blender components used during the initial testing

Power supply

Figure 83Power supply used for initial food processor trials
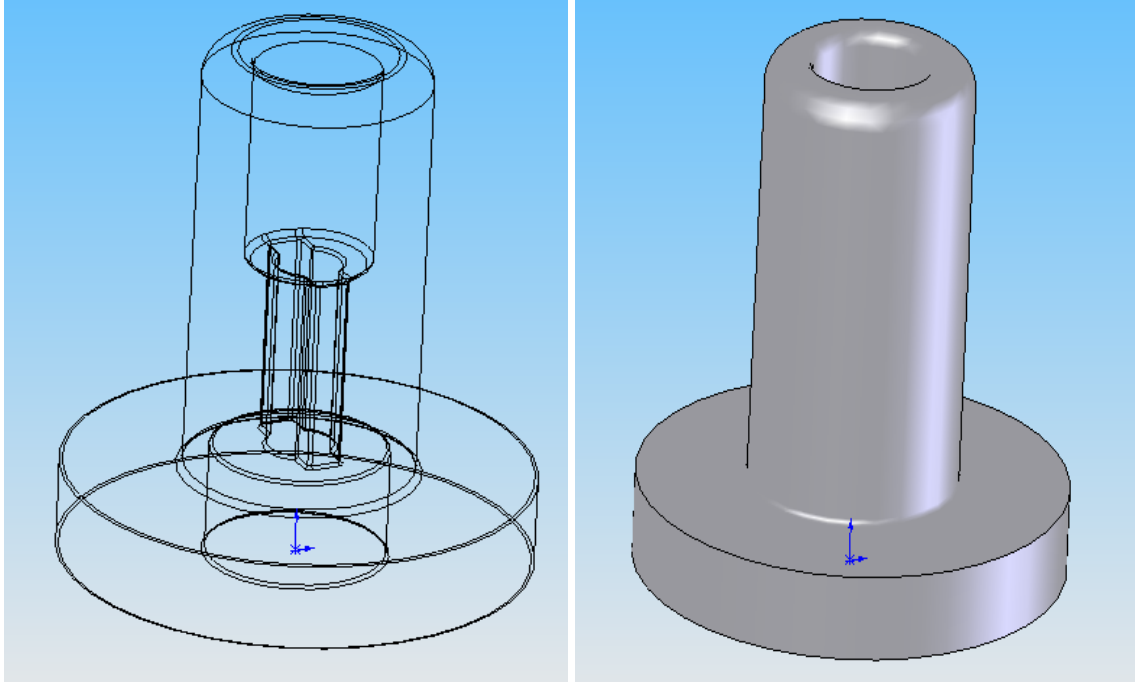
APPENDIX B: CAD MODELING

Figure 84 Bottom insert of cylinder. Transparent to show inner surfaces necessary to spin on the shaft. Solid for a final design look
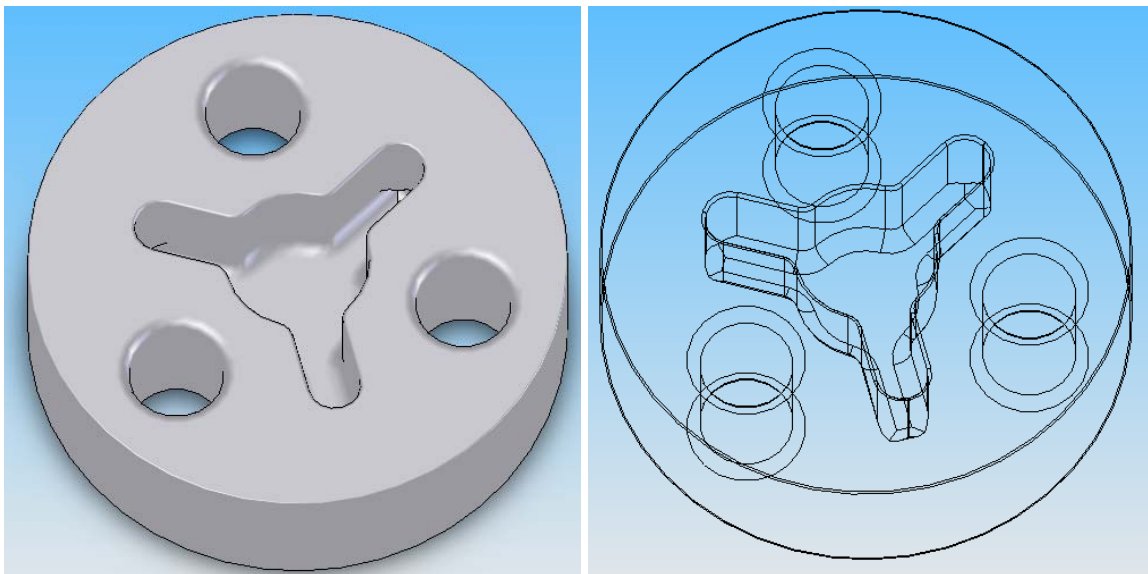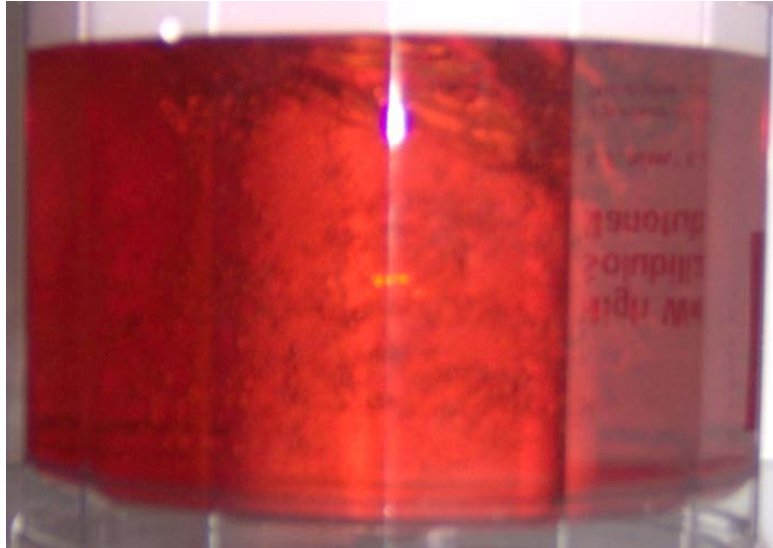

Figure 85 Top mount. Grooves match up with gearing of food processor

APPENDIX C: FLUID TESTING
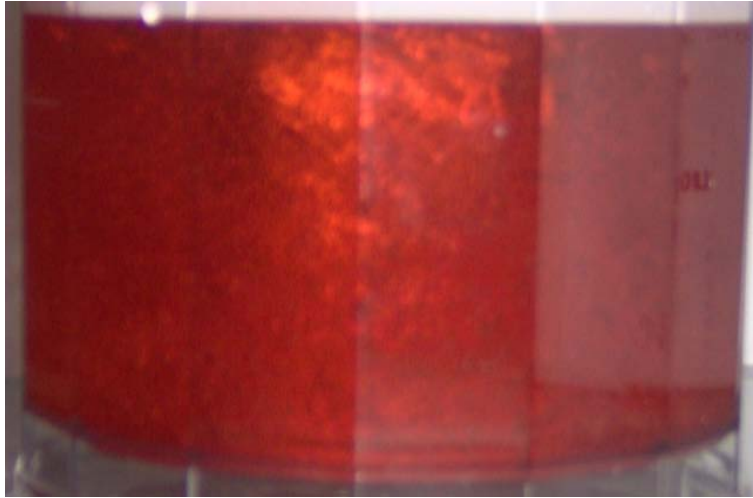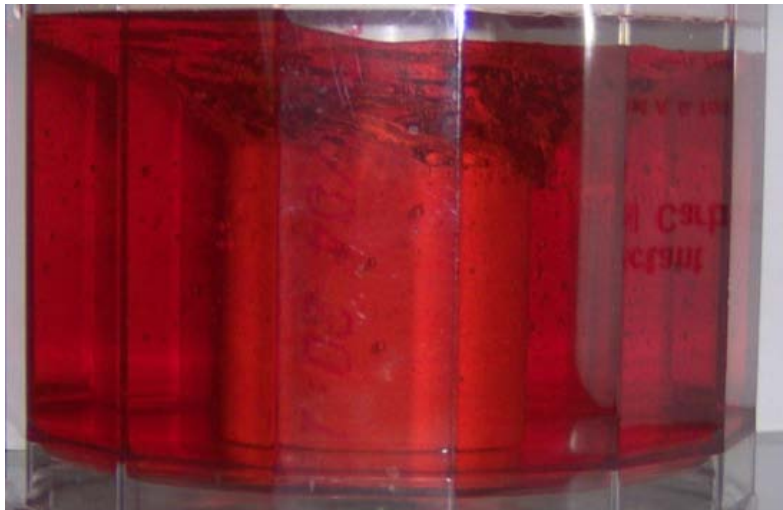
Diameter 4.25 cm: Speeds 1-3

Figure 86 Successive pictures of fluid motion using larger diameter inner cylinder.
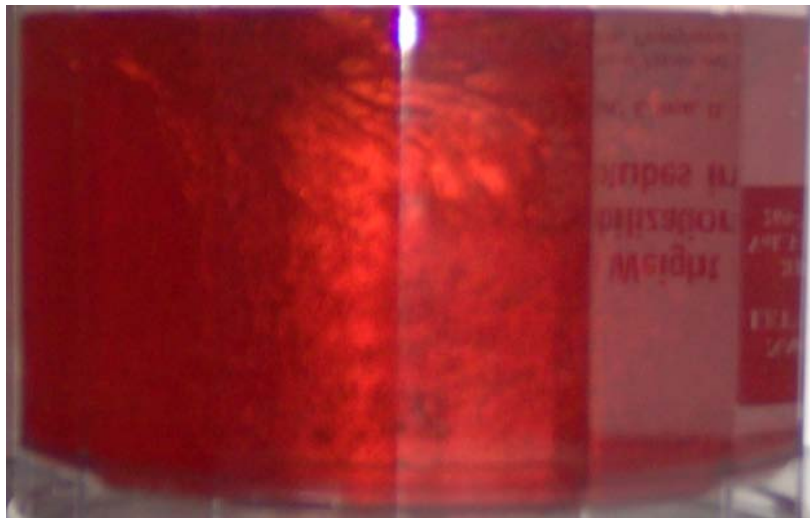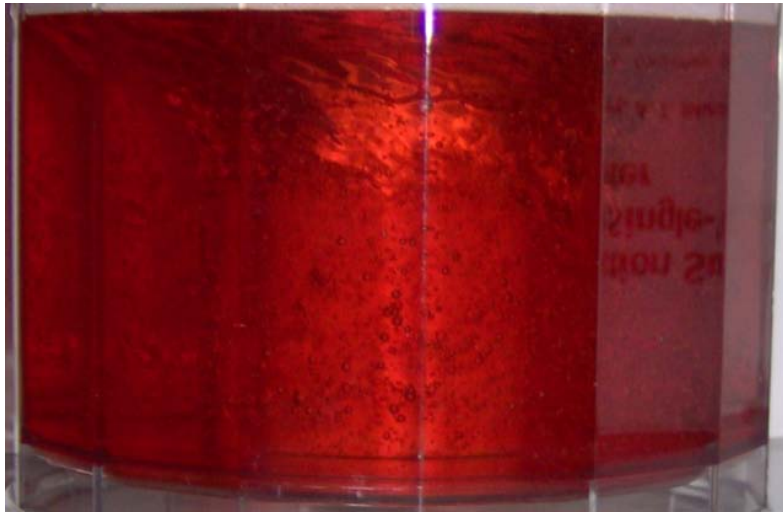
Diameter 3.4 cm: Speeds 1-3

Figure 87 Successive pictures of fluid motion using medium diameter inner cylinder.
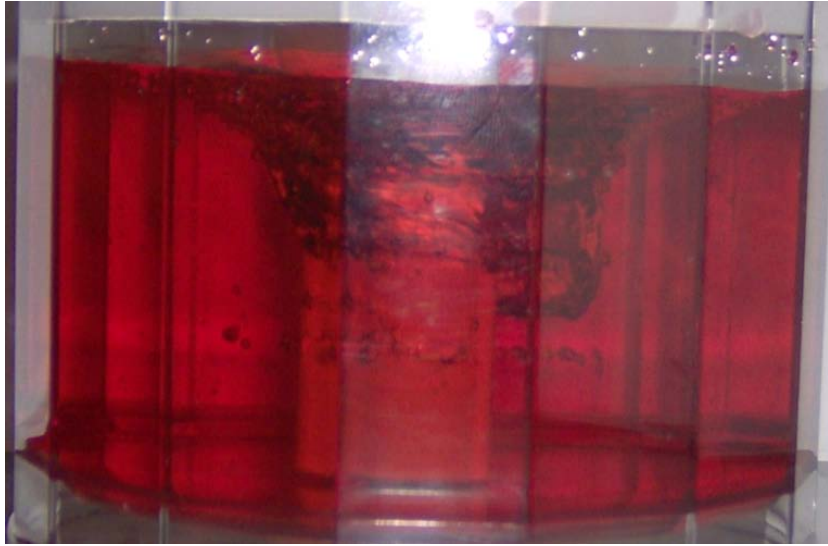
Figure 88 Successive pictures of fluid motion using smaller diameter inner cylinder.

REFERENCES

[1]   R. Bashir, D. Akin, R. Gomez, H. Li, W.J. Chang, and A. Gupta, "From BioMEMS to Bionanotechnology: Integrated Bio Chips for the detection of cells and microorganisms" *Materials Research Society Symposium Proceedings.*, vol. 773, pp. 117-124, 2003.

[2]   Munir, Cheryan. Ultrafiltration and Microfiltration Handbook. Lancaster, Pa: Technomic Pub. Co, 1998.

[3]   Sangho Lee, Richard M. Lueptow, "Rotating reverse osmosis for water recovery in space: influence of operational parameters on RO performance", Desalination, Volume 169, Issue 2, pp 109-120, 2004

[4]   Wereley, S.T., and Lueptow, R.M. "Inertial particle motion in a Taylor Couette rotating filter", Physics of Fluids, 11:325-333, 1999

[5]   D. Patel, T.C. Ford, D. Rickwood, "Fractionation of cells by sedimentation methods", Cell Separation a practical approach, pp 43-89, 1998

[6]   Carl G. Figdor, Frank Preijers, Richard Hujibens, Paul Ruijs, Theo J. M. deWitte, and Willy S. Bont, "Centrifugal Elutriation: A powerful Separation Technique in Cell Biology, Immunology, and Hematology", Cell Separation Methods and Applications, pp 43-59, 1998.

[7]   Michael Hausmann, Christopher Cremer, Roland Hartig, Hans-George Liebich, George H. Luers, Armin Saamuller, Reinhard Teichmann, "Free flow Magnetophoresis: Continuous Immunomagnetic Sorting of Cells and Organelles by Magnetic Deviation and Focusing", Cell Separation Methods and Applications, pp 209-235, 1998

[8]   Robert A. Hoffman and David W. Houck, "Cell Separation by Using Flow Cytometry", Cell Separation Methods and Applications, pp 237-269, 1998

[9]   P. Eggleton, "Separation of cells using free flow electrophoresis", Cell Separation a practical approach, pp 213-252, 1998

[10]   M. Durr et al., "Microdevices for manipulation and accumulation of micro- and nanoparticles by dielectrophoresis". Eletrophoresis **24**, pp 722–731, 2003

[11]   Ronald Pethig, Gerard H. Markx, "Applications of dielectrophoresis in biotechnology", Trends in Biotechnology, Volume 15, Issue 10, pp 426-432, 1997

[12]   Herbert A. Pohl and Ira Hawk, "Separation of Living and Dead Cells by Dielectrophoresis", Science **152**, pp 647-649, 1966

[13]   Joanne Deval, Patrick Tabeling, Chih-Ming Ho, "A dielectrophoretic Chaotic Mixer", Proc. MEMS'02, 15th IEEE Int. Workshop, pp 36-39, 2002

[14]   Peter R. C. Gascoyne and Jody Vykoukal, "Particle separation by Dielectrophoresis", Electrophoresis, **23**, pp 1973-1983, 2002

[15]   Chia-Fu Chou, Jonas O. Tegenfeldt, Olgica Bakajin, Shirley S. Chan, Edward C. Cox, Nicholas Darnton, Thomas Duke, and Robert H. Austin, "Electrodeless Dielectrophoresis of Single- and Double-Stranded DNA", Biophysical Journal, **83**, pp 2170-2179, 2002

[16]   Nicolas G. Green and Hywel Morgan, "Dielectrophoresis of Submicrometer Latex Spheres. 1. Experimental Results", J. Phys. Chem. B., **103**, pp 41-50, 1999

[17]   Nicolas G. Green, Hywel. Morgan, Joel J. Milner, "Manipulation and trapping of sub-micron bioparticles using dielectrophoresis", <u>Journal of Biochemical and Biophysical Methods</u>, **35**, Issue 2, pp 89-102, 1997

[18]   Hywel Morgan, Michael P. Hughes, and Nicolas G. Green, "Separation of Submicron Bioparticles by Dielectrophoresis", <u>Biophysical Journal</u>, **77**, pp 516-525, 1999

[19]   Russell. J. Donnelly, "Taylor-Couette flow: The early days," <u>Physics Today</u>, pp. 32-39, 1991

[20]   T. T. Lim, Y. T. Chew, and Q. Xiao, "A new flow regime in a Taylor–Couette flow," <u>Phys.Fluids</u>, **10**, pp 3233-3235, 1998

[21]   Ammar Mahamdia, Amir Dhaoni, and Ahcene Bouabdalla, "Aspect ratio influence on the stability of Taylor-Couette flow", <u>Journal of Physics Conference Series</u>, **137**, 2008

[22]   Karen L. Henderson, D. Rhys Gwynllyw, Carlo F. Barenghi, "Particle tracking in Taylor-Couette flow", <u>European Journal of Mechanics - B/Fluids</u>, **26**, Issue 6, pp 738-748, 2007

[23]   Ohmura, N., Suemasu, T., Asamura, Y. "Particle classification in Taylor vortex flow with an axial flow," <u>Journal of Physics: Conference Series</u>, **14**, pp 64–71, 2005

[24]   K. Min, R. M. Lueptow, "Circular Couette flow with pressure-driven axial flow and a porous inner cylinder", <u>Experiments in Fluids</u>, **17**, pp190-197, 1994

[25]   Arel Y. Weisberg, Joannis G. Kevrekidis and Alexander J. Smits, "Delaying transition in Taylor-Couette flow with axial motion of the inner cylinder", <u>Journal of Fluid Mechanics</u>, **348**, pp 141-151, 1997

[26]   Eric Serre, Michael A. Sprague, Richard M. Lueptow, "Staility of Taylor-Couette flow in a finite-length cavity with radial throughflow", <u>Physics of Fluids</u>, **20**, 034106, 2008

[27]   E. L. Koschmieder, <u>Benard Cells and Taylor vortices</u>, pp217, 1993